Identification of the Circadian Synaptic Transcriptome and the Role of DBHS Proteins in Synaptic Biology

---

Dissertation

zur

Erlangung der naturwissenschaftlichen Doktorwürde (Dr. sc. nat.)

vorgelegt der

Mathematisch-naturwissenschaftlichen Fakultät

der

Universität Zürich

von

Dennis Mircsof

von

Gossau, SG

Promotionskomitee

Prof. Dr. Jean-Marc Fritschy (Vorsitz)

Prof. Dr. Steven A. Brown (Leitung der Dissertation)

Prof. Dr. Michael Kiebler

Prof. Dr. Stephan Neuhauss

Zürich, 2015

Table of Contents

Abstract

Circadian rhythms are intrinsic oscillations, which occur periodically over the course of 24 hours and are conserved in many biological systems ranging from simple algae to complex organisms such as humans. These rhythms allow better anticipation of environmental changes such as the light-dark cycle or temperature fluctuations. It has been demonstrated that circadian clocks modulate daily changes of a variety of biological processes such as body temperature, hormone secretion, blood pressure, metabolism and many other functions. Interestingly, an increasing number of studies have demonstrated that alteration in the circadian system affect learning and memory consolidation. The biological basis of learning and memory is mainly regulated by synaptic plasticity through molecular mechanisms known as Long Term Potentiation (LTP) and Long Term Depression (LTD) and it has been shown that these forms of synaptic modifications require *de-novo* protein synthesis. Over the past few decades studies have demonstrated that the underlying protein translation in dendrites takes place in a small and localized compartment near the remodeling synapses by utilizing synaptic mRNA. Most of the studies that focused on mRNA dynamics at the synapse have been limited to the process of development or very short time periods during synapse activation. However, possible circadian dynamics in synaptic mRNAs has not been investigated so far, especially given the fact that learning and memory consolidation are regulated in a circadian fashion.

Therefore, the first goal of my thesis was to understand the possible role of circadian regulation of the local synaptic mRNA. By the implementation of biochemical isolation of synaptic nerve terminals called synaptosmomes and using next-generation sequencing of synaptosomal preparations, I could identify a total of 900 rhythmic expressed genes in the mouse brain and 180 rhythmic synaptic transcripts. Interestingly, I observed very poor overlap between these populations of rhythmic mRNA indicating that oscillations of mRNA at the synapse are independent of the nuclear circadian transcription process.

Synaptic mRNA transcripts are transported by neuronal RNA granules along microtubules control local protein synthesis in response to synaptic activity. Among these proteins two RNA-binding proteins namely NONO and SFPQ which belong to the DBHS family have been described to be components of RNA transport granules. Interestingly, these proteins are also linked to the circadian system. The role of NONO and other DBHS proteins such as SPFQ and PSPC1 in transcription and circadian clock regulation is very well known. However, their possible function in synapse morphology is up to now unclear.

In the second part of my thesis, I demonstrated that NONO and PSPC1 modulate inhibitory post-synaptic structures of gephyrin and $GABA_A$ receptor α2 both *in-vitro* as well *in-vivo* using a mouse model deficient of the corresponding protein. Interestingly NONO and PSPC1 knockout mice exhibit opposite gephyrin and $GABA_A$ receptor α2 morphology as well GABRA2 mRNA levels. In addition, I could show that disrupting paraspeckles by depletion of the long-noncoding nuclear RNA Neat1 dramatically increases gephyrin and $GABA_A$ receptor α2 clustering in the mouse hippocampus.

To understand in detail the functional consequences of these morphological changes I used NONO deficient mice as a model. I could demonstrate that NONO deficient mice exhibit craniofacial anomalies as well as global transcriptional dysregulation in fibroblasts and hippocampal tissue. Behaviorally, mice showed impaired performance in the Morris Water Maze as well as a marked anxiety phenotype documented via prepulse inhibition, open field exploration and light-dark preference testing. This results are strongly supported by the finding that null mutations in the NONO gene in humans are a novel cause of X-linked syndromic intellectual disability characterized by facial features as well as shy, gentle and cheerful behavior. These observations highlight for the first time the key role of a DBHS protein in learning and memory and the role of DBHS proteins in the functional organization of GABAergic synapses.

Zusammenfassung

Zirkadiane Rhythmen sind intrinsisch Oszillationen, die in regelmässigen Abständen über den Verlauf von 24 Stunden auftreten und sind in vielen biologischen Systemen welche von einfachen Algen über komplexere Organismen wie zum Beispiel den Menschen reichen konserviert. Diese natürliche Rhythmen erlauben die Antizipation von täglichen Umweltschwankungen, wie den hell-dunkel Zyklus oder Temperatur-schwankungen und es wurde gezeigt, dass diese Schwingungen in einer Vielzahl von biologischen Prozessen, wie Körpertemperatur, Hormon-sekretion, Blutdruck, Stoffwechsel und viele anderen Funktionen beteiligt sind. Darüber hinaus haben immer mehr wissenschaftliche Studien gezeigt, dass Veränderungen im zirkadianen System das Lernen und Gedächtnis beeinflussen. Die biologische Basis für Lernen und Gedächtnis ist hauptsächlich durch synaptische Plastizität geregelt welche den molekularen Mechanismen wie Langzeit-Potenzierung (LTP) und Langzeit-Depression (LTD) unterliegt und es hat sich gezeigt, dass diese Formen der synaptischen Änderungen von Grund auf neue Proteinsynthese erfordern. In den letzten Jahrzehnten haben Studien gezeigt, dass die zugrunde liegende Proteintranslation in Dendriten in einer kleinen und lokalisierten Weise direkt neben der umgestaltenden Synapsen durch die Verwendung von synaptischer mRNA stattfindet. Obwohl diese mRNA Dynamik an der Synapse während der Entwicklung von Organismen und sehr kurze Zeiträume während Synapsen-Aktivierung bereits untersucht wurden, ist die zirkadiane Dynamik der synaptischen mRNAs über einen Zeitraum von 24 Stunden noch nicht erforscht, vor allem angesichts der Tatsache, dass Lernen und Gedächtnis einem zirkadianen Prozess unterliegen.

In dieser Arbeit beschreiben wir die Identifikation der zirkadianen synaptischen Transkripte im Maushirn durch die Implementierung der biochemischen Isolierung von synaptischen Nervenendigungen (genannt Synaptosomen). „Next-Generation-Sequencing“ (NGS) von Synaptosomen identifizierte 900 rhythmisch exprimierte Gene im Maushirn und 180

rhythmische synaptische Transkripte. Interessanterweise zeigen die beiden Gruppen nur eine geringe Überlappung, was darauf hinweist, dass die Rhythmik an der Synapse vor allem unabhängig von der Expression der Transkripte im Zellkern angetrieben ist.

Synaptische mRNA-Transkripte werden durch RNA-Granulate entlang der Mikrotubuli transportiert und zwei Komponenten der RNA-Transport Maschinerie sind NONO und SFPQ welches Mitglieder des DBHS Familie von RNA-bindenden Proteinen darstellen. Interessanter Weise wurden diese Proteine ebenfalls mit dem zirkadianen System in Verbindung gebracht.

Während die Rolle NONO und anderen DBHS Proteinen in Transkription und der zirkadianen Uhr bekannt ist, ist seine Funktion in synaptischer Morphologie und Funktion bis jetzt unklar. In dieser Arbeit haben wir gezeigt, dass sowohl NONO und PSPC1 die Struktur von inhibierenden Synapsen sowohl *in-vitro* als auch *in-vivo* in einem Maus-Modell in welchem das entsprechende Protein fehlt signifikant beeinflusst. Interessanterweise zeigen NONO und PSPC1 defiziente Mäuse gegensätzliche Gephyrin und $GABA_A$-Rezeptor α2 Morphologie sowie GABRA2 mRNA Spiegel. Darüber hinaus habe ich gezeigt, dass die Zerstörung von „Paraspeckles“ durch reduzierung des langen-nichtkodierenden nuklearen RNA Neat1 sich die Anzahl Gephyrin und GABAA Rezeptor α2 Clustern im Hippocampus der Maus signifikant erhöht. Angesichts der morphologischen Veränderungen in NONO defizienten Mäusen, welche im zweiten Teil der Arbeit beschrieben wurden, habe ich die funktionellen Eigenschaften von NONO näher studiert. Ich habe gezeigt, dass NONO defiziente Mäuse sowohl Verhaltens- als auch und kraniofaziale Anomalien, sowie globale transkriptionelle Dysregulation in Fibroblasten und Hippocampus-Gewebe zeigen. Diese Ergebnisse werden stark von der Erkenntnis dass Mutationen im NONO Gen beim Menschen eine neue Ursache für X-chromosomale syndromale geistige Behinderung, welche durch abnormale Gesichtszüge gekennzeichnet ist, unterstützt. Diese Erkenntnisse verknüpfen NONO mit dem Lernprozess und Gedächtnis und zeigen die Schlüsselrolle der DBHS Proteine in der funktionalen Organisation der GABAergen Synapsen.

1. General Introduction

Thanks to its circadian clock, an organism is able to anticipate diurnal environmental changes in an adaptive fashion. Yet, these diurnal changes and the physiological responses to them also serve as timing cues to the clock, setting it to better match its environment. This chapter explores the molecular basis of this elegant interrelationship and its relevance for learning and memory.

1.1 Circadian Clocks

A circadian rhythm is an endogenously driven pattern of behavior or physiology in an organism that repeats periodically approximately each day. Such patterns exist in organisms throughout evolution, from bacteria to plants and animals (*1*). In metazoans, the prototypical example of a behavior that demonstrates a circadian rhythm is the sleep-wake cycle, with its alternating intervals of activity and with restfulness that recur with a periodicity approximating the 24-hour day-night cycle. Not only do circadian rhythms govern sleeping patterns, but in mammals they also play a part in controlling body temperature, hormone secretion, blood pressure, metabolism, and many other functions.

1.2 Concept of Biological Clocks

The mechanism underlying circadian rhythms is a biological “circadian clock.” Conceptually, circadian clocks can be divided into three quasi-independent processes: input pathways, which relay environmental information to a central pacemaker (clock); a circadian pacemaker, which generating the oscillation; and output pathways, through which the pacemaker regulates molecular and biochemical pathways that lead to rhythms in physiology and behavior. Circadian clocks, as opposed to other biological oscillators like the cell cycle or the menstrual cycle, meet four general criteria (*2-4*): i) their period length,

the time taken for one complete cycle, is about twenty-four hours (hence the word “circadian”, from the Latin *circa diem,* or “about a day”). ii) The rhythm must persist under constant environmental conditions, maintaining its periodicity of approximately 24 hours. iii) The rhythm exhibits temperature compensation, keeping roughly the same period length at different environmental temperatures. A normal biochemical reaction will approximately double its speed with every 10 degrees Celsius that the temperature increases, but circadian clocks do not. iii) The rhythm can be synchronized by environmental cues, commonly called *zeitgebers* (German for “timing cues”). This synchronization, or entrainment, allows the clock to change its phase, or internal time, to better match local external time.

Thus, environmental *zeitgebers* induce molecular changes in the circadian oscillator that adjust it to the environment. One of the most potent of these cues is light, which is capable of changing clock phase in either direction depending upon the time that it is perceived, and thereby altering the timing of daily behaviors such as rest-activity cycles and feeding. Interestingly, however, both behavior (i.e. exercise) and feeding themselves can shift clock properties at a molecular level. The result is an oscillator that responds both to the exigencies of the environment and the reality of an organism’s behavior in it. In the following pages, we first outline the mammalian circadian oscillator at a molecular and systemic level, and then summarize current knowledge about its entrainment.

1.3 Molecular Basis of Circadian Clocks

Knowledge of the molecular components of the circadian clock was first established in the fruit fly *Drosophila melanogaster*, where mutation of the gene *period* (*per*) caused altered circadian rhythms (*5*). Subsequent isolation of the affected gene showed that that both *per* RNA and protein are expressed rhythmically (*6*). Evidence that the PER protein product repressed transcription of its own gene led to the theory that regulation of the circadian rhythm on a molecular level is controlled by interlocking autoregulatory

feedback loops of transcription and translation that involve a set of clock genes and their protein products (*7*).

In mammals, the molecular set-up of the circadian clock may be schematically imagined as consisting of positive and negative elements (*7-9*). Positive components include the two transcription factors CLOCK (circadian locomotor output cycle kaput) and BMAL1 (Brain and Muscle ARNT like 1) and their homologs. These transcription factors form heterodimers through their PAS and HLH regions and bind cis-acting E-Box sequences (consensus sequence: CACGTG) present in the promoter regions of many clock and clock-controlled genes. Among the genes so activated are the three period genes (*mPer1–mPer3* in the mouse) and two cryptochrome genes (*mCry1* and *mCry2*), the key negative components of this feedback loop.

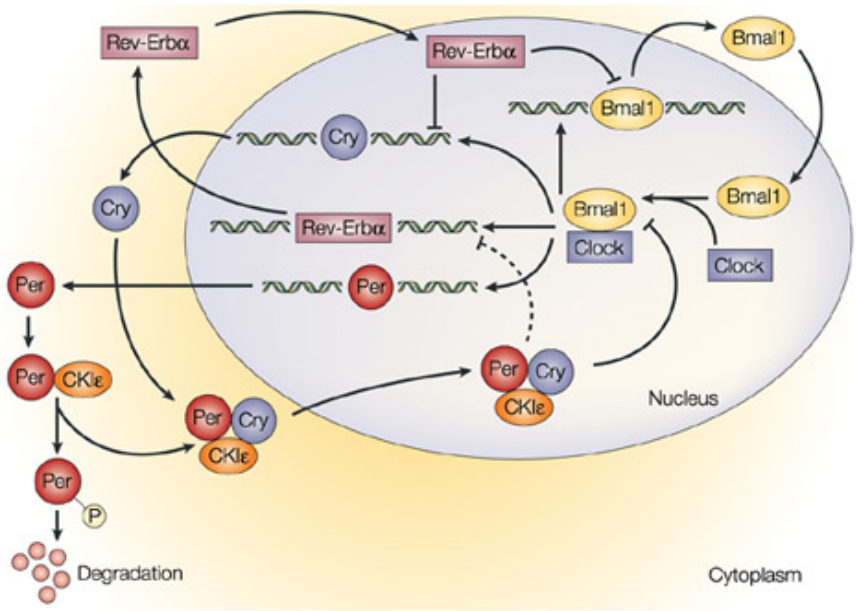

Figure 1. Core clock components of the mammalian transcriptional - translational feedback loops. The positive elements of the primary feedback loop are represented by the CLOCK and BMAL1, which heterodimerize and initiate the transcription of target genes containing E-box cis regulatory enhancer sequences including Periods (Per1, Per2, Per3) and Cryptochromes (Cry1, Cry2). Negative feedback is achieved by PER: CRY heterodimers that translocate back into the nucleus and repress their own transcription. Casein Kinase 1 epsilon and delta are critical factors that regulate the core circadian turnover in mammals. The second regulatory loop induced by CLOCK- BMAL1 heterodimers activates the transcription of retinoic acid-related orphan nuclear receptors (Rev-erbα, Rorα) that consequently compete to bind retinoic acid-related orphan receptor response elements (ROREs) in the Bmal1 promote. RORs activate transcription of Bmal1, whereas REV-ERBs repress the transcription process. (Fu & Lee; 2003)

To close this feedback loop, *Per* and *Cry* transcripts are translated in the cytoplasm several hours later and form multimeric complexes of unknown stoichiometry that are translocated back into the nucleus. There, they negatively regulate their own expression by repressing the transcriptional activity of CLOCK/BMAL1. A subsequent decline in PER and CRY protein levels through both lack of transcription and active post-translational modification, proteasome targeting, and degradation finally leads to a re-activation of CLOCK/BMAL1 driven transcription and initiation of the next cycle. This basic feedback loop recurs autonomously on a daily basis.

Other clock genes play a role in stabilizing the circadian rhythm by forming additional interlocked feedback loops. For example CLOCK/BMAL1 heterodimers not only regulate transcription of *Per* and *Cry* loci, but also of retinoic acid-related orphan nuclear-receptor genes *Rev-Erbα* and *RORα* (*10*). The REV-ERBα protein represses *Bmal1* transcription by binding to retinoic acid-related orphan receptor-response element (RORE) sequences in the *Bmal1* promoter. Similarly, RORα also binds the RORE sequences in the *Bmal1* promoter, but in contrast to REV-ERBα, RORα activates *Bmal1* transcription (*10, 11*). Therefore transcription of *Bmal1* is the result of competition between REV-ERBs and RORs at their specific response elements (RORE), interconnecting positive and negative feedback loops of the clock.

In addition to transcriptional regulation, posttranslational mechanisms such as protein phosphorylation have been found to be critical in generating circadian oscillations (*12*). For instance, casein kinase ε and δ(CK1ε/δ) are essential components of the feedback loops that generate circadian rhythm in mammals . CK1ε phosphorylates PER, CRY, and BMAL1 proteins (*12*) . CK1δ, a close paralog of CK1ε, has also been found to be associated with PER/CRY complexes and may therefore perform a similar function. Although phosphorylation of clock proteins at different sites leads to varying effects, one key role of this modification is to favor ubiquitinylation and subsequent proteasome-mediated degradation of proteins thus modified.

1.4 Master and Peripheral Clocks

From single-celled organisms to mammals, the basic circadian clockwork is cell-autonomous and present in most cells and tissues. Thus, individual cells (neurons, fibroblasts, hepatocytes, etc.) show circadian oscillations of gene expression, even in isolation. Nevertheless, in complex organisms like mammals, these clocks are arranged in a hierarchy (*13*). The master pacemaker of the mammalian circadian clock is located in the suprachiasmatic nucleus (SCN) of the anterior hypothalamus. The SCN is a heterogeneous tissue comprised of at least two broad regions. SCN neurons of the ventrolateral part (core) are heavily innervated by the retinohypothalamic tract and possess the unique property of inducing the expression of several genes, including *Per1* and *Per2,* in response to light stimulation. However, their intrinsic circadian oscillations are weak. In contrast, cells of the dorsomedial part (shell) receive most of their information from the hypothalamus and limbic areas as well as from the core, and show strong autonomous rhythmicity but only weak activation by photic input.

SCN-lesioned animals lose global circadian rhythmicity of diurnal behavior and physiology in constant conditions – e.g. corticosterone rhythm, drinking behavior and locomotor activity – and SCN grafts restore these rhythms. Thus, the SCN is responsible for entraining and synchronizing cellular clocks throughout the brain and body.

1.5 Clock Genes In The Hippocampus

The SCN is considered as master clock, coordinating circadian input such as light via different projections. A recent publication has identified around 35 brain projections to the SCN and not less than 15 efferent signaling pathways (*14*). As previously mentioned, light is the main Zeitgeber for the SCN, Exposure to light leads to depolarization of RGCs, which innervate the SCN via the retinohypothalamic tract (RHT). The monosynaptic RHT fibers end directly on SCN neurons in the ventrolateral part of the nucleus. This information is further processed and projected to the dorsal medial

hypothalamus (DMH) through the subparaventricular zone. (sPVz), which in turn forwards in formation to other hypothalamic structures, which contain which projects to various regions in the hypothalamus, including the ventrolateral preoptic area (VLPO), the lateral hypothalamus (LH) and the paraventricular nucleus (PVN) (*15, 16*). The role hypothalamic structures include various biological processes such as thermoregulation, food anticipation, sleep-wake arousal and hormone secretion via the hypothalamo-pituitary-adrenal (HPA) axis and the hypothalamo-pituitary-gonadal (HPG) axis, which will be discussed later. Evidence for the functional connection between the SCN and the hippocampus, a key region in memory formation and learning are however poorly understood. Indirect connections via the dorsal medial hypothalamus target to the locus coeruleus, which is a region activating cortical and hippocampal structures.

Although the SCN serves as a master clock, several studies have shown that clock driven rhythms can be found in various tissues including the brain. For example, circadian rhythms of clock genes have been shown for brain structures such as the prefrontal cortex (*17*), olfactory bulb (*18*) and the hippocampus (*17, 19*), brain structure crucial for neuronal plasticity and memory processing. Using detailed biochemical gene expression studies combined with morphological immunohistochemical analyses, the authors demonstrate a robust circadian oscillation of core clock genes such as *Per1, Cyr1/2, Clock* and *Bmal1,* but not *Per2* in the hippocampus of wildtype mice (*19*). Immunohistochemical colabeling studies revealed that clock gene protein expression was detected exclusively in in nuclei of cells of the *Stratum pyramidale* and the *Stratum granulosum* of hippocampal neurons, including parvalbumine positive interneurons, but not in astrocytes. Moreover, mice in which *Per1* expression was disrupted showed significant disturbed expression profiles for core clock genes.

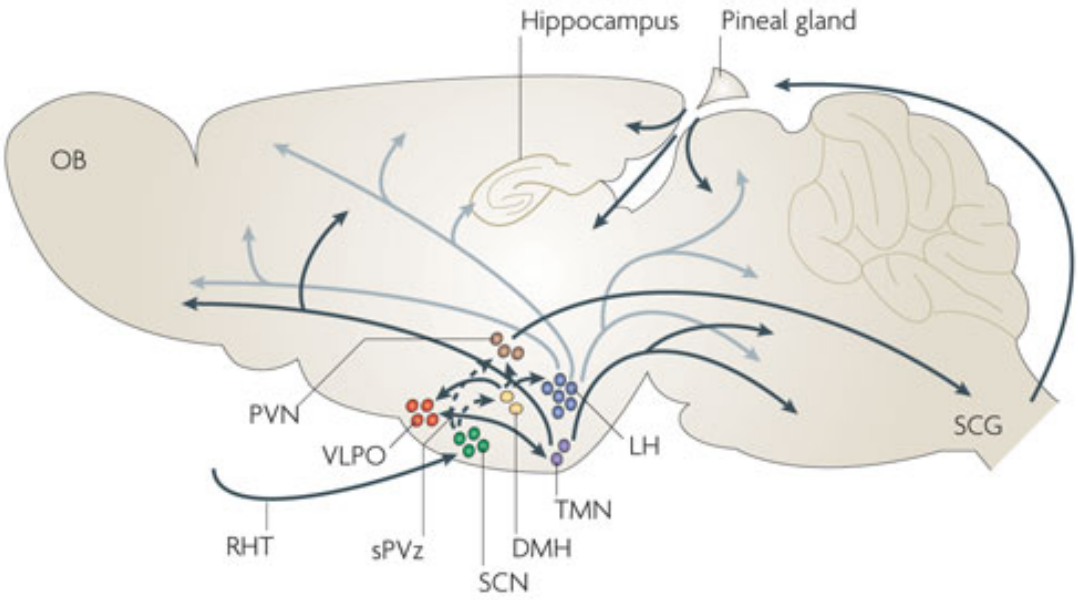

Figure 2. Anatomical circadian pathways in mice. In the mouse (*Mus musculus*), the suprachiasmatic nucleus (SCN) receives photic input through the retinohypothalamic tract (RHT). The SCN projects to the dorsal medial hypothalamus (DMH) through the subparaventricular zone (sPVz), which projects to various regions in the hypothalamus, including the ventrolateral preoptic area (VLPO), the lateral hypothalamus (LH) and the paraventricular nucleus (PVN). There are reciprocal connections between the VLPO and the tuberomammilary nucleus (TMN), which are thought to be partly responsible for the proper timing of sleep–wake rhythms. Functional connections between a circadian centre and a memory forming-centre, such as the hippocampus, are not well known. They may be partially gated through hypocretin- or orexin-expressing cells of the LH, or by melatonin secretion from the pineal gland following signaling from the PVN to the superior cervical ganglion (SCG). Note that C57BL/6J mice lack melatonin. OB, olfactory bulb. (Gerstner & Yin; 2010)

In a large ex-vivo screen, neuronal tissue from rat containing *Per1*-luciferase transgene were used to monitor intrinsic *Per1* expression in culture. Although many *Per*-expressing brain areas were arrhythmic in culture, 14 of the 27 areas examined were rhythmic (*17*). Despite the high expression of *Per1* in the hippocampus, the authors were not able to demonstrate intrinsic rhythmicity, whereas other tissues with comparable expression were able to recapitulate oscillations with a near 24h period for multiple cycles. Even though cell death could be excluded as a potential explanation for the lack of circadian oscillations, because forskolin evoked a healthy response, it is possible that the hippocampus failed to show circadian rhythmicity because culture conditions might have adversely affected those oscillations (e.g. by dispersion of interconnected neurons). A second explanation might be the fact that the SCN acts as the sole pacemaker that drives circadian rhythmicity in

the hippocampus. In line with this findings, *Per2* oscillation in the amygdala and dentate gryrus of SCN lesioned Syrian hamster has been shown to be abolished, strengthening the slave oscillator hypothesis (*20*). Controversially, a similar study using luciferase labeled *Per2* knockin mice, has demonstrated clear circadian rhythms of *Per2*-luciferase bioluminescence in the mouse hippocampus when monitored in the luminometer (*21*). This identified rhythmicity was claimed to be autonomous as they were present in isolated hippocampal slices which maintained in culture and thus independent of the SCN.

1.6 Circadian Rhythms And Memory

In the SCN of nocturnal rodent, neurons have been shown to exhibit diurnal changes in the spontaneous firing (SFR) and resting membrane potential (RMP) (*22-27*). This observation of course raises the possibility, that the SCN might drive time-dependent physiological and neuronal events downstream of the central pacemaker, including processes such as learning and memory.

Despite the controversy of precise clock gene expression and regulation in the hippocampus, most of the studies argue for a strong role of circadian rhythms in learning and memory. In the hippocampus, two opposing mechanisms called long-term potentiation (LTP) and long-term depression (LTD) are widely believed to be the molecular basis of learning and memory (*28*). Based on their recent activity, a synapse can modify its efficiency to either fire more strongly by LTP, or less strongly via LTD. Although the molecular mechanisms underlying LTP and LTD is still under investigation, this sort of plasticity has been shown to change depending on the time of day in various nocturnal rodents (*29-33*). In a pioneer study, it has been shown that excitability of the rat denatate gyrus, a substructure of the hippocampus, indeed exhibits a circadian component (*29*). Interestingly, the peak of LTP in the dentate gyrus was found during the dark phase, while in contrast LTP in the CA1 area of the hippocampus was during the light phase. Involvement of circadian rhythms in LTP formation in the hippocampus was also proved in a

study performed in Syrian hamster (*34*) and mice (*33*). Although excitability of the CA1 region in Syrian hamster peaked in the light phase as described for rats, in contrast to the previous studies the tissue was harvested the opposite time of the day. This means, that LTP in the Syrian hamster was higher in the CA1 area from tissue, which has been harvested during the light period and then tested in the dark period. A further study performed in mice, has investigated the role of tissue harvesting and examination in respect to LTP in the CA1 region of the hippocampus (*33*). Hippocampal tissues harvested from mice during the light period, LTP was greater when examined in the dark period than during the light period, which is in contrast to the previously reported rat study. Finally, a study by Nakatsuka and coworkers performed in rats tried to answer this discrepancy, by applying theata-burst stimulation (TBS) instead of high-frequency stimulation (HFS) of the Schaffer collateral of the hippocampus (*35*). Recordings of population spikes (PS)-LTP during the light and the dark phase has revealed, that the magnitude of the LTP was larger during the dark phase compared to the light phase. Taken together, this studies implicate, that the time of testing is more crucial then time of harvesting and indicates that these circadian variations are rather autonomous and therefore independent of the central pacemaker. This idea fit with the previously observation, that isolated hippocampal slices maintained *Per2* rhythmicity independent of the SCN. Additionally the circadian magnitude of LTP in the hippocampus is synchronized with the locomotor activity of these nocturnal rodents.

To better understand the physiological consequences of clock genes upon learning and memory, several mode organisms ranging from fruit flies to mice deficient of core clock genes have been examined for memory defects. Mice lacking the core clock genes *Cry1* and *Cry2* (*Cry* double knockout mice) learned to avoid unpleasant sensory experiences (mild foot shock) and could locate a food reward in a spatial learning task (place preference) (*36*). These mice failed, however, to learn time-place associations. (*36*). However, the situation for the *Period*-gene is still a matter of debate: In a study, using *Per1/Per2* double mutant mice, which exhibit an arrhythmic locomotor phenotype, no significant difference in terms of time-place learning compared

to wild-type mice was shown (*37*). Additionally, no deficiencies in short-term spatial working memory in *Per* mutant mice could been demonstrated. Moreover, both Per mutant and wild-type mice showed similar long-term memory for contextual features of a paradigm (a mild foot shock), measured in trained mice after a 2-month nontesting interval. (*37*). In line with this findings, examination of *Per1/Per2* double mutant mice using two different learning and memory paradigms, a water-maze place navigation task and contextual fear conditioning, showed that none of these learning types were affected by the mutations, which suggests that *Per* does not play a major role in the regulation of hippocampus-dependent learning and memory (*38*). In contrast to these findings, *Per1* deficient mice were accompanied by the loss of daytime-dependent differences in spatial working memory performance (*39*), which was related to the loss of circadian phosphorylation of cAMP response element-binding protein (CREB), a cellular transcription factor, in the hippocampus. Finally, the authors have been able to demonstrate physiological perturbations of LTP, a cellular correlate for long-term memory, upon *Per1* depletion (*39*). In addition, a similar study on *Per1* knockout animals has demonstrated a severe perturbation in a hippocampus-dependent long-term spatial learning paradigm (*19*), supporting the idea that *Per1* is indeed involved in the circadian learning behavior. Finally, *Per2* mutant mice exhibit deficits in the recall of trace, but not cued, fear conditioning (*21*).

Circadian dependency on cognitive performance and memory formation have been shown in several behavioral paradigms (*40-42*). Surprisingly, circadian rhythms of locomotor activity are not an accurate predictor of the timing of optimal performance in memory tasks over the course of the day. For example, while the peak of memory performance of diurnal organisms such as zebrafish (D. rerio) (*43*) or the sea slug (A. californica) (*44, 45*) is shown during their active phase, fruitflys (D. melanogaster) and nocturnal rodents such as mice show highest cognitive performance during their inactive phase. (*45, 46*). These findings indicate, that locomotor activity is not the cause of circadian memory formation, because there is clear separation between resting state and memory performance in the different studied model

organisms. These results raise the question of the driving mechanism, which govern circadian memory and learning behavior. Beside the cellular and molecular core clock mechanisms, other factors such as neurotransmitter release, which regulates synaptic excitability and activity or hormones could potentially contribute to the circadian memory enhancement.

One hormone, which is associated with circadian rhythms is melatonin. Melatonin is secreted by the pineal gland and it is under the circadian control of the SCN (*47*). The temporal release of melatonin is regulated in a circadian fashion in a wide range of organisms such as humans (*48*), zebrafish (*49*), sea slugs (*50*), mice (*51*), fruit flies (*52*) and low melatonin levels have been reported in autism spectrum disorders in the human (*53-55*). A study performed in zebrafish has shown, a clear time-of-day effect in acquisition (learning) and memory formation (*43*). This learning paradigm was then negatively correlated with high levels of melatonin: High melatonin levels during the night were resulted in lower periods of performance. Pinealectomy or treatment with a melatonin receptor antagonist ultimately rescued reduced cognitive performance during the dark phase, supporting the idea that melatonin is supporting memory and learning behavior (*43*). Studies performed in C57Bl/6J mice, which lack melatonin and C3H mice, which express melatonin has shown, that mice deficient of melatonin show less time-of-day-dependent changes in hippocampal LTP than mice secreting melatonin (*33*). However, circadian learning performance cannot be attributed completely to melatonin because mice deficient for melatonin still show time-of-day-dependent changes in memory formation (*46*) and therefore additional factor must contribute to diurnal memory performance.

A second class of hormones are glucocorticoids, which are produced by the adrenal gland, regulate a variety of physiological processes such as metabolism, immune response, cardiovascular activity, and brain function and his highly associated with stress response (*56*). Glucocorticoids can bind the glucocorticoid receptor (GR) a nuclear hormone receptor found in many cell types but not in the SCN (*57*) and it has been shown to exhibit both ultradian and circadian rhythmicity (*52, 57, 58*). Disruptions of the SCN by targeted

lesions have shown that circadian aspects of the rhythmic release of glucocorticoids indeed underlie the central pacemaker (*59-61*). Many studies have shown, that excessive glucocorticoid secretion upon chronic stress affect learning and memory in a negative fashion (*62-64*) and that they are able to regulate spine development and plasticity *in-vivo* (*65*). A recent study by the laboratory of Liston and coworkers has shown that thin spine development and plasticity is tightly tied to the circadian rhythmicity of corticosteroid secretion and are differentially regulated by glucocorticoid and mineralocorticoid receptor-dependent mechanisms (*66*). Taken together, these results show that circadian oscillations of glucocorticoids are important for learning-dependent synaptic formation and maintenance.

As mentioned previously, in addition to hormones neurotransmitter could potentially modulated circadian learning and memory behavior. One of the major inhibitory neurotransmitter in the central nervous system (CNS) of mammals is gamma-aminobutyric acid (GABA). The study by Ruby and coworkers elegantly connects the role of circadian learning performance via the neurotransmitter GABA. Instead of disrupting the circadian rhythm by SCN lesions, Siberian hamsters (Phodopus sungorus) have been made arrhythmic by a single 2h exposure to light during the night which was followed by a 3h phase delay the next day (*67*). Control hamster showed circadian performance in the novel object recognition (NOR) task, a memory test which is under the control of the hippocampus. By contrast, hamsters, which have been made arrhythmic, did not exhibit circadian learning pattern and in addition performed significantly worse compared to control wildtype littermates. Furthermore, the authors have shown that disturbed sleep patterns during the experiment in these animals could be excluded as cofounding factor since sleep deprivation did not restore learning impairment in arrhythmic hamsters. Surprisingly the GABA antagonist pentylenetetrazol completely restored the circadian sensitivity of learning the task indicating an important role of GABA in the circadian memory processing. A functional role for GABA in circadian LTP has been recently shown by the laboratory of Natsume and coworkers where local application of Gabazine, a $GABA_A$ receptor antagonist, mimicked nighttime disinhibition and thereby facilitated

LTP in the CA1 region of the rat hippocampus (Nakatsuka and Natsume, 2014).

1.6 Organization Of The Inhibotory GABAergic Synapse

Beside glycine, gamma-aminobutyric acid (GABA) is one the most important inhibitory neurotransmitter in the central nervous system (CNS) of mammals. While glycine primarily mediates fast inhibition in the brain stem and spinal cord, GABA acts mainly in the central brain. GABA is synthesized in presynaptic terminals of interneurons by the enzyme glutamic acid decarboxylase (GAD) and the vesicular GABA transporter (vGAT) enzyme enriches the neurotransmitter in presynaptic vesicles (*68*). Interestingly, both GAD activity and GABA levels have been shown to exhibit circadian oscillations in the rat SCN and regulates neuronal coupling (*69*). Upon arrival of an action potential at the presynaptic site, Ca^{2+} channels in the plasma membrane open, leading to depolarization by Ca^{2+} influx. This depolarization triggers the exocytosis of some of the presynaptic vesicles containing GABA into the synaptic cleft.

Upon binding of GABA, $GABA_A$ receptor ($GABA_AR$), a ionotropic chloride channel, mediate fast synaptic inhibition by activation whereas $GABA_B$ receptors ($GABA_BR$), a G-protein coupled receptor, mediate slow and prolonged neuronal inhibition by indirectly affecting downstream effector pathways via Gi/o associated proteins. $GABA_A$ receptors belong to the Cys loop superfamily of ligand-gated ion channels, which are encoded by a family of 19 subunits (α1-α6, β1-β3, γ1-γ3, δ, ε, π, θ, and ρ1-ρ3) and exhibit four transmembrane domains per subunit (*68*). The functional GABAA receptor complex has a pentameric structure existing in a variety of possible combinations of protein subunits.

Through the proximity of the receptor to the transmitter release site within the synapse, the kinetics of the IPSP is tightly controlled. Phasic inhibition plays a key role in synchronizing neuronal activity. Tonic inhibition, on the other hand,

is mediated by extrasynaptic receptors generating low amplitude currents evoked by ambient GABA spilling over from the synaptic cleft. Extrasynaptic $GABA_AR$ are involved in the regulation of neuronal excitability and plasticity (*72*). Synaptic GABA receptor exhibit a lower affinity for GABA than the extrasynaptic receptors

In the brain, most $GABA_A$ receptors are composed of two α, two β and one γ/δ/ε subunit. Differential composition of the pentameric receptor by subunit combinations defines specific localization, kinetics properties and pharmacological profile. For instance, receptors mediating fast inhibition contain mainly α, β and the γ2 subunit and are located adjacent to the presynaptic inhibitory bouton while receptors containing the δ or ε subunit in place of the γ subunit, are benzodiazepine insensitive and are exclusively located at extrasynaptic sites and typically they exhibit a higher affinity for GABA than synaptic receptors (*70, 71*). Synaptic GABA receptors regulate a process called inhibitory postsynaptic potential (IPSP), which is a fast, high amplitude phasic current, generated by the release of presynaptic GABA and fast clearance from the synaptic cleft be neurotransmitter reuptake through dedicated transporters. This inhibition is believed to play a major role in synchronizing neuronal activity. In contrast to synaptic receptor, extrasynaptic receptors are involved tonic inhibition generating relatively low amplitudes and prolonged receptor activation mainly by a spillover of synaptic GABA. Tonic inhibition is involved in the regulation of neuronal excitability and plasticity (*72*).

Various brain regions perform different tasks and therefore require different molecular specialization, which translates to distinct signaling profiles. Therefore, it is not surprising, that specific GABAR subunits are localized in a specific manner in the brain to satisfy this needs. The expression of seven major $GABA_AR$ subunits has been studied in detail by immunohistochemistry in the adult rat brain (*73*). For example, the α1 subunit which shows the fastest decay kinetics among the α subunits has been shown to be highly expressed throughout the brain, while other subunits exhibit more specific sublocalization (*74*). In the adult brain, the α2 subunit is highly expressed in

the hippocampus and shows a distribution pattern, which is opposite to the α1 subunit, being highly, expressed where α1 subunit expression is low relatively low. The α3 subunit distribution is similar to that of α2, although expression levels are reduced. The α5 subunit has been shown to be expressed in the olfactory bulb, hippocampus and spinal trigeminal nucleus. The γ2 subunit, which is essential for postsynaptic localization of GABA receptors, is ubiquitously expressed, while in contrast γ1 subunit expression is mainly restricted to the hypothalamus, amygdala, parts of the basal ganglia and the inferior olivary nucleus. The subunits β2 and β3 subunit has been shown to co-localize with α1 or α2 subunits in the adult brain, although β1 expression is relatively low compared to β1. Finally, extrasynaptic $GABA_A$ receptors typically are characterize by the assembly of two α4, α5 or α6 subunits, together with two β and the δ or γ2 subunit (*75*). The δ subunit is expressed in the forebrain together with the α4 subunit or the α6 subunit in the cerebellum. (*73*)

Functional studies of the relevance of GABAAR subunit composition was studied by targeted gene deletion. Depletion of the GABRA1 gene, which codes for the α1 subunit, showed strong compensation by increased expression of α2 and α3 in the thalamus and cerebellum but ultimately did not result in any major behavioral changes (*76*). Disruption of the α2 subunit in mice resulted in receptor rearrangements in CA1 pyramidal cells, but no replacement by the α1 subunit was observed. Interestingly, electrophysiological recordings in CA1 pyramidal cells from α2-KO mice showed a significant decrease in GABAergic mIPSC frequency, with unchanged amplitude and kinetics (*77*). Among all the GABA receptor subunits, the γ2 subunit is probably the most crucial for proper receptor function and development, since it's disruption causes postnatal lethality (*78*).

The majority of excitatory (symmetric) synapses in the mammalian brain are found on protrusions of the neuron, also referred as spines, whereas most inhibitory (asymmetric) synapses are formed on the dendritic shaft, as well as on the soma and axonal initial segment (*79*). Therefore, specific mechanisms must exist in order guarantee the correct localization of the postsynaptic

receptors with the presynaptic terminal.

The inhibitory postsynaptic density (PSD) is an asymmetric, electron dense structure adjacent to the presynaptic active zone and contains a high concentration of ligand-gated ion channels. In addition, further proteins allow the bridging between pre- and postsynaptic site and the proper scaffolding of inhibitory receptors to the postsynaptic membrane, preventing the lateral diffusion out of the synaptic cleft. Different effector proteins, kinases, and phosphatases are concentrated at the PSD and facilitate fast signal transduction.

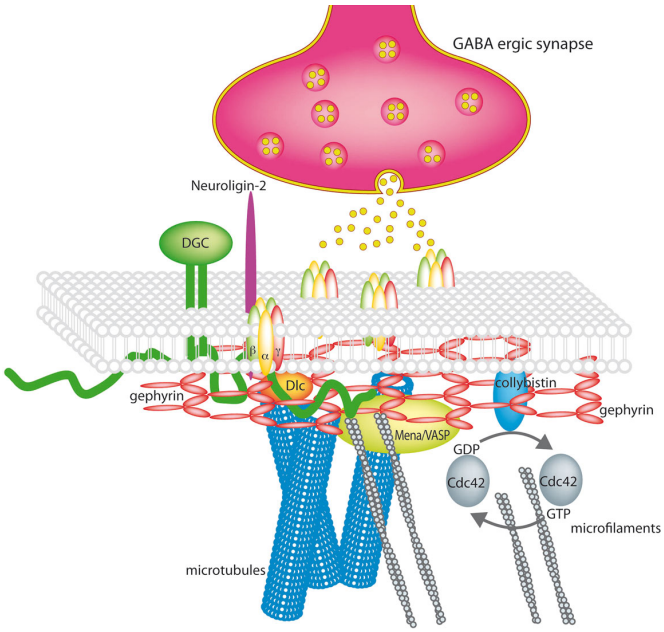

Figure 3. The GABAergic synapse. Synaptic GABAA receptors are stabilized by a submembranous lattice of gephyrin by direct interaction. Cytoskeleton associated proteins are Dlc1/2 and Mena/VASP. Collybistin, a guanine nucleotide exchange factor is membrane associated and interacts with gephyrin. The dystrophin-glycoprotein complex (DGC) stabilises the synapse and neuroligins bridge the synaptic cleft by interaction with presynaptic neurexins. Adapted from Tretter & Moss (2008).

One protein that has been strongly associated with the regulation and anchoring of GABAARs at inhibitory synapses is the multifunctional 93 kDA protein gephyrin, which self-assembles into a scaffold and interacts with the cytoskeleton. Initially, gephyrin was identified which by the interaction with glycine receptors, where directly binds to the intracellular domain of the β subunit of glycine receptors, stabilizing them at inhibitory synapses in the spinal cord (*75*). Gephyrin is a highly conserved multifunctional protein and despite the initial identification in the CNS gephyrin is also widely expressed in non-neuronal tissues required for the catalysis molybdenum cofactor (MoCo) biosynthesis (*80*). Subsequent studies have demonstrated that

GABAA receptors are anchored postsynaptically by gephyrin and binding to GABAA receptors is mediated by interaction sites that have been mapped within the intracellular loop of GABAA receptors α1, α2 and α3 subunits (*81, 82*), even though with lower binding affinity compared to the β subunit of glycine receptor (*83*). However, in contrast to glycine receptors, targeted depletion of α subunits has revealed, that not all receptor subtypes are clustered by gephyrin dependent mechanisms (*84*).

In vertebrates, the structure of gephyrin is highly conserved and consists of three domains, namely G, C and E domains (*74*). The flanking G and E domain are homologous the bacterial MogA and MoeA proteins, responsible for the MoCo synthesis and are linked by an unstructured C-domain. The flexible C-domain of gephyrin contains multiple sites for protein interaction and for post-translational modification and with proteins that regulate synapse formation and function. Due to the relatively high instability of the C-linker domain, the full-length structure of gephyrin by crystallography remains an unsolved task until today. Biochemical and structural analysis of isolated subdomains of gephyrin have shown a trimerization for the G domain as well as dimerization for the E domain (*85*). Taking this information into account, a hexagonal lattice structure was proposed for gephyrin at the postsynaptic site, forming a two-dimensional scaffold (*86*).

Depletion of gephyrin in mice neurons by targeted deletion or by gene silencing has shown, that absence of gephyrin significantly reduced postsynaptic clusters containing α2 and α3 $GABA_AR$ subunits (*78, 87*). Nevertheless, α1 subunit expression and localization was not impaired, thus indicating a clustering mechanism, which is gephyrin independent (*84*). Interestingly, gephyrin depends on the presence of $GABA_AR$ to form postsynaptic clusters in GABAergic synapses, and the size and density of gephyrin scaffolding can be correlated to strength and frequency of GABAergic transmission. Thus, gephyrin clustering is largely impaired in the mice lacking the $GABA_AR$ α2 subunit. Similarly in $GABA_AR$ α1 knockout mice gephyrin clustering at postsynaptic sites is impaired, leading to intracellular aggregates. This results show, that both gephyrin and $GABA_AR$ clustering

reciprocally regulate their clustering at the inhibitory postsynaptic site. In addition to GABAAR, gephyrin interacts with several other proteins at the PSD, including cytoskeletal, signaling, and trans-membrane proteins

As previously mentioned, the C-linker domain of gephyrin has been shown as a target for protein-protein interactions and posttranslational modifications and potentially modulate the clustering of GABAA receptors the synapse. Over the last decades, several phosphorylation residues on gephyrin have been identified. For instance, our laboratory has identified two relevant phosphorylation sites: Ser268 is phosphorylated by extracellular signal-regulated kinases 1 and 2 (ERK1/2) and overexpression of phosphor-deficient mutant in cultured neurons significantly increased gephyrin cluster size (*88*). These morphological changes are accompanied by changes of amplitude and frequency in miniature GABAergic postsynaptic currents. On the other hand, Ser270 is phosphorylated by glycogen synthase kinase 3β and overexpression of the phoso-deficient mimicking gephyrin construct in primary hippocampal neurons demonstrated a reduction in gephyrin cluster density (*89*). Thereby, the phosphorylation status of this identified residues can regulate the number and size of synaptic gephyrin and fine-tune synaptic plasticity. Beside phosphorylation, gehyrin has also been show to be target of further post-translational modifications such as palmitoylation or SUMOylation (*88-90*).

1.7 NONO – A Link between Circadian Rhythms And Memory?

Initially, our lab has identified the RNA binding protein NONO as a Per1 associated component (*91*). Disruption of NonA (the Drosophila homolog of NONO) function has shown that fruit flies harboring a hypomorphic allele show hyperactive behavior and mild arrhythmicity. Additionally, NonA deficient flies exhibit significantly decreased mRNA expression of the clock gene timeless as well as dampened rhythmicity. Interestingly, although NONO protein expression is constant, binding to the clock gene *Per1* has been demonstrated to occur in a circadian fashion. In a subsequent study, mice

which have been depleted for NONO have shown show only small changes in period length or clock gene expression (*92*) and thus the authors speculated that in mammals the lack of NONO may be compensated by other protein family members. NONO belongs to the highly conserved Drosophila Behavior Human Splicing (DBHS) protein family and this family includes three members in mammals, namely NONO, Paraspeckle Component 1 (PSPC1), and Splicing Factor Proline/Glutamine-Rich (SFPQ, also known as PSF). The speculations of the authors regarding compensation of NONO by other family members have been confirmed recently at least on the protein level since murine embryonic fibroblasts (MEFs) from mice lacking NONO exhibit significantly increased PSPC1 levels (*93*).

NONO, a Non-POU-domain-containing, Octamer-binding protein, was originally identified in mouse by Yang and coworkers in 1993 as the mammalian homolog of Drosophila NonA gene (*94*). Subsequently, the human homolog was found in HeLa cells where it was named p54/nrb for Nuclear RNA-Binding protein, 54 kDa and was included in the novel Drosophila Behavior, Human Splicing (DBHS) protein family together with the human Factor Proline/Glutamine-rich PSF/SFPQ and the Drosophila NONA/BJ6V as they all share the phylogenetically conserved protein segment of 320 amino acid, termed DBHS domain (*95*). P54NRB and SFPQ also share regions rich in proline and glutamine residues outside the main homology region. These proteins can form homo- and heterodimers in vivo (*96-99*) and are implicated in a wide variety of cellular processes, many of which are related to RNA.

First, NONO/P54NRB and PSF/SFPQ together with paraspeckle protein 1 PSPC1/PSP1, another DBHS protein family member, localize to paraspeckles (*100-106*). Paraspeckles are subnuclear bodies found in the interchromatin space of mammalian cell nuclei (*100, 107*). These ribonucleoprotein structures, built on the long non coding RNA (lncRNA) NEAT1 (also known as MENe/b) play a key role in the nuclear retention of adenosine-to-inosine hyperedited RNAs, and in storage and rapid release of certain RNAs under stress conditions (*108-110*). Second, NONO/P54NRB as well as PSF/SFPQ,

have also been shown to regulate DNA unwinding and pairing (*111, 112*), transcriptional activation and repression (*113-122*), pre-mRNA processing (*123-125*) and splicing (*126-128*). Third, P54NRB/NONO and PSF/SFPQ have been involved in DNA damage response (*93, 129-133*) and RNA transport in neurons (*134*). Other studies demonstrated that P54NRB/NONO and PSF/SFPQ are both phosphorylated during mitosis, altering their protein interactions or functional properties (*112, 135, 136*). Another study suggests that P54NRB/NONO could play a role in the maintenance of pH homeostasis in the nucleus through its Carbonic Anhydrase activity (*137*). Lastly, NONO/P54NRB and other DBHS family members serve as transcriptional cofactors necessary for correct circadian clock function in both flies and mammals (*91, 92, 138*), and through interaction with PER proteins can confer circadian clock regulation upon various downstream processes such as wound healing (*139*).

2. Aims of the Thesis

Sub-cellular localization of mRNA plays an essential role in cell function, especially during development and in neuronal plasticity. However, despite the recent progress in the identification of synaptic transcripts and RNA transport mechanism, little is know about the circadian regulation of mRNA transcripts at the synapse.

Therefore, in the first part of the thesis I wanted to address the question, weather there are synaptic enriched genes, which are regulated in a circadian fashion at the synapse. As a first step, the isolation of synaptic transcripts had to be established in order to identify synaptic enriched genes. After successful implementation of synapse purification, transcriptomic analysis of circadian synaptosomes has been performed to identify rhythmic transcript at the synapse. Finally, bioinformatical analysis has revealed that a specific subset of synaptically enriched transcripts indeed exhibits rhythmic behavior and in addition is independent of the circadian core clock.

The role of RNA binding proteins in synaptic morphology and plasticity is only poorly understood. Two components of RNA transport granules which also have been linked to the circadian system are NONO and SFPQ, members of the DBHS family of RNA-binding proteins. While the role of NONO and other DBHS proteins in transcription and circadian clock regulation is known, its function in synapse morphology and function is up to now unclear. Because of the involvement of the DBHS family of proteins in RNA transport in neurons and because they formed specific RNA holding structures in the nucleus, we guessed that these proteins might play a role in postsynaptic structure, perhaps through regulated RNA transport. The aim of the project is to characterize the function of DBHS proteins and paraspeckles in regulating synaptic morphology. As a first step to elucidate the role of these proteins in regulation of synaptic signaling, the influence on they assembly and stability of the inhibitory postsynaptic density was investigated *in-vitro* as well as *in-*

vivo with the main focus on gephyrin, which is a major scaffolding protein at inhibitory synapses in the CNS.

Finally, I wanted to understand some of the functional consequences of this regulation. It is presumed that changes in inhibitory synapse morphology, which is reported in the second chapter, are correlated with changes in the localization and function of neurotransmitter receptors. Therefore I have investigated the direct consequence of such changes in more detail for NONO deficient mice where I show, that NONO knockout mice have intellectual and anxiety-related deficits. We trace these effects to specific defects at inhibitory synapses, where NONO regulates both synaptic transcription and gephyrin scaffold structure. Our data identify NONO as a new neurodevelopmental disease gene and highlight the key role of the DBHS protein family in functional organization of GABAergic synapses

3. Results

STUDY I: Identification of the Circadian Synaptic Transcriptome

D. Mircsof[1,2], L. Opitz[3], S. K. Tyagarajan[2§] , S. A. Brown[1§]

[1]Chronobiology and Sleep Research Section, University of Zurich; [2]Neuromorphology Section; Institute of Pharmacology and Toxicology, University of Zurich; [3]Functional Genomics Center Zurich (FGCZ), University of Zurich

[§]Correspondance to:

Dr. Shiva K. Tyagarajan and Dr. Steven Brown and

Institute of Pharmacology and Toxicology, University of Zurich, Winterthurerstrasse 190, 8057 Zurich, Switzerland

Email: steven.brown@pharma.uzh.ch
tyagarajan@pharma.uzh.ch

Contribution of the first author

D. Mircsof designed and performed all biochemical experiments including synaptosomal preparation and RNA exteactions. All transcriptomic experiments and bioinformatics analysis were done by D. Mircsof with assistance of the Functional Genomics Center Zurich (FGCZ).

Abstract

Intrinsic circadian clocks allow organisms throughout the animal kingdom to synchronize their biology and behavior to the 24h light-dark changes and in humans, several observations link cognitive disorders to circadian rhythm anomalies. The molecular basis of memory and learning in the brain is thought to be a consequence of the phenomenon called as Long Term Potentiation (LTP) and Long Term Depression (LTD), causing constant remodeling of the synapse. This modification of the synapse induces short- and long lasting morphological and functional alterations at the synaptic entity and it has become clear, that these forms of synaptic plasticity require local protein synthesis. Recent findings have shown that, in dendritic processes, protein synthesis is operated on a small and localized scale directly next to the remodeling synapses. Over the last decades new techniques have greatly helped to better understand the process of local mRNA trafficking and the identification of synaptic transcripts in high spatial resolution. However, despite the recent progress in the identification of synaptic transcripts and RNA transport mechanism, little is know about the circadian regulation of mRNA transcripts at the synapse. Here, we describe the identification of circadian synaptic transcripts in the mouse brain. Next-generation sequencing has revealed totally 900 rhythmically expressed genes in the mouse brain and 180 rhythmic synaptic transcripts. Interestingly, both populations exhibit only a poor overlap, indicating that rhythmicity at the synapse is mainly driven independent of the nuclear transcriptional forward-feedback loop.

Introduction

A circadian rhythm is an endogenously driven pattern of behavior or physiology in an organism that repeats periodically approximately each day. Such patterns exist in organisms throughout evolution, from bacteria to plants and animals. In metazoans, the prototypical example of a behavior that demonstrates a circadian rhythm is the sleep-wake cycle, with its alternating intervals of activity and with restfulness that recur with a periodicity approximating the 24-hour day-night cycle. Not only do circadian rhythms govern sleeping patterns, but in mammals they also play a part in controlling body temperature, hormone secretion, blood pressure, metabolism, and

many other functions (*1*). Additionally, in humans several observations have link cognitive disorders to circadian rhythm anomalies (*2-7*).

Activity dependent synaptic changes are required for memory formation and storage in the brain described by the models of long-term potentiation (LTP) and long-term depression (LTD). A considerable aspect of this synaptic plasticity is determined postsynaptically by regulating the localization and the density of neurotransmitter receptors. It has now become evident that protein translation is required for the late phase of LTP and intermediate stages of LTD are dependent on new protein translation being independent of transcription. This compartmentalization between mRNA synthesis and translation of proteins, which are present in a repressed phase allows fast rapid local response to a certain stimuli. Trafficking of specific mRNA does not take place unattended, but accompanied by a whole set of proteins consisting of RNA-binding proteins, targeting specific mRNAs to the synapse.

Neurons, which are one of the main components in the brain of organisms exhibit a high degree of compartmentalization compared to other cell type, enabling fast signal processing. They are characterized by a soma, dendrites and synapses, and axonic processes which can be in the most extreme situations up to couple of meters long. Beside the rapid information propagation/transmission, this compartmentalization causes a significant biological hurdle in terms of protein transport. For example, synaptic molecules such as neurotransmitter receptors have to be first be synthesized in the soma, packaged in vesicles and transported along the dendrites using microtubules, sorted at branch point and finally integrated at site of interest.

The study of synaptic transcripts in neurons has been cumbersome for a very long time, mainly due to technical hurdles. However, over the last decades techniques such as Next-Generation Sequencing (NGS) and high-resolution in-situ analysis have greatly helped to better understand the process of local mRNA trafficking and the identification of synaptic transcripts. In a recent study, Schuman and coworkers have identified the transcriptome of the neuropil in the rat hippocampus combining microdissection (*8*), NGS and high-resolution in situ hybridization, yielding 2550 local transcripts. Within these genes, mRNA transcripts for proteins with known roles in

LTP/LTD such as calmodulin-dependent kinase IIα (CaMKIIα) or GABA receptors, have been identified, supporting the local protein synthesis model.

A circadian rhythm is an endogenously driven pattern of behavior or physiology in an organism that repeats periodically approximately each day and an increasing number of studies have demonstrated that alteration in the circadian system affect learning and memory. In Drosophila, the circadian clock controls daily changes in neuronal and synaptic structure (*9-12*). In zebrafish, induction and/or formation of long-term memory is modulated by a circadian clock and both learning and memory formation occur better during the day than during the night (*13*). In mice, circadian fluctuations are important for learning and memory by promoting learning-associated spine formation and elimination (*14*).

However, despite the recent progress in the identification of synaptic transcripts and RNA transport mechanism, little is know about the circadian regulation of mRNA transcripts at the synapse. Here, we describe the identification of circadian synaptic transcripts in the mouse brain using Next-generation sequencing.

Results

In a recent study it has been shown, that transmembrane proteins in synaptosomal preparation from rodent brain and in undisturbed synapses from brain slices highly correlate (*2*). To investigate the synaptic transcriptome, we established a protocol to isolate mRNA from synaptosomes. The successful isolation of synaptosomal mRNA from mouse brain was investigated biochemically by deep-sequencing showing enrichment for know genes such as CaMKIIα, GABRA2, Arc or Homer2 in synaptosomal compartment compared to total homogenate (see Study III). As expected, these results have been confirmed by qPCR analysis for GABRA2 and CamK2a mRNA, which showed 2-3 fold enrichment in synaptosomes compared to brain homogenate (see Study III). Additionally Neat1, a nuclear long-noncoding RNA was significantly reduced in the synaptosomal fraction, indicating a high quality purification procedure (see Study III).

As a next step, we have harvested mouse brain from animals under constant

darkness in a circadian fashion and subjected them to synaptosomal preparation. Total brain homogenate and synaptosomes were used to isolate mRNA and submitted to High-Throughput Sequencing and circadian expression of known core clock genes such as *Per1*, *Per2*, *Clock* and *Bmal* in total brain homogenate served as control for the successful circadian profile. Indeed, mRNA transcript levels of these genes were expressed in a rhythmic fashion, confirming circadian sampling and data processing (Figure 1A). To confirm successful isolation of synaptic components, transcript known to be enriched at synapse such as Kif5a and CaMKIIα were studied over the course of 24h showing constant high expression in synaptosomes (Figure 1B). Beta-Actin, which served as a marker for housekeeping gene, exhibits constant reduced expression levels in synaptosomes compared to total brain homogenate (Figure 1B).

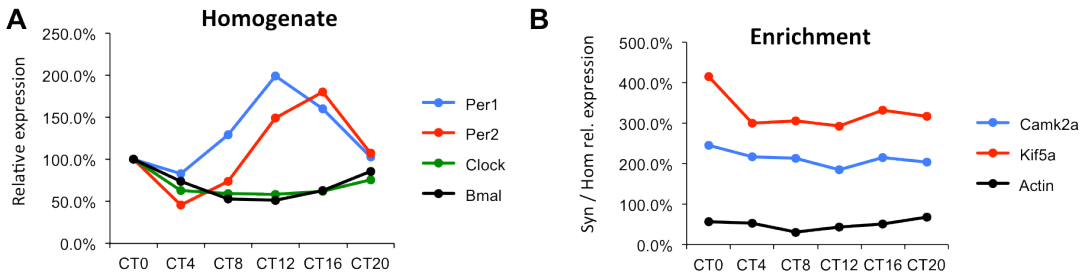

Figure 1. Circadian transcriptomic profile of clock genes and synaptic enriched genes around the clock. (A) Transcript level of circadian core clock genes Per1, Per2, Clock and Bmal at different circadian timepoints (CT) relative to CT0 in total mouse brain homogenate analyzed by High-Througput-Sequencing (HTS). (B) Enrichment of known synaptic localized transcript at CT0-CT20 in synpatosomes of the mouse brain compared to total homogenate. Actin is indicated as control. *n* = pool of 3 mice per time point.

To identify potential circadian fluctuations of mRNA at the synapse, it is important to separate circadian transcription from circadian transport or degradation of mRNA at the synapse. Ideally, constant transcript levels in the homogenate and circadian expression at the synapse would be indicative of such a phenomenon. Therefore, in a first step we have identified all the expressed genes in the mouse brain, which consisted of totally 13'050 genes. Next, to investigate genes with rhythmic expression, transcripts, which exhibit a maximum to minimum ratio of 1.5 during the period of 24h, were further considered for circadian expression (2826 genes). As a last step, this 2826 genes were further analyzed by JTK_CYCLE, a nonparametric

test for circadian expression, identifying totally 900 rhythmically expressed genes, which is 6.9% of totally expressed genes (Figure 2).

Secondly to identify rhythmic expressed synaptic transcripts, from the 13'050 expressed genes, we categorized mRNAs as enriched when they had an synaptosome/homogenate ratio of ≥1.5 and potentially rhythmic when they exhibit a amplitude-ratio (peak/trough) ≥1.5. Combining both tests, we have categorized 1307 genes, which were further submitted to analysis by JTK_CYCLE. From these genes, totally 180 have passed at least one of the statistical tests, representing synaptic enriched genes with circadian expression profile (Figure 2).

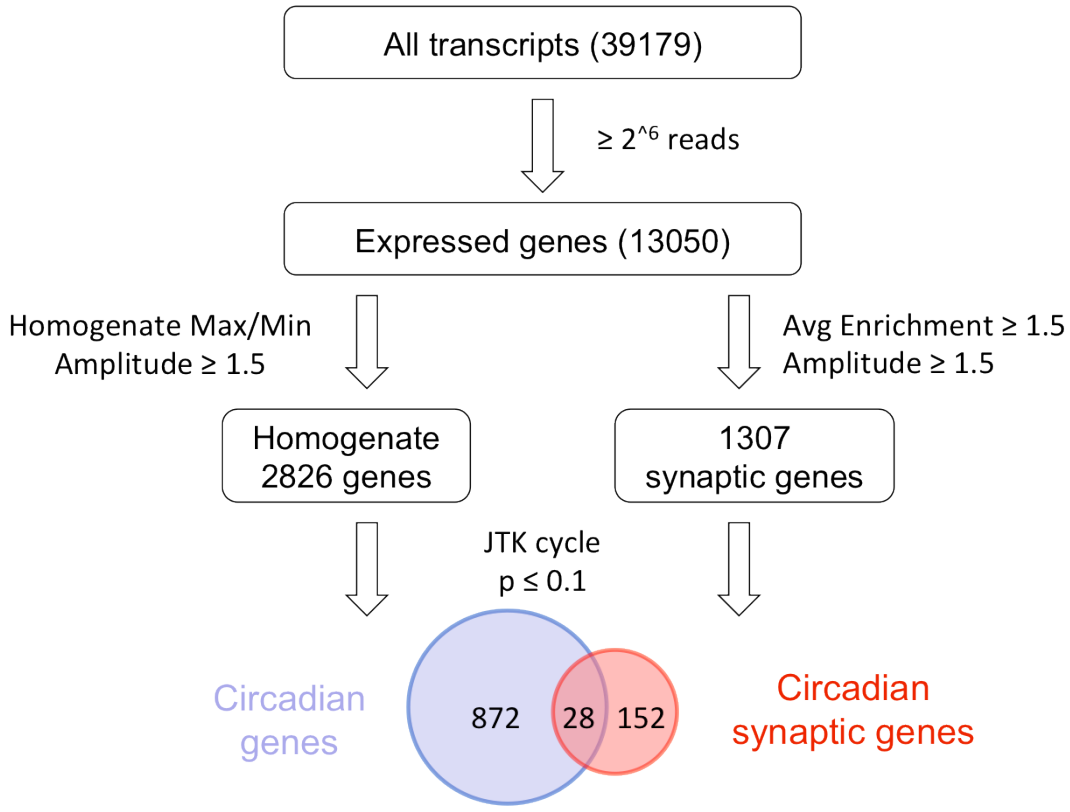

Figure 2. Flowchart of the identification of circadian synaptic genes.

Interestingly, the Venn diagram of those two categories shows only a poor overlap between circadian expressed genes in total brain tissue and synaptic enriched genes (Figure 2), indication that rhythmicity at the synapse is not driven by the main transcription translation feedback loop.

Visual selection of synaptic circadian expressed genes previously identified by the filtering method confirmed a circadian enrichment-profile, while transcript levels were constant in total homogenate. Among the identified genes, Tenascin C (Tnc), Glypican 2, cerebroglycan (GPC2), Adducin 3 (Add3) and Calcium-regulated heat stable protein 1 (Carhsp1) are potential candidates for the circadian transport of the mRNA (Figure 3).

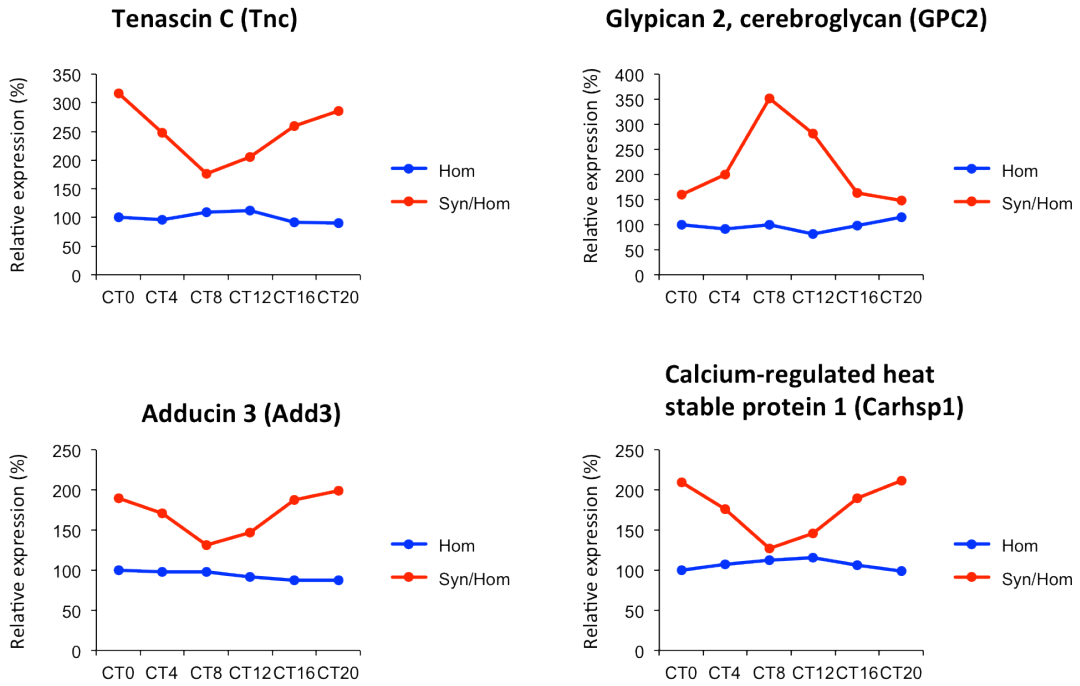

Figure 3. RNA-Seq expression plots for four examples of transcripts whose enrichment at the synapse is circadian while transcript levels are constant in total brain homogenate. Note that Glypica2 shows an inverted phase compared to Tenascin C, Adducin 3 or Calicium-regulated heat stable protein 1. *n* = pool of 3 mice per time point.

Discussion

The molecular mechanisms behind synaptic plasticity have not been completely characterized, but it become evident, that local protein synthesis in dendrites plays an important role. This compartmentalization between mRNA synthesis and translation of proteins allows fast rapid local response to a certain stimuli. Trafficking of specific mRNA does not take place unattended, but accompanied by a whole set of proteins consisting of RNA-binding proteins, targeting specific mRNAs to the synapse. While it has become clear, that a specific set of mRNA localizes to in

dendrites and synapses by a very dedicated RNA transport machinery, yet very little is known about the temporal resolution.

Here, we have identified transcripts, which in addition to their synaptic enrichment exhibit prominent circadian rhythmicity. Interestingly, among this identified transcripts, only 15.5% show rhythmicity in total brain extracts, indicating a mechanism, which mainly is driven independently by the circadian transcription of this transcripts. A plausible explanation for this phenomenon would be the circadian transport of mRNA from the soma along the microtubule to synapse. As a first step more research is needed to identity the proteins that bind these mRNA in the transport granule. Given the fact, that the identified transcripts show different circadian phase, probably different RNA transport granules might be involved at different circadian time points. Studies of RNA transport granule by Hirokawa and coworker have demonstrated a high complexity regarding protein composition (*15*). The analysis of RNA-transporting granules by gel electrophoresis and mass spectrometry revealed 42 proteins, some of them containing known RNA-binding properties like staufen, syncrip or DDX1/DDX3. Given the high complexity of these granules, the identification of mRNA composition remains still very challenging.

An alternative circadian mechanism, by which mRNA is regulated at the synapse would be the regulation of transcript stability. In mammals, mRNA localization and stability is highly regulated by its 3' untranslated region (UTR), especially by shortening of the poly(A) tail. For instance, poly adenyl binding protein (PABP) associates with the 3' end of mRNA to regulate polyadenylation and preventing the transcript from being degraded and therefore any factors that affect the rate of deadenylation will alter the half-life of the mRNA. One recently identified circadian deadenylase and potential target is Nocturnin (*16*). While the role of Nocturnin (*Noc*) has been extensively studied in peripheral processes such as lipid metabolism, adipogenesis, glucose homeostasis, inflammation and osteogenesis, however it's localization and role in the brain remains largely unknown.

Finally, there is increasing evidence that dendritic mRNA may be translationally silenced by miRNA in response to synaptic activity (*17*) and thereby promote the decay of their mRNA targets. A recent study by Gattfield and coworkers suggest, that

in hepatocytes miRNA targeted transcripts affect up to 30% of the rhythmic transcriptome (*18*). Given the fact, that miRNA's are highly expressed in the mammal brain, a similar mechanism might be involved in the regulation of rhythmic expression of synaptic transcripts. Besides of the molecular mechanism of circadian targeting of synaptic transcripts, the underlying physiological trigger remains largely elusive.

Material and Methods

Mice

All experiments were performed by using C57Bl6 adult wild type mice. Animal housing and experimental procedures are in agreement with veterinary law of the canton of Zurich. For circadian experiments, mice have been housed in constant darkness.

Synaptosome preparation

Synaptosomes have been prepared as described previously[45]. In brief, mouse brains were homogenized in 5 ml homogenization buffer (0.32 M sucrose, 1 mM EDTA pH 7.4, 1 mM dithiothreitol, phenylmethanesulfonyl fluoride solution (Sigma, 93482-50ML-F), complete mini-protease inhibitor (Roche Diagnostics) for 10 sec using a polytron. The homogenate was centrifuged at 1,000g for 10 min at 4 °C yielding the nuclear fraction (Nuc) and the supernatant (Sup). The supernatant was centrifuged at 31,000g for 5 min at 4°C using a discontinuous Percoll gradient. The layer between 3% and 10% of Percoll were collected, washed in 30 ml of homogenization buffer and further centrifuged at 22,000 × g for 15 min at 4°CT. The pellet was resuspended in lysis buffer for RNA extraction (GenElute Mammalian Total RNA Miniprep Kit, Sigma).

RNA extraction

RNA was extracted using a GenElute Mammalian Total RNA Miniprep Kit (Sigma, St Louis, MO, USA) according to the manufacturer's instructions. Total RNA was quantified by absorbance spectroscopy and RNA integrity and quality was assessed by 1.0% agarose gel electrophoresis

Transcriptome analysis

For transcriptome analysis using RNA-Seq, the quality of the isolated RNA was determined with a Qubit® (1.0) Fluorometer (Life Technologies, California, USA) and a Bioanalyzer 2100 (Agilent, Waldbronn, Germany). RNAs were then processed using The TruSeq Stranded mRNA Sample Prep Kit (Illumina, Inc, California, USA) according to the manufacturer recommendations. The TruSeq SR Cluster Kit v3-cBot-HS or TruSeq PE Cluster Kit v3-cBot-HS (Illumina, Inc, California, USA) was used for cluster generation using 8 pM of pooled normalized libraries on the cBOT. Sequencing was performed on a Illumina HiSeq 2000 system using the TruSeq SBS Kit v3-HS (Illumina, Inc, California, USA) with paired end 2 X100 reads or single end 1X100 reads.

RNA-seq reads were quality-checked with fastqc which computes various quality metrics for the raw reads. Reads were aligned to the genome and transcriptome with tophat v 1.3.3. Before mapping the low quality ends of the reads were clipped (3 bases from the read start and 10 bases from the read end). Tophat was run with default options. The fragment length parameter was set to 100 bases with a standard deviation of 100 bases. Based on these alignments the distribution of the reads across genomic features was assessed.Isoform expression was quantified with the RSEM algorithm (http://www.biomedcentral.com/1471-2105/12/323) with the option for estimation of the read start position distribution turned on.

For rhythmicity detection in transcript profiles we used a non-parametric test, JTK_CYCLE (Hughes et al., 2010).

References

1. Gachon, F., Nagoshi, E., Brown, S.A., Ripperger, J. & Schibler, U. The mammalian circadian timing system: from gene expression to physiology. *Chromosoma* **113**, 103-12 (2004).
2. Wilhelm, B.G. *et al.* Composition of isolated synaptic boutons reveals the amounts of vesicle trafficking proteins. *Science* **344**, 1023-8 (2014).
3. Nir, I. *et al.* Brief report: circadian melatonin, thyroid-stimulating hormone, prolactin, and cortisol levels in serum of young adults with autism. *J Autism Dev Disord* **25**, 641-54 (1995).
4. Kulman, L. While diet docs debate fats and carbs, weight loss still comes down to calories. *US News World Rep* **128**, 56 (2000).
5. Kulman, G. *et al.* Evidence of pineal endocrine hypofunction in autistic children. *Neuro Endocrinol Lett* **21**, 31-34 (2000).
6. Tordjman, S., Anderson, G.M., Pichard, N., Charbuy, H. & Touitou, Y. Nocturnal excretion of 6-sulphatoxymelatonin in children and adolescents with autistic disorder. *Biol Psychiatry* **57**, 134-8 (2005).
7. Melke, J. *et al.* Abnormal melatonin synthesis in autism spectrum disorders. *Mol Psychiatry* **13**, 90-8 (2008).
8. Cajigas, I.J. *et al.* The local transcriptome in the synaptic neuropil revealed by deep sequencing and high-resolution imaging. *Neuron* **74**, 453-66 (2012).
9. Mehnert, K.I. *et al.* Circadian changes in Drosophila motor terminals. *Dev Neurobiol* **67**, 415-21 (2007).
10. Fernandez, M.P., Berni, J. & Ceriani, M.F. Circadian remodeling of neuronal circuits involved in rhythmic behavior. *PLoS Biol* **6**, e69 (2008).
11. Pyza, E. & Gorska-Andrzejak, J. External and internal inputs affecting plasticity of dendrites and axons of the fly's neurons. *Acta Neurobiol Exp (Wars)* **68**, 322-33 (2008).
12. Damulewicz, M. & Pyza, E. The clock input to the first optic neuropil of Drosophila melanogaster expressing neuronal circadian plasticity. *PLoS One* **6**, e21258 (2011).
13. Rawashdeh, O., de Borsetti, N.H., Roman, G. & Cahill, G.M. Melatonin suppresses nighttime memory formation in zebrafish. *Science* **318**, 1144-6 (2007).

14. Liston, C. *et al.* Circadian glucocorticoid oscillations promote learning-dependent synapse formation and maintenance. *Nat Neurosci* **16**, 698-705 (2013).
15. Kanai, Y., Dohmae, N. & Hirokawa, N. Kinesin transports RNA: isolation and characterization of an RNA-transporting granule. *Neuron* **43**, 513-25 (2004).
16. Stubblefield, J.J., Terrien, J. & Green, C.B. Nocturnin: at the crossroads of clocks and metabolism. *Trends Endocrinol Metab* **23**, 326-33 (2012).
17. Nalavadi, V.C., Muddashetty, R.S., Gross, C. & Bassell, G.J. Dephosphorylation-induced ubiquitination and degradation of FMRP in dendrites: a role in immediate early mGluR-stimulated translation. *J Neurosci* **32**, 2582-7 (2012).
18. Du, N.H., Arpat, A.B., De Matos, M. & Gatfield, D. MicroRNAs shape circadian hepatic gene expression on a transcriptome-wide scale. *Elife* **3**, e02510 (2014).

STUDY II: The Role of DBHS Proteins in Regulating Inhibitory Synapse Structure and Function

D. Mircsof[1,2], M. Žnidarič[1], K. Airich[2], S. Nakagawa[3], J.-M. Fritschy[2], S. A. Brown[1§], S. K. Tyagarajan[2§]

[1]Chronobiology and Sleep Research Section; [3]Neuromorphology Section; Institute of Pharmacology and Toxicology, University of Zurich; Switzerland

[3]RNA Biology Laboratory, RIKEN Advanced Research Institute, Wako, Saitama 351-0198, Japan

[§]Correspondance to:

Dr. Steven A. Brown and Dr. Shiva K. Tyagarajan

Institute of Pharmacology and Toxicology, University of Zurich, Winterthurerstrasse 190, 8057 Zurich, Switzerland

Email: tyagarajan@pharma.uzh.ch
steven.brown@pharma.uzh.ch

Contribution of the first author

D. Mircsof designed and performed all biochemical and morphological experiments with assistance of M. Žnidarič and K. Airich.

Abstract

Subcellular localization of mRNAs plays an important role for regulation of local protein synthesis, especially in the context of development and neuronal plasticity. In recent years specialized RNA-binding proteins have been identified and functionally characterized such DBHS proteins, consisting of three homologous proteins NONO, PSPC1 and SFPQ, each of which contains two RNA recognition motifs (RRMs). DBHS proteins are nuclear proteins forming homo- and heterodimers in vivo, and have been previously described in various aspects of RNA production such as transcriptional activation and repression, splicing, pre-mRNA processing and RNA transport in neurons and other cell types. Additionally, they are major components of nuclear paraspeckles, where they associate with the long noncoding RNA *Neat1* which have been recognized as nuclear RNA-holding structures for edited RNAs. While the role of DBHS proteins in transcriptional regulation is known, its function in regulating synaptic morphology and function is up to now unclear. Here we demonstrate, that overexpression of all three NOPS proteins alters synaptic structure in primary neurons and mutations in its RNA recognition site have the opposite effect upon gephyrin clustering. Additionally, the RNA binding proteins NONO and PSPC1 are highly expressed in the mouse hippocampal pyramidal neurons and dentate gyrus, where they particularly affect inhibitory synapse morphology by regulation the postsynaptic scaffolding molecule gephyrin as well as the GABRA2 receptor. Furthermore, examination of GABAergic synaptic structure in Neat1 knockout mice showed strong increase in numerical density of gephyrin as well as GABAA receptor alpha2 clusters in in the CA3 region of the hippocampus. Transcriptional analysis of the hippocampus of NONO and PSPC1 deficient mice showed specific regulation of the GABA receptor alpha2 subunit transcript in a circadian fashion. However, we were unable to trace these changes in transcription in Neat1 deficient neurons. Concluding, this study demonstrates the involvement of the DBHS protein family in inhibitory synaptic biology and suggests new role for paraspeckles, a nuclear sub-compartment, which is built on the long-nocoding RNA Neat1.

Introduction

Activity dependent synaptic changes are required for memory formation and storage in the brain described by the models of long-term potentiation (LTP) and long-term depression (LTD) (*1*). A considerable aspect of this synaptic plasticity is determined postsynaptically by regulating the localization and the density of neurotransmitter receptors. It has now become evident that protein translation is required for the late phase of LTP and intermediate stages of LTD are dependent on new protein translation being independent of transcription (*2*). This compartmentalization between mRNA synthesis and translation of proteins, which are present in a repressed phase allows fast rapid local response to a certain stimuli.

The ability of mRNAs to move in the cytoplasm of eukaryotic cells is essential for sorting sites of synthesis for specific proteins. Studies analysing the mechanisms of mRNA localization have demonstrated the existence of complex mRNA transport systems (*3*). These and other studies have provided strong support for the idea that localized mRNAs are actively transported on cytoskeletal filaments. Two components of such RNA transport granules are NONO and SFPQ, members of the NOPS family of RNA-binding proteins (*4*). This family consists of three homologous proteins NONO, PSPC1 and SFPQ, each of which contains two RNA recognition motifs (RRMs) (*5-7*). NONO (also known as p54nrb in humans) has been shown to regulate a variety of processes which include transcriptional activation and repression (*8-10*), pre-RNA processing(*11-13*), and RNA transport (*4*). For example, it has been shown to regulate the transcriptional activation of the TORC family of growth and metabolic factors (*8*). In an apparently unrelated nuclear function, it also mediates the nuclear retention of edited RNAs in nuclear paraspeckles, RNA holding structures (*14, 15*). These structures contain the related factors NONO, SFPQ, and PSPC1, as well as the noncoding scaffolding RNA Neat1 (*6, 14-20*). In addition, they have been found to play an important role in the circadian clock, where they might act as transcription factors (*21*). While the role of NONO and other DBHS proteins in transcription and circadian clock regulation is known, its function in synapse morphology and function is up to now unclear.

An important component of the macromolecular complex at inhibitory synapses is Gephyrin, a highly conserved multifunctional protein also responsible for molybdenum cofactor synthesis (*22*). In neurons Gephyrin is found co-localizing exclusively with GABAergic and glycinergic synapses and loss of Gephyrin expression results in a loss of GABAergic synaptic transmission. (*23, 24*) While direct interaction between gephyrin and glycine receptor beta subunit is well established, direct interaction with GABAA receptor subunit is except for the alpha2 subunit still unclear. Many gephyrin interacting protein have been identified, that includes some of the prominent members of the cytoskeleton binding proteins.

A previous study (Mircsof et al.) has shown that shown, that NONO regulates inhibitory synaptic biology. To better understand the underlying mechanism, in this study we investigated the role of DBHS proteins and nuclear paraspeckles on inhibitory synaptic morphology. Mechanistically, over-expression of DBHS proteins in primary rat neurons induced changes in the numeric density of gephyrin in a RNA motif dependent manner.

Results

NONO and PSPC1 are highly expressed in the nucleus of pyramidal cells and granule cells of the mouse hippocampus

To study the distribution and localization of NONO and PSPC1 protein in the mouse brain, immunohistochemical staining were performed using antibodies validated using tissues lacking NONO or PSPC1 respectively (Supplementary Fig. 1) By immunofluorescence, NONO and PSPC1 were detected widely in brain including hippocampus and cortex (Figure 1C). Expression for NONO as well as PSCP1 was detected most strongly in the nucleus of NeuN positive neurons in CA1 and CA3 pyramidal neurons and in granule cells of the dentate gyrus, which exhibited high levels. Additionally NONO and PSPC1 positive cells were also detected sparsely in CA1 and CA3 *Stratum radiale* and *Stratum oriens*, which were positive for NeuN. In the neocortex, NONO and PSPC1 were again most strongly expressed by neurons, particularly in layer II/III and V showing selective expression in NeuN but not GFAP

positive cells. However, NONO immunofluorescence was also detected in layer I of the cortex which were NeuN and GFAP negative, which resemble most likely oligodendrocytes (Figure 1B). Finally, morphological analysis of NONO and PSPC1 distribution show complete colocalization between both proteins (Figure 1C). Altogether, its cellular localization and expression profile indicate that NONO and PSPC1 operate mainly in neurons of CA1 and CA3 pyramidal cells and dentate gyrus granule cells of the hippocampus.

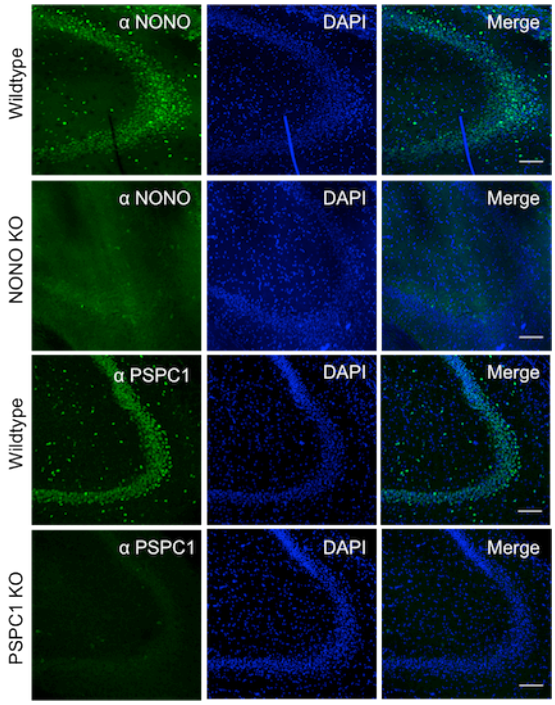

Supplementary Figure 1: Immunofluorescence labeling of NONO in wildtype NONO knockout (bottom) mouse coronal brain sections and PSPC1 in wildtype PSCP1 knockout (bottom) mouse coronal brain sections in CA3 region of the hippocampus. Scale bar = 100µm.

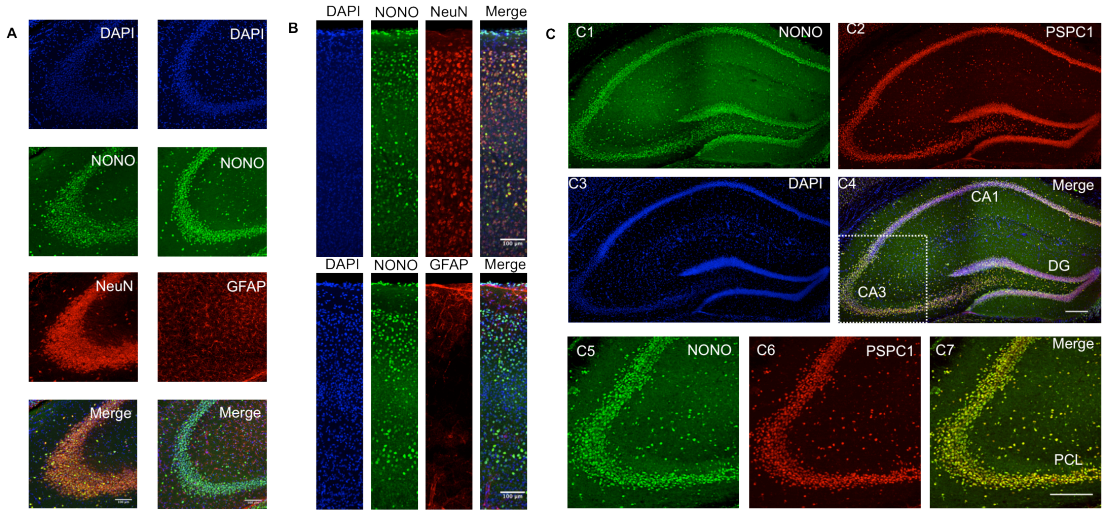

Figure 1.Cell type and layer-specific localization of NONO and PSPC1 in mouse brain. (**A**) Staining of hippocampal cell nuclei by DAPI (blue), anti-NONO (green), and neuron-specific anti-NeuN or astrocyte-specific anti-GFAP (red, left or right column respectively). (**B**) Identical staining of cortex Scale bar 100µm (**C**) Immunofluorescence labeling of NONO (green) and PSPC1 (red) in wildtype mouse coronal brain sections of the hippocampus. NONO and PSPC1 show strong immunoreactivity of principal neurons of the pyramidal cell layer (PCL) and the dentate gyrus (DG). (C5-7) Magnification of CA3 region of the mouse hippocampus labeled for NONO and PSCP1. Scale bar 200µm.

DBHS protein regulates inhibitory synapse structure by the RNA binding domain

Because of the involvement of the NOPS family of proteins in RNA transport in neurons and because they formed specific RNA holding structures in the nucleus, we guessed that these proteins might play a role in postsynaptic structure, perhaps through regulated RNA transport. To investigate whether these proteins might play a specific role in dendritic structure, we focused on gephyrin, which is a major scaffolding protein at inhibitory synapses in the CNS. Previous research has shown, that overexpression of the inhibitory scaffolding gephyrin in primay rat neurons localizes to endogenous postsynaptic inhibitory sites and does not affect morphological or functional properties of the transfected cell, thus enabling the use of GFP tagged gephyrin as an inhibitory marker (*89*).

To better understand the role of DBHS protein regulating inhibitory synapse structure, vectors expressing mCherry tagged DBHS proteins were co-transfected into cultured primary rat hippocampal neurons together with eGFP-tagged gephyrin at 8 days in vitro (DIV8). Postsynaptic gephyrin clusters were identified by

immunofluorescence staining to directly visualize and quantify the distribution of gephyrin clusters 7 days later (DIV8+7) on the basis of colocalization with presynaptic vGAT. Analysis of gephyrin clusters in dendrites of cells expressing mCherry-NONO and mCherry-SFPQ showed significant increase in eGFP-gephyrin density compared to eGFP-gephyrin transfected neurons, while overexpression of mCherry-PSCP1 significantly reduced eGFP-gephyrin density (Figure 2).

Hirokawa and co-workers have shown, that NOPS proteins bind RNA using their RNA recognition motif (RRM) and regulate mRNA localization (*134*) and thereby potentially regulate inhibitory morphology through their RRM motif. To answer this hypothesis, DBHS constructs containing 4 point mutations in their RNA recognition motif, disrupting RNA binding, were co-expressed with GFP-Gephyrin in analogy to the previously described assay. Interestingly, over expression of the mutated DBHS constructs had the opposite effect on gephyrin density as it has been show for the wildtype construct (Figure 2). This results suggest, that gehpyrin oligomerization at inhibitory synapse is regulated by the RNA binding property of the DBHS proteins.

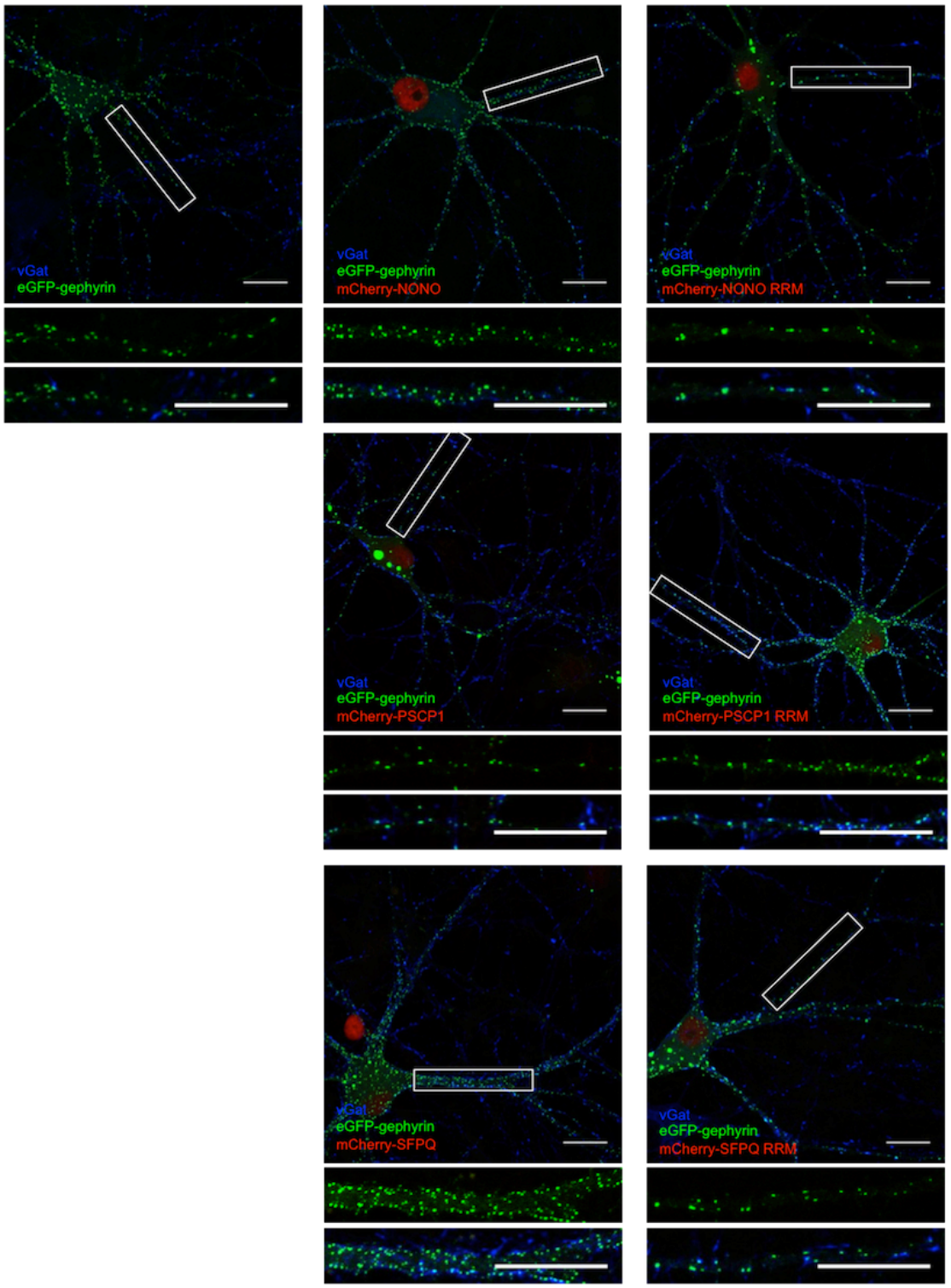

Figure 2. Primary hippocampal rat neurons expressing control GFP-gephyrin alone, or co-expressed with myc-DBHS proteins, or co-expressed with RNA binding-deficient myc-DBHS-RRM. Boxed region is magnified beneath. Postsynaptic clustering is demonstrated by apposition of eGFP-gephyrin clusters (green) to vGat -positive terminals (blue). Scale bar 20µm.

GABRA2 and gephyrin cluster densitiy are reduced in the hippocampus of NONO knockout mice

To investigate whether NONO proteins plays a specific role in dendritic inhibitory structure in-vivo, cytological studies were performed using antibodies against native gephyrin and GABA-A Receptor α2 subunit of brain sections from wildtype, NONO and PSPC1 deficient mice. The CA3 area of the hippocampus is a brain region with distinct synapse distribution conditional to specific layers. For our confocal images we decided to analyse the strata radiatum, because other regions with high density of clusters precluded determining their numbers. Analysis in the CA3 region of the hippocampus showed, that gephyrin and GABA-A Receptor α2 subunit as postsynaptic markers are significantly reduced (30.7% and 35.1% respectively) in NONO KO mice while PSCP1 deficient neurons show significant increased gephyrin (39.1%) and GABAAR α2 (12.3%) density (Figure 3 and 4). Size of synaptic gephyrin and GABA-A Receptor α2 subunit were however not affected by NONO or PSPC1 deficiency (Figure 3 and 4). In general, vGAT positive terminals in the Hippocampus could be shown to be distributed around pyramidal cells, however throughout the examined brain regions vGAT staining was found to be inconsistent, suggesting weak antibody-stability.

Both ribonucleoproteins NONO and PSPC1 are a part of the nuclear sub-structure called paraspeckle, which are built on the long non coding RNA (lncRNA) NEAT1. To test the hypothesis, that this specific structure is involved in inhibitory morphology, we performed immunohistological studies of brain sections from wildtype and Neat1 deficient mice, using antibodies against the GABA-A Receptor α2 subunit, as well as the synaptic scaffolding protein gephyrin as previously described. Interestingly, hippocampi from Neat1 deficient mice showed a significant increase in the numeric density of the inhibitory marker gephyrin (40.2%) and GABA-A Receptor α2 subunit (23.6%) (Figure 5). Again, the average cluster size of these markers was not affected in Neat1 deficient mice compared to wildtype littermates (Figure 5). Overall analysis of gephyrin, GABA-A Receptor α2 subunit and vGAT immunoreactivity expressed in the GABAergic interneurons in the CA3 layer of the hippocampus regions revealed that paraspeckle depletion causes profound reduction of gephyrin and GABAAR α2 clustering at postsynaptic sites.

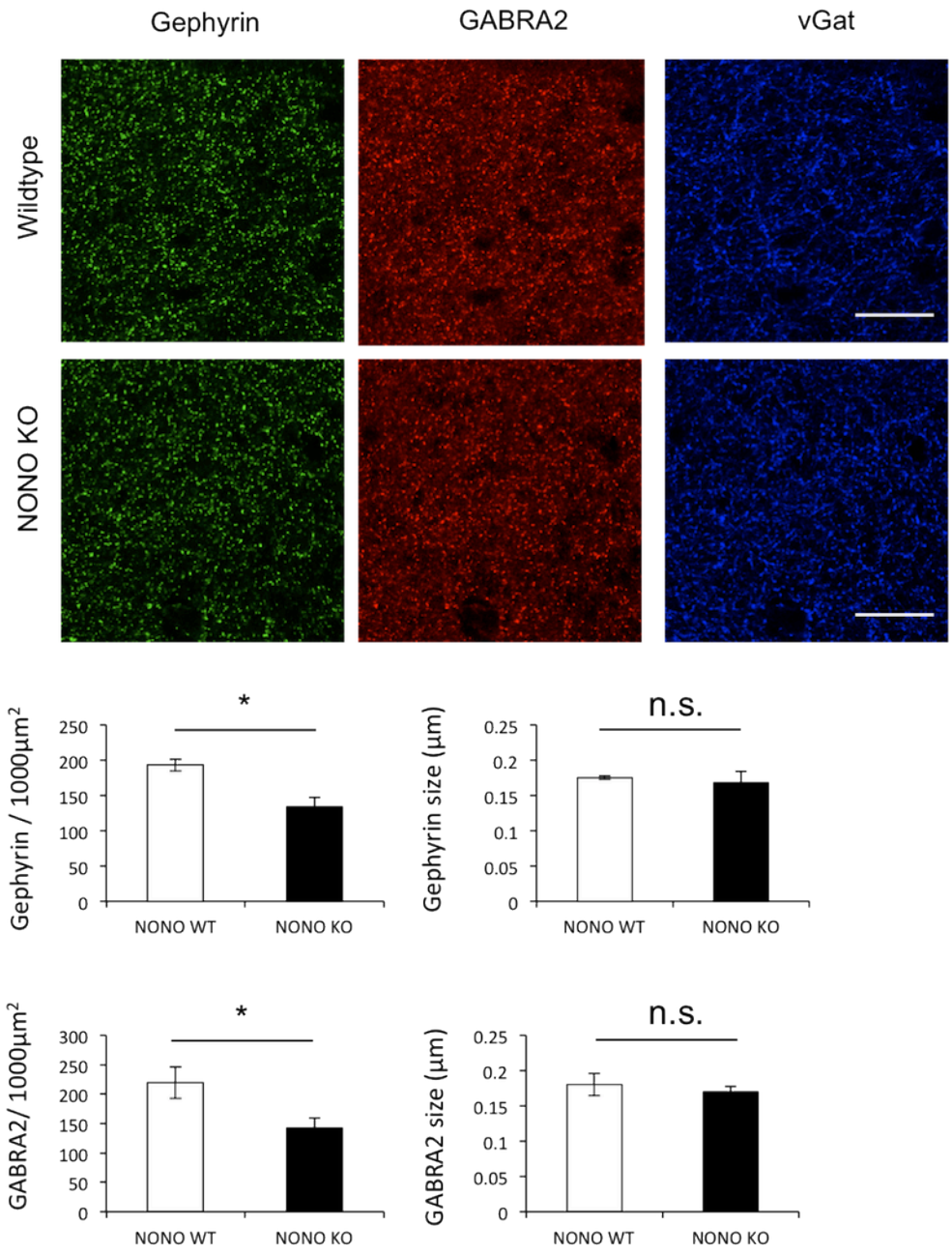

Figure 3. **Effects of NONO deficiency upon synaptic biology.** Immunohistochemical staining for inhibitory postsynaptic marker gephyrin (green), GABA type II receptor (red), and the presynaptic marker vGat (blue) in wildtype and NONO KO mice in the stratum radiatum CA3 of the hippocampus (top). Scale bar 25µm. Quantification of gephyrin and GABA type II receptor density (left) and cluster size (right). Means ± SD are shown, $^{*}P < 0.05$ using Student's *t*-test (top). *n* = 3 mice per genotype

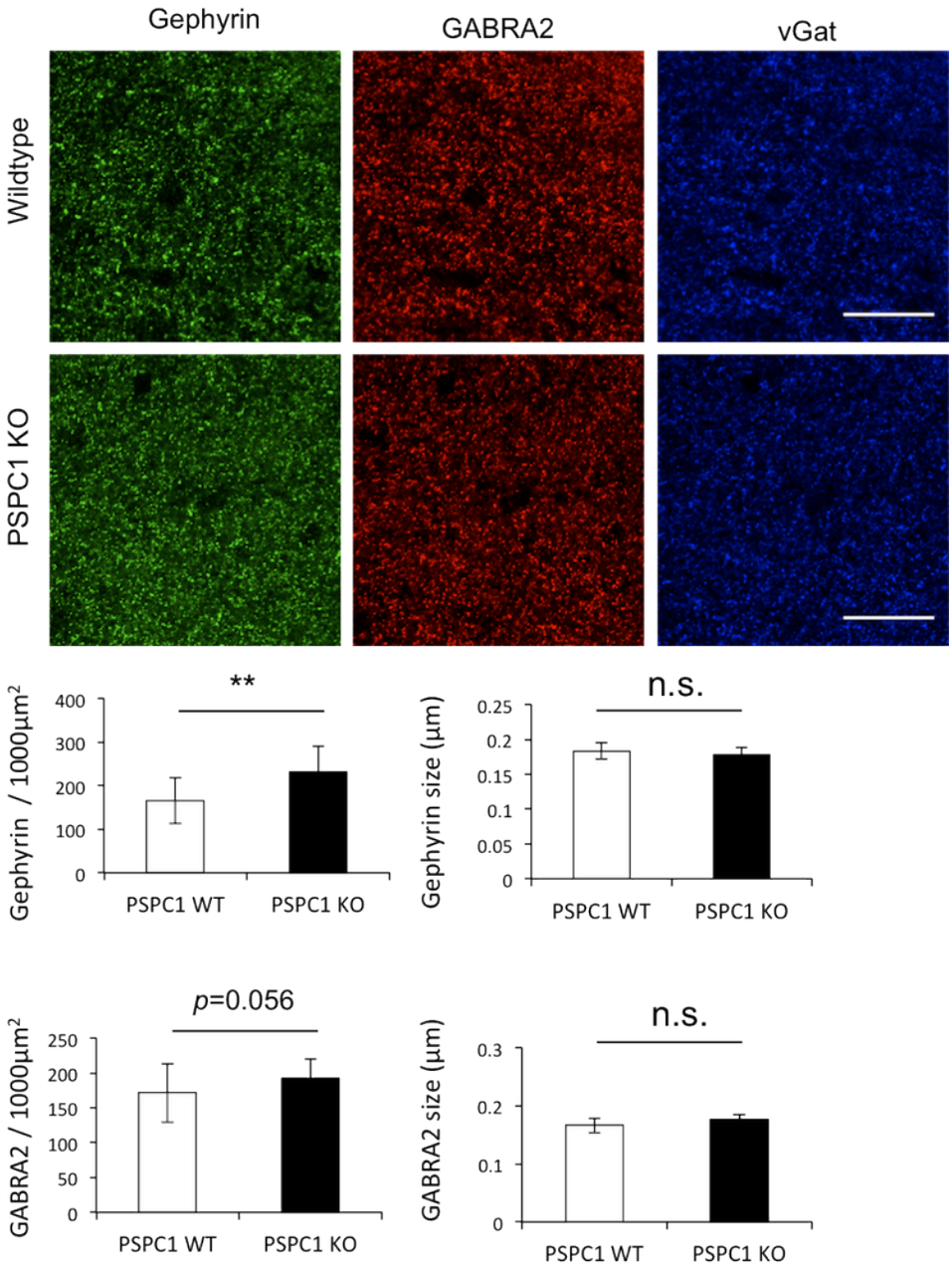

Figure 4. **Effects of PSPC1 deficiency upon synaptic biology.** Immunohistochemical staining for inhibitory postsynaptic marker gephyrin (green), GABA type II receptor (red), and the presynaptic marker vGat (blue) in wildtype and PSPC1 KO mice in the stratum radiatum CA3 of the hippocampus (top). Scale bar 25µm. Quantification of gephyrin and GABA type II receptor density (left) and cluster size (right). Means ± SD are shown, $^{**}P < 0.005$ using Student's *t*-test (top). *n* = 3 mice per genotype.

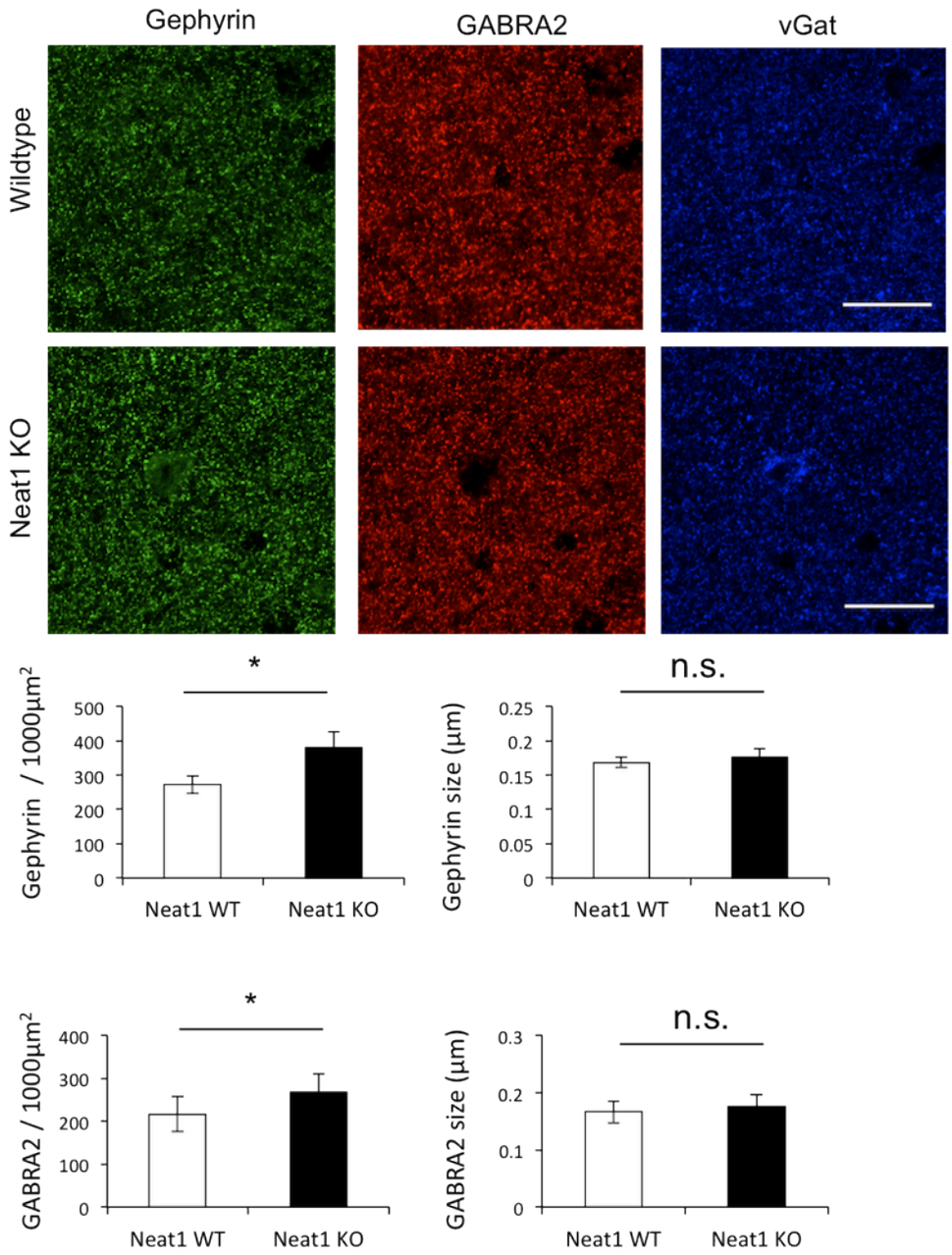

Figure 5. **Effects of Neat1 deficiency upon synaptic biology.** Immunohistochemical staining for inhibitory postsynaptic marker gephyrin (green), GABA type II receptor (red), and the presynaptic marker vGat (blue) in wildtype and Neat1 KO mice in the stratum radiatum CA3 of the hippocampus (top). Scale bar 25µm. Quantification of gephyrin and GABA type II receptor density (left) and cluster size (right). Means ± SD are shown, $^{*}P < 0.05$ using Student's *t*-test (top). *n* = 3 mice per genotype.

NONO and PSPC1 regulate GABRA2 mRNA levels in-vivo

Since DBHS proteins have been described in transcriptional regulation (*113, 115, 154*) as well as the circadian clock (*91*), it is essential to separate these two processes. For this, we have investigated the transcription of GABAergic synaptic components in

mouse brain around the clock. For this, wildtype mouse brains were harvested over the period of 24h in constant dark conditions and inhibitory transcripts were analyzed by qPCR. Transcription profiles of key GABAergic regulatory molecules revealed that GABA-A Receptor α2 subunit was expressed in a circadian fashion (p=0.016), while GABAAR α1 (p=0.82), Collybistin (p=0.1) or Gephyrin (p=0.33) showed significant alterations (Figure 6).

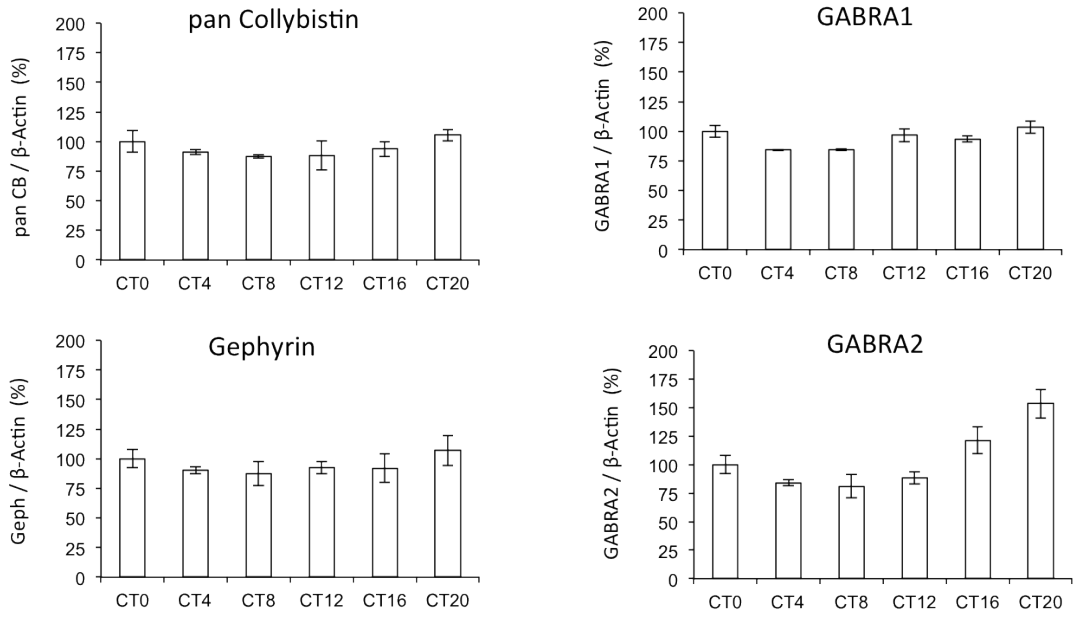

Figure 6. Expression analysis of inhibitory synaptic components around the clock. mRNA expression profile for inhibitory synaptic gene components at circadian timepoint (CT) 0-20 by RT-PCR. Gene expression levels were normalized to beta-Actin and CT0. *n* = 3 mice per genotype. Means ± SD are shown.

Thus, we further focused on the expression levels of these molecules at circadian timepoints (CT) 10 and 22, since GABA-A Receptor α2 peaked at these timepoints. Again, components of GABAergic inhibitory synapses such as gephyrin, collybistin and GABRA2 were compared in wildtype, NONO and PSPC1 deficient hippocampi. Transcriptional analysis showed, that gephyrin, collybistin and GABRA1 was not affected in NONO and PSPC1 deficient neurons (Supplementary Figure 2).

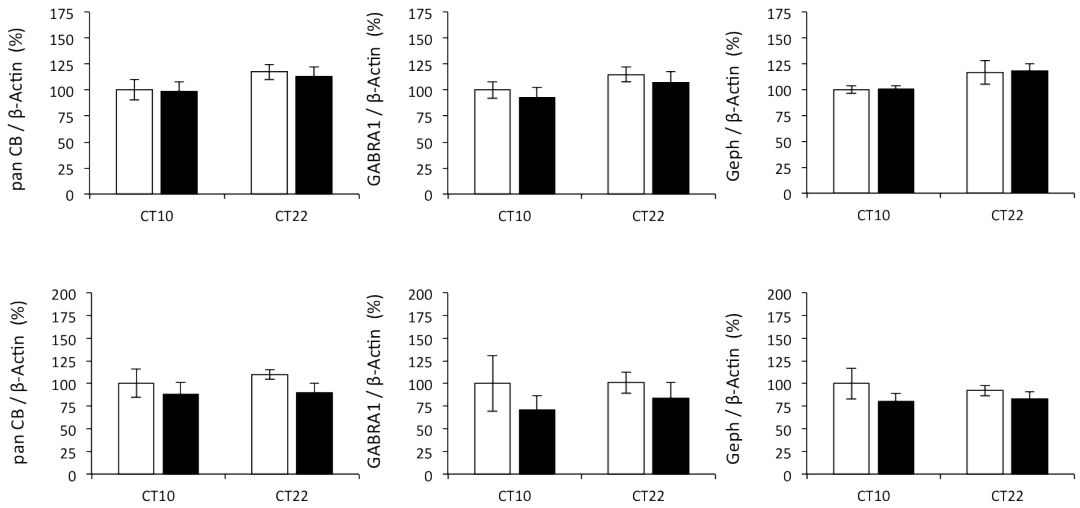

Supplementary Figure 2: mRNA expression profile for inhibitory synaptic gene components at circadian timepoint (CT) 10 and 20 by RT-PCR in wildtype (white), NONO knockout (top, black) and PSPC1 knockout (black, bottom) hippocampal samples. Gene expression levels were normalized to beta-Actin and CT10. Means ± SD are shown. *n* = 3 mice per genotype

Analysis of GABRA2 transcript levels at CT10 and CT22 showed significant differences as expected from the previous circadian profile. Interestingly, mice lacking NONO, showed a striking reduction of GABRA2 at both circadian timepoints, while PSCP1 depleted hippocampi showed a significant increase at CT10 but not at CT10 (Figure 7), indicating a possible role of PSPC1 but not NONO in the circadian transcription of GABRA2. Since the morphological inhibitory synaptic defects could potentially created/generated by disturbed transcription of the the GABA-A Receptor α2 subunit, we tested GABRA2 mRNA levels in Neat1 deficient mice as previously described. Unfortunately, qPCR analysis could not identify any significant differences of GABRA2 levels between wildtype and Neat1 KO mice (Figure 7), indicating a more complex underlying mechanism. However, it has to be noted, that GABRA2 mRNA levels did not change significantly between CT10 and CT22 as previously expected.

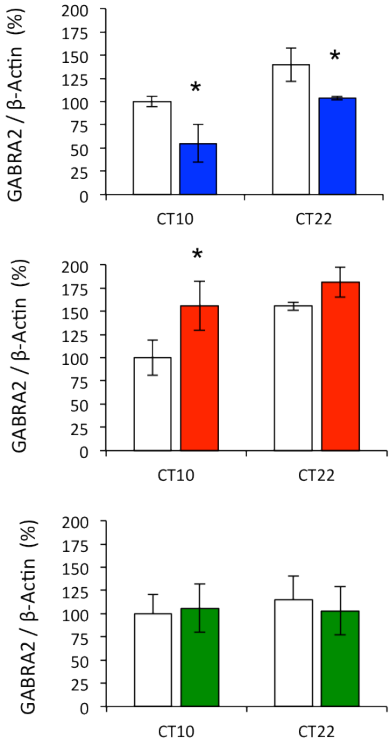

Figure 7. GRABR2 mRNA expression levels in the mouse hippocampus. Quantification of GABRA mRNA levels in the mouse hippocampus in wildtype (white), NONO knockout (blue), PSPC1 knockout (red) and Neat1 knockout (green) mice by RT-PCR at circadian timepoint (CT) 10 and 22. GABRA2 expression levels were normalized to beta-Actin and CT10. Means ± SD are shown, $^{*}P < 0.05$ using Student's *t*-test (top). *n* = 3 mice per genotype

Discussion

While the role of DBHS proteins in transcriptional regulation is known, its function in regulating synaptic morphology and function is up to now unclear. Here, we have demonstrated the involvement of thes proteins in inhibitory morphology and postulate a new function for nuclear paraspeckles. NONO and PSCP1 are highly expressed in neurons of the mouse hippocampus und modulate clustering of GABA-A Receptor α2 subunit as well as gephyrin, a key scaffolding molecule at inhibitory synapse. NONO and SFPQ, another DBHS protein family member, together with PSP1, localize to so called nuclear paraspeckles (*14, 15, 17-19, 26*). These ribonucleoprotein structures, built on the long non-coding RNA (lncRNA) NEAT1 and elimination of Neat1 leads to the disruption of paraspeckles (*14, 18-20*).

To support the hypothesis, that DBHS modulate inhibitory synaptic structure by their localization to paraspeckles, our immunocytological studies show, that elimination of the essential paraspeckle component Neat1 leads to increased gephyrin and GABA-A Receptor α2 subunit density in analogy to PSPC1 deficient neuron. Additionally, while NONO depletion lead to reduced GABRA2 mRNA levels, PSPC1 deficiency

shows the opposite effect. This phenomenon could be explained by two hypothetical models which have been previously demonstrated for the DBHS proteins: In the first case, both NONO and PSCP1 compete as negative transcription factors with different repressive potentials for GABRA2 repression, in which NONO would be a weaker repressor compared to PSPC1 (*8, 27, 28*). In a second model, NONO would act as a positive transcription factor, while PSPC1 inhibits the transcription of GABRA2 (*9, 29-31*).

In contrast to NONO and PSPC1 KO mice, Neat1 knockout mice did not show transcriptional deregulation of GABRA2 mRNA levels in the hippocampus, indication that both NONO/PSCP1 might affect GABRA2 levels independently of the paraspeckle. However, recent studies added a new layer of complexity taking the nubnuclear localization of DBHS proteins into account (*32, 33*). In this model, the fraction of DBHS proteins bound to paraspeckles through Neat1 and nucleoplasmic DBHS proteins are in homeostasis. For example, disruption of Neat1 leads to significant increase of freely available DBHS proteins and thereby might enhance gene transcription by promoter binding.

Therefore, we hypothesize that mechanistically nuclear enriched Neat1 regulates either synaptic gene expression and/or retention by modulating the differential association or activity of DBHS proteins from promoter regions to paraspeckles. In order to distinguish translation and nuclear retention, gene expression analysis in nuclear as well as synaptosomal fractions of NONO, PSPC1 and Neat1 deficient mouse brains should shed light into this open question.

Previous studies have shown a strong association of the hippocampus and the inhibitory system in memory and anxiety (*34*). Considering the strong expression of NONO and PSPC1 in the mouse hippocampus, where they regulate GABAergic inhibitory morphology additional functional studies by electrophysiology as well as behavioral can help to better understand the functional implication of paraspeckles in the brain.

Material and Methods

Plasmids

The eGFP–gephyrin P1 variant has been described previously (Lardi-Studler et al., 2007). Overexpression of myc-DBHS and myc-DBHS RRM, were conducted using the plasmids described in Kuwahara et al.

Cell culture

Primary hippocampal neuron cultures were prepared as described previously (Buerli et al., 2007). Hippocampal cultures were transfected with 0.5 µg of either eGFP–gephyrin or the specific myc–NONO construct according to the protocol described previously (Buerli et al., 2007). Cells were transfected after 8 DIV and processed for immunofluorescence 7 days later (referred to as 8+7 DIV). In co-transfection experiments the total DNA concentration was maintained at 1.5 µg.

Mice

Generation of NONO and Neat1 knockout mice was described previously in. (*139, 163*). Chimeric mice were obtained from PSPC1gt ES cells (C57Bl6 genotype) via standard blastocyst injection into SV129 mice by the University of California, Davis. Individual chimeric mice were back-crossed 4–10 generations against C57Bl6 All experiments were performed by comparing adult wild type and mutant littermates (2-3 months old). Animal housing and experimental procedures are in agreement with veterinary law of the canton of Zurich. For circadian experiments, mice have been housed in constant darkness.

RNA extraction and quantitative real-time PCR analysis

RNA was extracted using a GenElute Mammalian Total RNA Miniprep Kit (Sigma, St Louis, MO, USA) according to the manufacturer's instructions. Total RNA was quantified by absorbance spectroscopy and RNA integrity and quality was assessed by 1.0% agarose gel electrophoresis. Total RNA (1 µg) was transcribed to cDNA with SuperScript II (Invitrogen, Carlsbad, CA, USA) using random hexamer primers according to the manufacturer's instructions. For quantitative real-time PCR (qPCR), 20 ng of cDNA was used, and single transcript levels of genes were detected with the

HOT FIREPol EvaGreen qPCR Mix (Solis BioDyne, Tartu, Estonia) and an AB7900 thermocycler. Primers used for detection of synaptic transcripts were as follows:

β-Actin Fwd	AGTGTGACGTTGACATCCGTA
β-Actin Rev	GCCAGAGCAGTAATCTCCTTCT
GABRA1 Fwd	GGTTGACCGTGAGAGCTGAA
GABRA1 Rev	CTACAACCACTGAACGGGCT
pan Collybistin Fwd	CAATGATGATCCCCACCTCAGT
pan Collybistin Rev	AGTGTTGATAGCGGCTGTCCTT
GABRA2 Fwd	CAGTGGCCCATAACATGACAAT
GABRA2 Rev	GGACATTCGGCTTGGACTGT
Gephyrin Fwd	GGCGACCGAGGGAATGAT
Gephyrin Rev	CCACCCAACAAAGAAGGATCTT

Data were analyzed using the comparative CT method (Schmittgen & Livak, 2008).

Immunohistochemistry

Mouse anti-gephyrin antibody (mAb7a, 1:3000; or 3B11, 1:10000; Synaptic Systems, Gottingen, Germany), rabbit anti-vGAT antibody (1:3000, Synaptic Systems, Gottingen, Germany), guinea pig anti-GABAAR α2 subunit antibody (Fritschy and Mohler, 1995), mouse anti-Myc (1:10000, Roche), rabbit anti-NONO (1:500, Brown, 2011), mouse anti-PSPC1 (1:500; SAB4200503 Sigma-Aldrich), NeuN (1:1000; MAB377 Milipore), GFAP (1:1000, Z0334 DAKO and MAB360, Millipore) and secondary antibodies coupled to Cy3 or Cy5 (1:500-1000, Jackson ImmunoResearch).

Immunocytochemistry on cells was performed as described previously (Tyagarajan et. Al 2011). In short, cells were rinsed in PBS and fixed for 10 minutes in 4% paraformaldehyde at room temperature. Cells were permeabilized with 0.01% Triton X-100 and detection of intracellular proteins were achieved by incubation for 60 minutes at room temperature with primary antibodies diluted in PBS containing 10% normal serum, followed by incubation with secondary antibodies coupled to Cy3 or Cy5 (1:500, Jackson ImmunoResearch) for 30 minutes at room temperature. Finally, coverslips were mounted with fluorescent mounting medium (Dako Cytomation, Carpinteria, CA). The GABAARα2 subunit antibody was incubated in living cultures for 90 minutes in culture medium (Brünig et al., 2002)

Staining and immunhistochemical analysis of synaptic components was performed as previously described (Notter et. al., 2013). Briefly, mice were anesthetized with pentobarbital and perfused intracardially with ice-cold, oxygenated ACSF. The brain was extracted and cut in blocks containing the regions of interest for analysis (e.g. hippocampal formation). The Tissue was plunged into ice-cold, freshly prepared fixative (4% PFA in PBS) and postfixed for 90 min, rinsed with phosphate-buffered saline (PBS), cryoprotected overnight in 30% sucrose in PBS and frozen with powdered dry ice and stored at –80 °C.

Sections were cut from frozen blocks with a sliding microtome at a thickness of 40 µm and were collected free-floating in PBS. They were incubated under continuous agitation in primary solution (Tris buffer (pH 7.4) containing 0.2 Triton X-100, 2% normal serum and the primary antibodies) for 15–48 h at 4 °C, washed in Tris buffer and incubated for 30–60 min at room temperature in secondary antibodies coupled to a fluorochrome.

Image analysis

Immunofluorescence images were captured by laser scanning confocal microscopy, using a 20x, 40x or 64x lens respectively (NA 1.4, 1024 x 1024 pixels, Zeiss LSM 710). Final illustrations were prepared from the maximal intensity projection of stacks of images spaced at 0.5 µm. Signals were quantified, using a custom macro created with the ImageJ software. Images were back- ground-subtracted and filtered with a Gaussian filter, but no change in brightness and contrast was applied.

References

1. Martin, S.J., Grimwood, P.D. & Morris, R.G. Synaptic plasticity and memory: an evaluation of the hypothesis. *Annu Rev Neurosci* **23**, 649-711 (2000).
2. Kelleher, R.J., 3rd, Govindarajan, A. & Tonegawa, S. Translational regulatory mechanisms in persistent forms of synaptic plasticity. *Neuron* **44**, 59-73 (2004).
3. Hirokawa, N. mRNA transport in dendrites: RNA granules, motors, and tracks. *J Neurosci* **26**, 7139-42 (2006).
4. Kanai, Y., Dohmae, N. & Hirokawa, N. Kinesin transports RNA: isolation and characterization of an RNA-transporting granule. *Neuron* **43**, 513-25 (2004).

5. Fox, A.H., Bond, C.S. & Lamond, A.I. P54nrb forms a heterodimer with PSP1 that localizes to paraspeckles in an RNA-dependent manner. *Mol Biol Cell* **16**, 5304-15 (2005).
6. Fox, A.H. *et al.* Paraspeckles: a novel nuclear domain. *Curr Biol* **12**, 13-25 (2002).
7. Fox, A.H. & Lamond, A.I. Paraspeckles. *Cold Spring Harb Perspect Biol* **2**, a000687 (2010).
8. Amelio, A.L. *et al.* A coactivator trap identifies NONO (p54nrb) as a component of the cAMP-signaling pathway. *Proc Natl Acad Sci U S A* **104**, 20314-9 (2007).
9. Dong, X., Sweet, J., Challis, J.R., Brown, T. & Lye, S.J. Transcriptional activity of androgen receptor is modulated by two RNA splicing factors, PSF and p54nrb. *Mol Cell Biol* **27**, 4863-75 (2007).
10. Park, Y., Lee, J.M., Hwang, M.Y., Son, G.H. & Geum, D. NonO binds to the CpG island of oct4 promoter and functions as a transcriptional activator of oct4 gene expression. *Mol Cells* **35**, 61-9 (2013).
11. Buxade, M., Morrice, N., Krebs, D.L. & Proud, C.G. The PSF.p54nrb complex is a novel Mnk substrate that binds the mRNA for tumor necrosis factor alpha. *J Biol Chem* **283**, 57-65 (2008).
12. Kaneko, S., Rozenblatt-Rosen, O., Meyerson, M. & Manley, J.L. The multifunctional protein p54nrb/PSF recruits the exonuclease XRN2 to facilitate pre-mRNA 3' processing and transcription termination. *Genes Dev* **21**, 1779-89 (2007).
13. Rosonina, E. *et al.* Role for PSF in mediating transcriptional activator-dependent stimulation of pre-mRNA processing in vivo. *Mol Cell Biol* **25**, 6734-46 (2005).
14. Chen, L.L. & Carmichael, G.G. Altered nuclear retention of mRNAs containing inverted repeats in human embryonic stem cells: functional role of a nuclear noncoding RNA. *Mol Cell* **35**, 467-78 (2009).
15. Prasanth, K.V. *et al.* Regulating gene expression through RNA nuclear retention. *Cell* **123**, 249-63 (2005).
16. Andersen, J.S. *et al.* Directed proteomic analysis of the human nucleolus. *Curr Biol* **12**, 1-11 (2002).
17. Bond, C.S. & Fox, A.H. Paraspeckles: nuclear bodies built on long noncoding RNA. *J Cell Biol* **186**, 637-44 (2009).
18. Clemson, C.M. *et al.* An architectural role for a nuclear noncoding RNA: NEAT1 RNA is essential for the structure of paraspeckles. *Mol Cell* **33**, 717-26 (2009).

19. Sasaki, Y.T., Ideue, T., Sano, M., Mituyama, T. & Hirose, T. MENepsilon/beta noncoding RNAs are essential for structural integrity of nuclear paraspeckles. *Proc Natl Acad Sci U S A* **106**, 2525-30 (2009).
20. Sunwoo, H. *et al.* MEN epsilon/beta nuclear-retained non-coding RNAs are up-regulated upon muscle differentiation and are essential components of paraspeckles. *Genome Res* **19**, 347-59 (2009).
21. Brown, S.A. *et al.* PERIOD1-associated proteins modulate the negative limb of the mammalian circadian oscillator. *Science* **308**, 693-6 (2005).
22. Tyagarajan, S.K. & Fritschy, J.M. Gephyrin: a master regulator of neuronal function? *Nat Rev Neurosci* **15**, 141-56 (2014).
23. Fritschy, J.M., Harvey, R.J. & Schwarz, G. Gephyrin: where do we stand, where do we go? *Trends in neurosciences* **31**, 257-64 (2008).
24. Tyagarajan, S.K. & Fritschy, J.M. GABA(A) receptors, gephyrin and homeostatic synaptic plasticity. *The Journal of physiology* **588**, 101-6 (2010).
25. Tyagarajan, S.K. *et al.* Regulation of GABAergic synapse formation and plasticity by GSK3beta-dependent phosphorylation of gephyrin. *Proc Natl Acad Sci U S A* **108**, 379-84 (2011).
26. Wilusz, J.E., Sunwoo, H. & Spector, D.L. Long noncoding RNAs: functional surprises from the RNA world. *Genes Dev* **23**, 1494-504 (2009).
27. Ishitani, K. *et al.* p54nrb acts as a transcriptional coactivator for activation function 1 of the human androgen receptor. *Biochem Biophys Res Commun* **306**, 660-5 (2003).
28. Kuwahara, S. *et al.* PSPC1, NONO, and SFPQ are expressed in mouse Sertoli cells and may function as coregulators of androgen receptor-mediated transcription. *Biol Reprod* **75**, 352-9 (2006).
29. Mathur, M., Tucker, P.W. & Samuels, H.H. PSF is a novel corepressor that mediates its effect through Sin3A and the DNA binding domain of nuclear hormone receptors. *Mol Cell Biol* **21**, 2298-311 (2001).
30. Song, K.S., Kim, K., Chung, K.C., Seol, J.H. & Yoon, J.H. Interaction of SOCS3 with NonO attenuates IL-1beta-dependent MUC8 gene expression. *Biochem Biophys Res Commun* **377**, 946-51 (2008).
31. Kowalska, E. *et al.* Distinct roles of DBHS family members in the circadian transcriptional feedback loop. *Mol Cell Biol* **32**, 4585-94 (2012).

32. Hirose, T. *et al.* NEAT1 long noncoding RNA regulates transcription via protein sequestration within subnuclear bodies. *Mol Biol Cell* **25**, 169-83 (2014).
33. Imamura, K. *et al.* Long noncoding RNA NEAT1-dependent SFPQ relocation from promoter region to paraspeckle mediates IL8 expression upon immune stimuli. *Mol Cell* **53**, 393-406 (2014).
34. Bannerman, D.M. *et al.* Hippocampal synaptic plasticity, spatial memory and anxiety. *Nat Rev Neurosci* **15**, 181-92 (2014).
35. Kowalska, E. *et al.* NONO couples the circadian clock to the cell cycle. *Proc Natl Acad Sci U S A* **110**, 1592-9 (2013).
36. Nakagawa, S., Naganuma, T., Shioi, G. & Hirose, T. Paraspeckles are subpopulation-specific nuclear bodies that are not essential in mice. *J Cell Biol* **193**, 31-9 (2011).

STUDY III: NONO mutations are a novel cause of syndromic intellectual disability and inhibitory synaptic defects

Dennis MIRCSOF[1,2*] and Maéva LANGOUËT[3*], Marlène RIO[3,4], Sébastien MOUTTON[3], Karine SIQUIER-PERNET[3], Christine BOLE-FEYSOT[5], Nicolas CAGNARD[6], Patrick NITSCHKE[6], Ludmila GASPAR[1], Matej ŽNIDARIČ[1], Olivier ALIBEU[5], Ann-Kristina FRITZ[7], David P. WOLFER[7], Aileen SCHRÖTER[8], Giovanna BOSSHARD[2], Markus RUDIN[8], Christina KOESTER[2], Florence CRESTANI[2], Petra SEEBECK[9], Nathalie BODDAERT[3,10], Jean-Marc FRITSCHY[2], Arnold MUNNICH[3], Jeanne AMIEL[3,4], Steven A. BROWN[1§*] and Shiva K. TYAGARAJAN[2§*], and Laurence COLLEAUX[3§*]

[1]: Chronobiology and Sleep Research Group, and [2]: Neuromorphology Group, Institute of Pharmacology and Toxicology, University of Zurich, 190 Winterthurerstrasse, 8057 Zurich
[3]: INSERM UMR 1163, Laboratory of Molecular and pathophysiological bases of cognitive disorders, Paris Descartes– Sorbonne Paris Cité University, Imagine Institute, Necker-Enfants Malades Hospital, 75015 Paris
[4]: Service de Génétique, Hôpital Necker-Enfants Malades, AP-HP, Paris
[5]: Genomic platform, INSERM UMR 1163, Paris Descartes– Sorbonne Paris Cité University, Imagine Institute
[6]: Bioinformatic platform, INSERM UMR 1163, Paris Descartes– Sorbonne Paris Cité University, Imagine Institute
[7]: Institute of Anatomy, University of Zürich
[8]: Molecular Imaging and Functional Pharmacology Group, University of Zurich
[9]: Center for Integrative Rodent Physiology, University of Zurich
[10]: Service de radiologie pédiatrique, Hôpital Necker-Enfants Malades, AP-HP,Paris

*These authors contributed equally to this work.

[§]Correspondance to:

Dr. Laurence COLLEAUX
INSERM UMR 1163, Institut IMAGINE, 24 boulevard du Montparnasse, 75015 Paris, France
Email: laurence.colleaux@inserm.fr, phone: +33 1 42 75 42 96,/ fax: 33 1 42 75 42 21

Drs. Shiva TYAGARAJAN and Steven BROWN
Institute of Pharmacology and Toxicology, University of Zurich, Winterthurerstrasse 190, 8057 Zurich, Switzerland
Email: tyagarajan@pharma.uzh.ch, steven.brown@pharma.uzh.ch

Abstract

Identifying causes of sporadic intellectual disability remains a considerable medical challenge. Here, we demonstrate that null mutations in the *NONO* gene, a member of the Drosophila Behavior Human Splicing (DBHS) protein family, are a novel cause of X-linked syndromic intellectual disability. Comparing patients to *Nono*-deficient mice revealed related behavioral, craniofacial, and transcriptional anomalies. In brain, these mice also showed deregulation of a large number of synaptic transcripts including the GABA receptor alpha2 subunit, as well as impaired postsynaptic scaffolding of gephyrin, a master organizer of inhibitory synapses. Importantly, alteration of synaptic scaffolding could be rescued by over-expression of *Gabra2* in NONO-compromised neurons, suggesting that aspects of this syndrome are potentially treatable. Our data identify *NONO* as a new neurodevelopmental-disease gene and highlight the key role of DBHS proteins in functional organization of GABAergic synapses.

Results

Intellectual disability (ID) is characterized by significant limitations in intellectual functioning and adaptive behavior. Recent developments in next-generation sequencing (NGS) and whole-exome sequencing (WES) have considerably empowered detection of disease variants in ID (1-3). WES was carried out in parallel in two unrelated male ID patients (MCCID1 and 2), who presented the same slender built-macrocephaly gestalt, facial features, shy behavior, a thick corpus callosum and a smaller cerebellum (Fig. 1a and 1b, Table S1 and Supplementary Note). Hypothesizing that the same disease gene was shared by the two patients, only the X-linked *NONO* (Non-octamer-containing, POU-domain DNA-binding protein, also known as *p54NRB*) gene emerged as a candidate (Supplementary Table 2). Capillary sequencing confirmed the *de novo* occurrence of a splice site variant affecting the last base of exon 10 in patient MCCID1 (NM_001145408.1:c.1131G>A; p.Ala377Ala) (Supplementary Fig.1). The variant identified in patient MCCID2 was a one-base-pair insertion in the last coding exon (NM_001145408.1:c.1394dup ; p.Asn466Lysfs*13) inherited from his healthy mother (Supplementary Fig.1). Immunoblot analyses of cultured skin fibroblast lysates using an anti-NONO antibody

showed a markedly reduced amount of NONO proteins in patient cells compared to controls (Fig 1c, d). These results were confirmed by immuno-cytochemistry using the same antibody (Fig. 1e).

NONO belongs to the highly conserved Drosophila Behaviour Human Splicing (DBHS) protein family. This family includes three members in mammals, namely NONO, paraspeckle component 1 (PSPC1), and Splicing Factor Proline/Glutamine-Rich (SFPQ, also known as PSF). DBHS proteins are nuclear proteins forming homo- and heterodimers *in vivo* (4,5) and previous literature documents their involvement in various aspects of RNA production (6). Studies *in vitro* suggest that they play a role in transcriptional activation and repression (7-9), splicing (10,11), pre-mRNA processing (12) and RNA transport (13,14). In addition, they are major components of nuclear paraspeckles, which have been recognized as nuclear RNA-holding structures for edited RNAs (15,16) that likely play a role in stress-mediated regulation *via* nuclear retention of transcripts (17-19). NONO and other DBHS family members also serve as transcriptional cofactors for correct circadian clock function in both flies and mammals, where they regulate the circadian clock *via* interaction with PER proteins (20-23). However, no study so far has linked impaired function of these proteins to human disease.

Consistent with the established role for the NONO protein within the circadian clock, cultured skin fibroblasts from patients showed reduced amplitude of circadian oscillations (Supplementary Fig. 2). Microarray analysis of cultured skin fibroblast RNAs in patients compared to controls also revealed a marked modification in the global pattern of gene expression between the two groups. Indeed, hierarchical clustering analysis showed that the patient group formed an independent cluster away from the control RNAs, as illustrated by the corresponding heatmap (Fig. 2a). A total of 389 differentially expressed genes were shared by the two patients with 372 transcripts being similarly affected (213 down regulated and 159 up regulated), whereas only 17 transcripts were deregulated in opposite orientation (Fig. 2b, Supplementary Table 3). Notably, increased levels of *PSPC1* (2.22 and 2.78 fold respectively) and *SFPQ* transcripts (1.54 and 1.71 fold respectively) were detected in patients compared to controls. Expression data were confirmed by Western blot

analysis showing increased amounts of PSPC1 and SFPQ proteins in patient fibroblasts compared to controls (Fig 1c,d).

To further characterize the physiological role of NONO upon brain development, we analyzed a mouse model in which the *Nono* gene had been disrupted by genetrap (*gt*)23. Visual inspection and CT scan revealed that mutant mice displayed a flattened nose mimicking the facial anomalies observed in the patients (Fig. 3a-c, Supplementary Table 4). Similarly, a smaller cerebellum was observed in mutant mice (Fig 3d, S2, Supplementary Table 4) and patients (Fig. 1b, Supplementary Table 1), as well as other structural anomalies (Supplementary Fig. 3, Supplementary Table 1, 4). Behaviorally, mice showed impaired performance in the Morris Water Maze (Fig 3e,f) reflective of the cognitive defects observed in patients, as well as a marked anxiety phenotype documented via prepulse inhibition, open field exploration, and light-dark preference testing (Supplementary Fig. 4). Gene expression analysis in adult dermal fibroblasts from wild type and *Nonogt* mice also revealed global transcriptional deregulation in the mutant mice compared to controls in patterns similar to that of human patients and controls. When human and mouse data sets were merged and submitted to a hierarchical clustering with the Spearman correlation similarity measure, the samples were split in two main groups. *Nonogt* mice samples segregated with the patients group, whereas wild type mice samples segregated with the human control samples (Fig. 2c and Supplementary Table 5). Taken together, these data demonstrated a regulatory role of NONO conserved through evolution and supported the relevance of the *Nonogt* model for further elucidation of the disease mechanism in patients.

Immunofluorescence analysis using anti-Nono antibodies detected strong immunoreactivity in mouse brain, including cortex and hippocampus (Fig. 4a). Staining was strongest in neuronal nuclei (NeuN-positive) in CA1 and CA3 pyramidal regions and granule cells of the dentate gyrus, but absent from neighboring astrocytes (GFAP-positive) (Supplementary Fig. 5). Gene expression analysis in hippocampi of wildtype and *Nonogt* mice identified 882 differentially expressed genes (Fig. 4b), including the two other DBHS family members *Sfpq* and *Pspc1* (Supplementary Fig. 6), as observed in fibroblasts from NONO-deficient patients (Supplementary Table 3). Protein levels of these orthologs were also overexpressed

in *Nonogt* hippocampi (Supplementary Fig. 7). Interestingly, mRNA levels of *Gabra2*, the GABAA receptor alpha2 subunit, were markedly reduced in hippocampi of *Nonogt* mice compared to controls, a result confirmed by qRT-PCR and Western blot analyses (Supplementary Fig. 6,9). Finally, pathway analyses suggested that NONO-regulated genes were markedly enriched in Gene Ontology categories related to synaptic functions (Supplementary Table 5). To support this *in silico* prediction, we compared the synaptosomal transcriptomes from *Nonogt* and control mice. RNA was extracted from synaptosomal fractions obtained by density gradient ultracentrifugation (24). The quality of this fractionation was confirmed by verifying enrichment of known synaptically transported RNAs and depletion of known nuclear RNAs relative to whole transcriptome (Fig S7A-C). We found that 30.5% of synaptosomal transcripts, including *Gabra2* (Fig S6D), were deregulated in samples from *Nonogt* mice when compared to controls, a significant over-representation compared to whole transcriptome (Table S6, p=0.0007). Hence, our data suggest that NONO might play an important role in the regulation of synaptic RNAs.

Gabra2 codes for a subunit of the GABAA receptors that potentiate the majority of fast synaptic inhibition in the brain. Previous studies have demonstrated that GABAA receptors are anchored postsynaptically by gephyrin, which self-assembles into a scaffold and interacts with the cytoskeleton. Gephyrin binding to GABAA receptors is mediated by interaction sites that have been mapped within the intracellular loop of of GABAA receptors α1, α2 and α3 subunits (25). We thus tested the consequences of loss of NONO at inhibitory synapses by immunohistological studies of brain sections from wild type and *Nonogt* mice, using antibodies directed against GABAAR α2 and gephyrin respectively. Post-synaptic punctate staining for gephyrin and GABAAR α2 was significantly reduced in the CA3 hippocampal region of *Nonogt* mice, while staining of the presynaptic vesicular GABA transporter marker (VGAT) was unaffected (Fig. 4c). Quantitative evaluations showed that the number of gephyrin clusters was significantly reduced, but average cluster size was conserved (Fig. 4d). Western blot analyses showed markedly reduced GABAAR α2 levels in total brain lysates and synaptosomes (Supplementary Fig. 9). By contrast, gephyrin levels were similar in wild type and *Nonogt* in all compartments analyzed (Supplementary Fig. 9). Taken together, these data suggest that reduced GABAAR α2 levels in *Nonogt* mice

are likely due to transcriptional deregulation. On the other hand, altered gephyrin clustering is likely a downstream consequence of altered synaptic composition.

In principle, the anomalies observed in *Nonogt* mice could arise from either cellular synaptic defects, or broader neurodevelopmental changes. To distinguish between these possibilities and uncover potential cell-autonomous phenotypes, we used high-resolution fluorescent *in situ* hybridization to analyse dissociated hippocampal neurons from wildtype and *Nonogt* mice. As in intact brain slices, we observed a significant reduction of *Gabra2* transcripts in *Nono*-deficient neurons but unchanged transcript levels for other postsynaptic markers (collybistin, *Gabra1*) (Supplementary Fig. 10). At the protein level, these cultures showed the same reduction of gephyrin scaffolding puncta and GABAAR α2 levels, demonstrating that primary culture neurons from these mice recapitulated the key cytological features observed in *Nonogt* mouse hippocampi. This cellular model was therefore used for functional analysis of NONO in post-synaptic biology.

It has been previously established in cultured primary neurons that over-expression of green fluorescent protein-tagged gephyrin (GFP-gephyrin) has no apparent effect on gephyrin clustering. This tool was used to examine in more detail the effects of NONO upon post-synaptic structures (26). Inversely to what was observed in *Nono*-deficient mouse neurons, over-expression of Myc-tagged NONO in wildtype primary hippocampal neurons expressing GFP-gephyrin caused a significant increase in density of GFP-gephyrin puncta compared to neurons transfected with GFP-gephyrin alone. By contrast, a reduction in GFP-gephyrin density was observed in cells transfected with a construct over-expressing a mutant form of the NONO protein, myc-NONO RRM (Fig. 4e,f). This construct contains four point mutations in the RNA recognition motif (RRM), and is therefore unable to bind to single-stranded RNAs. Thus, we can conclude that the function of NONO upon synaptic biology is RNA-dependent.

Gephyrin depends on the presence of GABAAR to form postsynaptic clusters in GABAergic synapses, and the size and density of gephyrin scaffolding can be correlated to strength and frequency of GABAergic transmission (25,26). Thus, gephyrin clustering is largely impaired in the mice lacking the GABAAR α2 subunit

(*Gabra2*-KO) (27). Therefore, we hypothesized that the altered gephyrin distribution observed in NONO-deficient neurons might be the consequence of *Gabra2* transcript deregulation, and furthermore that this defect might be rescued by over-expressing GABAAR α2. Indeed, transfection of plasmids expressing *Gabra2* could rescue the reduced gephyrin cluster density observed in cultured neurons transfected with myc-NONO RRM (Fig. 4g,h), further supporting the view that NONO alters postsynaptic structure by regulating *Gabra2* levels.

Discussion

In this study, we have shown that *NONO*-null mutations cause a novel, clinically recognizable ID syndrome, with slender built-macrocephaly, malar hypoplasia and thick corpus callosum. A mouse model deficient in NONO recapitulates the major features of this syndrome. Studying brains and neurons from these mutant mice suggested that NONO plays an unsuspected role in regulating inhibitory synaptic biology, results also consistent with intellectual and anxiety phenotypes of these mice. Previous studies have identified NONO as a member of a neuronal RNA transport complex (13) and demonstrated increased NONO abundance at synapses in response to synaptic activity (28), but no study has yet linked dysfunction in NONO or other DBHS proteins to any human disease. Our studies clearly demonstrate that, in the brain, NONO function is primarily mediated by its role in the regulation of RNA expression, and suggest that it may contribute to the local regulation of RNA metabolism underlying activity-dependent regulation of dendritic spine morphology. Finally, because inhibitory synapse structural defects caused by NONO dysfunction could be rescued by increasing the number of GABA-α2 receptors, this study opens reasoned opportunities for therapeutic trials in this novel intellectual disability syndrome.

Acknowledgments

We are grateful to the patients and their family members for their participation in our study, and to the Functional Genomics Center Zürich (FGCZ) for transcriptomic services. This program has received a state subsidy managed by the National

Research Agency under the "Investments for the Future" program bearing the reference ANR-10-IAHU-01.This study was also supported by the Centre National de la Recherche Scientifique (CNRS), the Fondation pour la Recherche Médicale (DEQ20120323702) and the Ministère de la Recherche et de l'Enseignement Supérieur, as well as by the Swiss National Science Foundation, the Zurich Clinical Research Priority Program "Sleep and Health", the Zurich Fonds zur Förderung des akademischen Nachwuchses, and the Zurich Neurozentrum (ZNZ). DM and SAB and SKT are affiliates of the ZNZ Life Sciences Zurich graduate program, and SAB is a member of the Zürich Center for Interdisciplinary Sleep Research (ZIS).

Author Contributions

LC, SAB, and SKT designed the study. JA and MR recruited and evaluated the study subjects. NB performed and analysed the human brain imaging, and DM, PS, AS, and MR performed and analysed the mouse brain imaging. ML analyzed WES data, performed transcriptional analysis and WB analysis on patient cells, and LG performed circadian analyses on patient cells. SM contributed to WES data analysis. CBF performed WES. NC and PN performed the bioinformatic studies. DM executed and analysed all experiments on mouse tissues, and DM and MZ executed and analyzed experiments in rodent cells. DM, CK, FC, AKF, and DPW performed and analysed mouse behavioral experiments. All authors contributed to writing and editing the manuscript.

Competing Financial Interests

The authors declare no competing financial interests.

References

1. de Ligt, J. *et al.* Diagnostic exome sequencing in persons with severe intellectual disability. *N Engl J Med* **367**, 1921-9 (2012).
2. Rauch, A. *et al.* Range of genetic mutations associated with severe non-syndromic sporadic intellectual disability: an exome sequencing study. *Lancet* **380**, 1674-82 (2012).
3. Vissers, L.E., de Vries, B.B. & Veltman, J.A. Genomic microarrays in mental retardation: from copy number variation to gene, from research to diagnosis. *J Med Genet* **47**, 289-97 (2010).
4. Fox, A.H., Bond, C.S. & Lamond, A.I. P54nrb forms a heterodimer with PSP1 that localizes to paraspeckles in an RNA-dependent manner. *Mol Biol Cell* **16**, 5304-15 (2005).
5. Myojin, R. *et al.* Expression and functional significance of mouse paraspeckle protein 1 on spermatogenesis. *Biol Reprod* **71**, 926-32 (2004).
6. Shav-Tal, Y. & Zipori, D. PSF and p54(nrb)/NonO--multi-functional nuclear proteins. *FEBS Lett* **531**, 109-14 (2002).
7. Amelio, A.L. *et al.* A coactivator trap identifies NONO (p54nrb) as a component of the cAMP-signaling pathway. *Proc Natl Acad Sci U S A* **104**, 20314-9 (2007).
8. Dong, X., Sweet, J., Challis, J.R., Brown, T. & Lye, S.J. Transcriptional activity of androgen receptor is modulated by two RNA splicing factors, PSF and p54nrb. *Mol Cell Biol* **27**, 4863-75 (2007).
9. Park, Y., Lee, J.M., Hwang, M.Y., Son, G.H. & Geum, D. NonO binds to the CpG island of oct4 promoter and functions as a transcriptional activator of oct4 gene expression. *Mol Cells* **35**, 61-9 (2013).
10. Kim, K.K., Kim, Y.C., Adelstein, R.S. & Kawamoto, S. Fox-3 and PSF interact to activate neural cell-specific alternative splicing. *Nucleic Acids Res* **39**, 3064-78 (2011).
11. Patton, J.G., Porro, E.B., Galceran, J., Tempst, P. & Nadal-Ginard, B. Cloning and characterization of PSF, a novel pre-mRNA splicing factor. *Genes Dev* **7**, 393-406 (1993).

12. Kaneko, S., Rozenblatt-Rosen, O., Meyerson, M. & Manley, J.L. The multifunctional protein p54nrb/PSF recruits the exonuclease XRN2 to facilitate pre-mRNA 3' processing and transcription termination. *Genes Dev* **21**, 1779-89 (2007).
13. Izumi, H., McCloskey, A., Shinmyozu, K. & Ohno, M. p54nrb/NonO and PSF promote U snRNA nuclear export by accelerating its export complex assembly. *Nucleic Acids Res* **42**, 3998-4007 (2014).
14. Kanai, Y., Dohmae, N. & Hirokawa, N. Kinesin transports RNA: isolation and characterization of an RNA-transporting granule. *Neuron* **43**, 513-25 (2004).
15. Bond, C.S. & Fox, A.H. Paraspeckles: nuclear bodies built on long noncoding RNA. *J Cell Biol* **186**, 637-44 (2009).
16. Nakagawa, S. & Hirose, T. Paraspeckle nuclear bodies--useful uselessness? *Cell Mol Life Sci* **69**, 3027-36 (2012).
17. Chen, L.L., DeCerbo, J.N. & Carmichael, G.G. Alu element-mediated gene silencing. *EMBO J* **27**, 1694-705 (2008).
18. Prasanth, K.V. *et al.* Regulating gene expression through RNA nuclear retention. *Cell* **123**, 249-63 (2005).
19. Zhang, Z. & Carmichael, G.G. The fate of dsRNA in the nucleus: a p54(nrb)-containing complex mediates the nuclear retention of promiscuously A-to-I edited RNAs. *Cell* **106**, 465-75 (2001).
20. Brown, S.A. *et al.* PERIOD1-associated proteins modulate the negative limb of the mammalian circadian oscillator. *Science* **308**, 693-6 (2005).
21. Duong, H.A., Robles, M.S., Knutti, D. & Weitz, C.J. A molecular mechanism for circadian clock negative feedback. *Science* **332**, 1436-9 (2011).
22. Kowalska, E. *et al.* NONO couples the circadian clock to the cell cycle. *Proc Natl Acad Sci U S A* **110**, 1592-9 (2013).
23. Kowalska, E. *et al.* Distinct roles of DBHS family members in the circadian transcriptional feedback loop. *Mol Cell Biol* **32**, 4585-94 (2012).
24. Dunkley, P.R., Jarvie, P.E. & Robinson, P.J. A rapid Percoll gradient procedure for preparation of synaptosomes. *Nat Protoc* **3**, 1718-28 (2008).
25. Tyagarajan, S.K. & Fritschy, J.M. Gephyrin: a master regulator of neuronal function? *Nat Rev Neurosci* **15**, 141-56 (2014).

26. Tyagarajan, S.K. *et al.* Regulation of GABAergic synapse formation and plasticity by GSK3beta-dependent phosphorylation of gephyrin. *Proc Natl Acad Sci U S A* **108**, 379-84 (2011).

27. Panzanelli, P. *et al.* Distinct mechanisms regulate GABAA receptor and gephyrin clustering at perisomatic and axo-axonic synapses on CA1 pyramidal cells. *J Physiol* **589**, 4959-80 (2011).

28. Zhang, G., Neubert, T.A. & Jordan, B.A. RNA binding proteins accumulate at the postsynaptic density with synaptic activity. *J Neurosci* **32**, 599-609 (2012).

Figure Legends

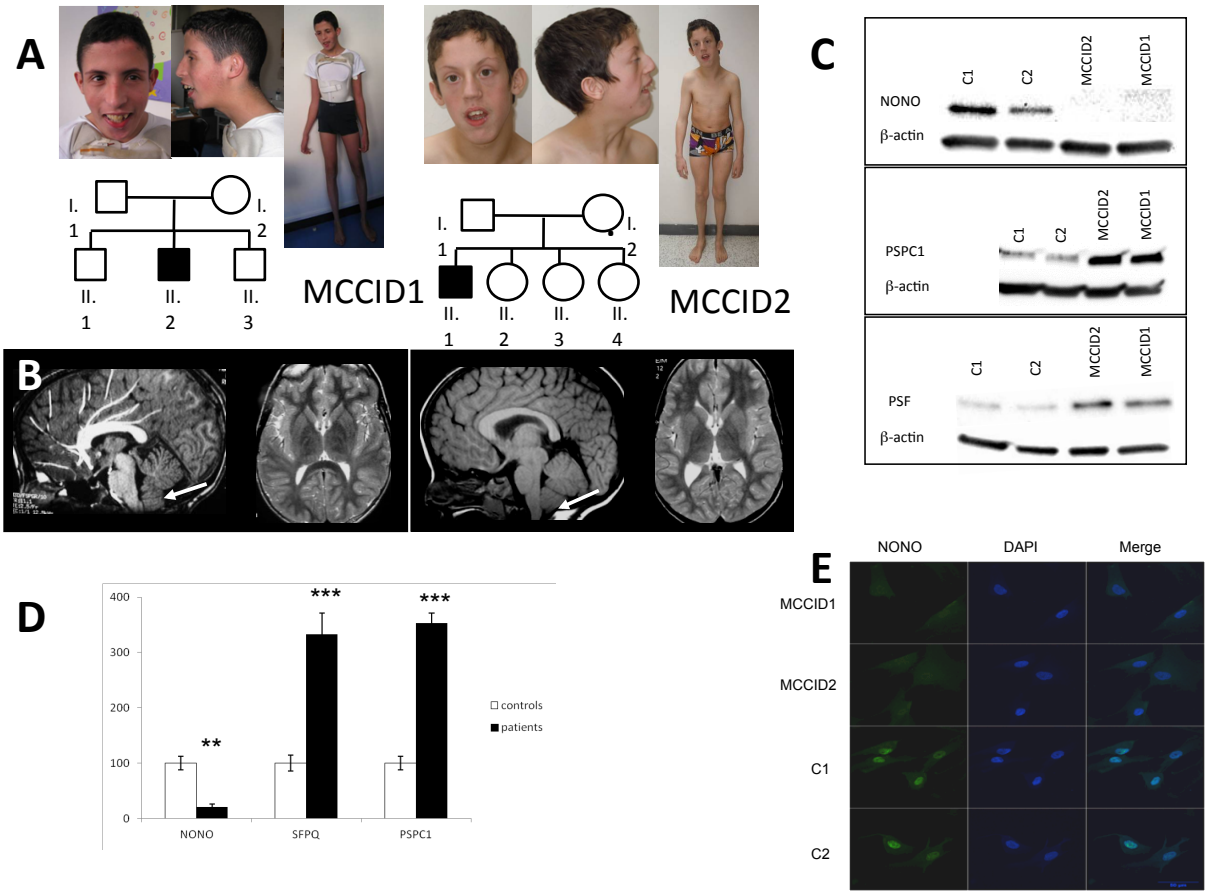

Figure 1: *P54NRB/NONO* mutations and their functional consequences (**a**) Photographs and pedigree of both patients**.** Shaded symbols indicate the affected individuals. (**b**) Sagittal T1 and axial FSE T2 brain MRI of patient MCCID1 at 9 years-old (left panel) and patient MCCID2 at 8 years old (right panel) showing a thick corpus callosum, a small cerebellum and a Chiari I malformation (arrows). (**c**) Immunoblots showing a complete absence of the NONO protein and overexpression of PSPC1 and SFPQ proteins in patients' cells compared to controls. (**d**) Densitometry analyses. Means ± standard error (SEM) for the three DBHS proteins relative to the amount of total proteins are given from two independent experiment and expressed as a percentage of the control values (100%). Significance was calculated using two-way analysis of variance (ANOVA) test with Tukey correction. Here and in subsequent figures, ∗ P value < 0.05, ∗∗ P value < 0.01, ∗∗∗ P value < 0.001 (**e**) Immunofluorescence showing the complete absence of the NONO protein in patients' cells compared to controls.

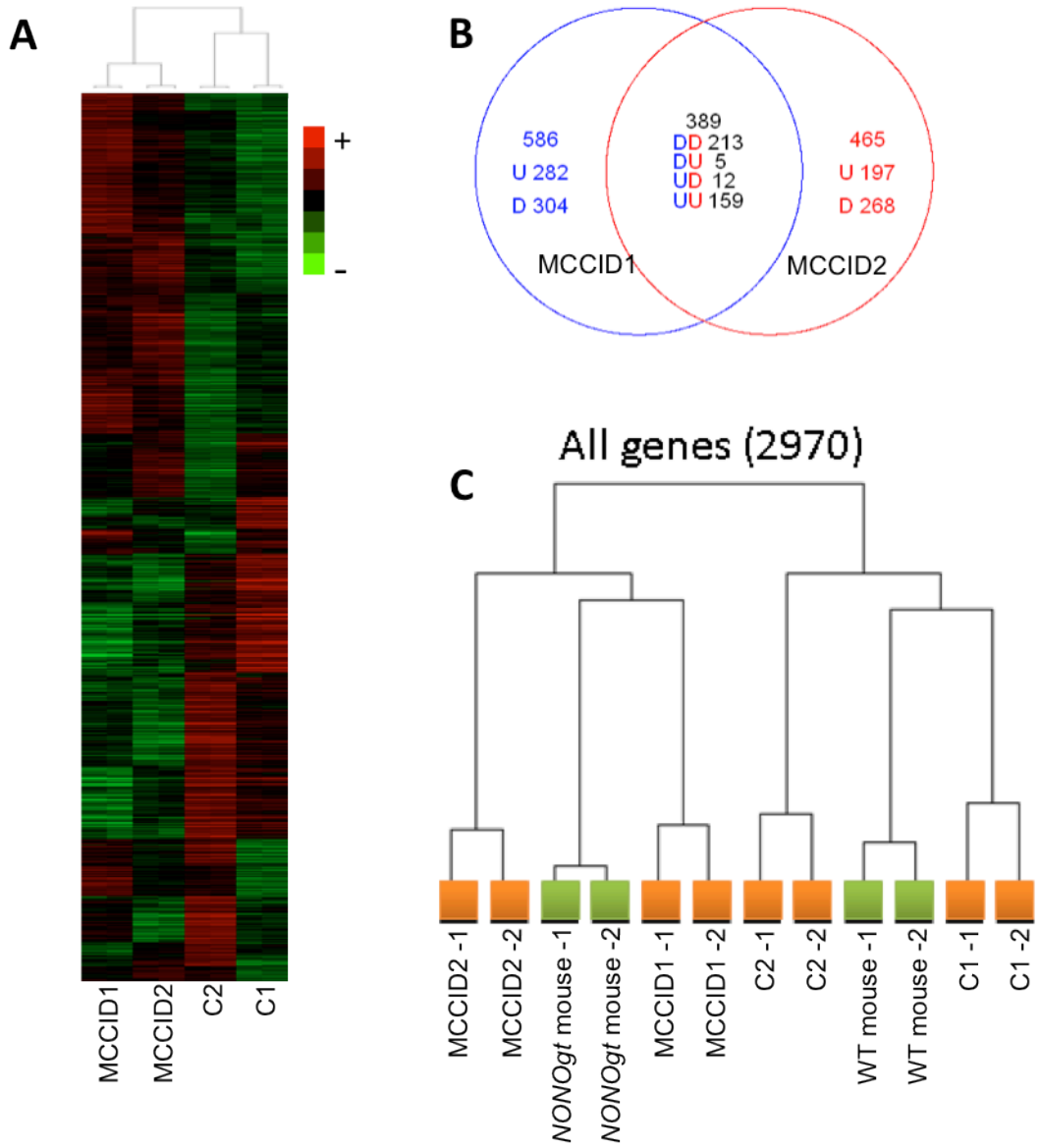

Figure 2. Transcriptome analysis in human and mouse cells (a) Heatmap cluster analyses indicating similarity in expression profile among probes from the two patients and differences compared to the two controls. High detection signals relative to the mean were colored in red. Low detection signals were colored in green. The cut-off for inclusion in the heatmap was a 1.5-fold alteration of probe expression for both patients. **(b)** Venn diagram showing the number of genes commonly or differentially expressed in the two patients compared to the mean of the two controls. Significant differences are based on a 1.5-fold difference and a P-value of<.05. U= up, D= down. (**c**) Hierarchical clustering analysis of combined mouse and human orthologous genes, resulting in a striking separation highlighting similarity of mouse and human transcriptional dysregulation.

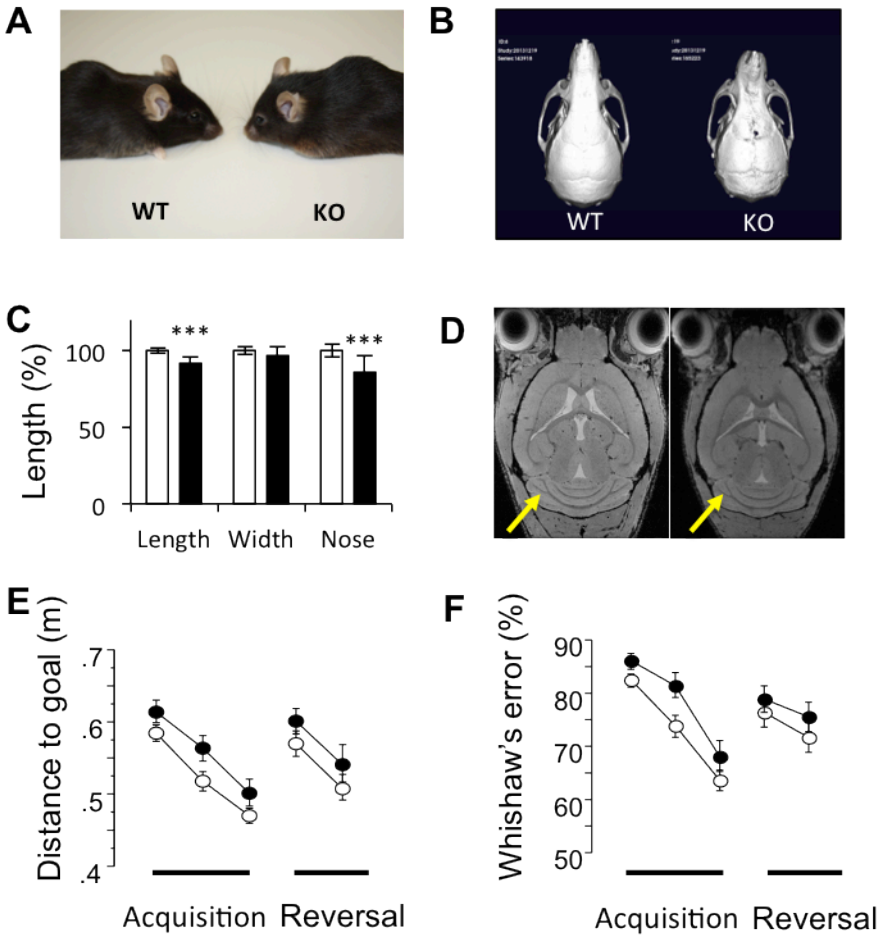

Figure 3. Functional consequences of NONO deficiency in mice. (**a**) Side view of representative *Nono*^{gt} mouse (right) compared to wildtype littermate (left). (**b**) CTscan analysis indicating a flattened and distorted nose in *Nono*^{gt} mice (right) compared to WT (left). (**c**) Quantification of skull length, width and nose length in *Nono*^{gt} mice (black) compared to wildtype littermate (white). *n* = 20 mice per genotype. $^{***}P < 0.001$; Student's *t*-test. Bars represent mean ± SD. **(d)** MRI scan of representative *Nono*^{gt} mouse (right) compared to wildtype littermate (left). Yellow arrow indicates cerebellum. Also see Supplementary Fig 3 and Supplementary Table 4. (**e-f**) Behavior of *Nono*^{gt} mice and WT littermates in Morris water maze, n=16-20 per genotype. Black circles, *Nono*^{gt}; open circles, WT. Unless otherwise noted in this and subsequent figure, bars represent means ± SEM. (**e)** Gallagher's proximity test scores, i.e. average distance of mice from goal as fraction of total distance. Repeated ANOVA, gene p<0.0237, time p<0.001, gene x time n.s. (**f**) Whishaw's error, i.e. % path outside an 18cm-wide corridor connecting release point and goal. Gene p<0.0215, time p<0.001, gene x time n.s.

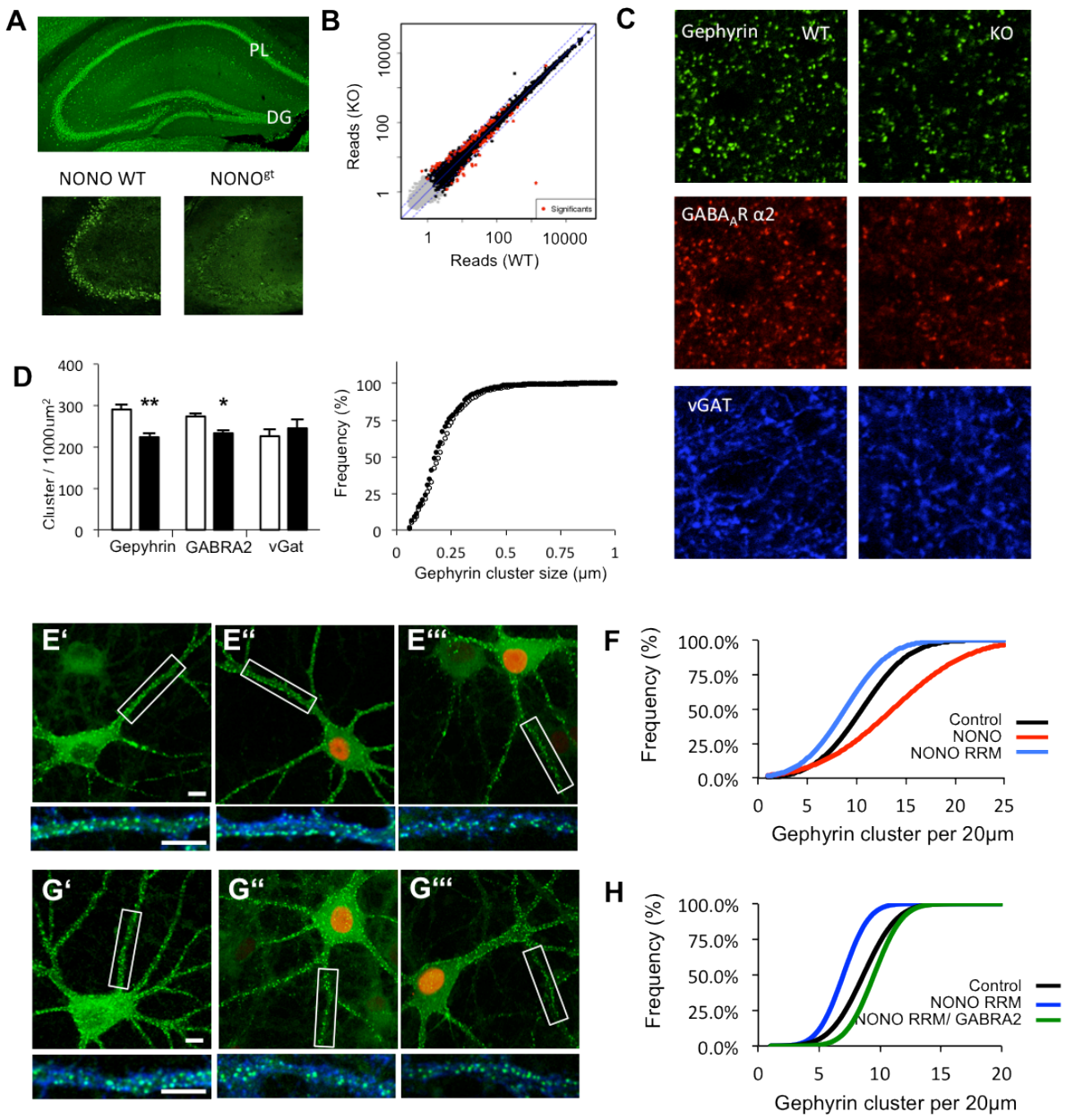

Figure 4. Effects of NONO deficiency upon synaptic biology. (**a**) Immunofluorescence labeling of NONO in wildtype (top) and *Nono*^{gt} (bottom) mouse coronal brain sections. PL = pyramidal cell layer, DG = dentate gyrus. (**b**) Scatter plot of hippocampal transcriptome from WT and *Nono*^{gt} mice. Red, diffrentially expressed genes, $p \leq 0.01$ and log ratio ≥ 0.5. (**c**) Immunohistochemical staining for inhibitory postsynaptic marker gephyrin (green), GABA type II receptor (red), and the presynaptic marker vGat (blue) in wildtype and *Nono*^{gt} mice in the *stratum radiatum* CA3 of the hippocampus. (**d**) Quantification of gephyrin, GABA type II receptor and vGat density (left) and gephyrin cluster size (right). Means ± SD are shown, $^{*}P < 0.05$, $^{**}P < 0.01$; Student's *t*-test (top) and Kolmogorov-Smirnov test (bottom). (**e-h**) Immunofluorescence analysis of inhibitory synapse morphology *in-vitro.* (**e**) Primary hippocampal rat neurons expressing control GFP-gephyrin alone, or (**e'**) co-expressed with myc-NONO, or (**e''**) co-expressed with RNA binding-deficient myc-NONO-RRM,. Boxed region is magnified beneath. Postsynaptic clustering is

demonstrated by apposition of eGFP-gephyrin clusters (green) to vGat -positive terminals (blue). (**f**) Quantification of cluster density distribution in 9 neurons from 3 independent experiments., Control x NONO $^{*}P < 0.05$, Control x NONO- RRM $^{*}P < 0.05$ using Kolmogorov-Smirnov test. (**g**) Primary hippocampal rat neurons expressing control GFP-gephyrin alone, or (g') co-expressed with myc-NONO-RRM, or (g'') co-expressed with myc-NONO-RRM and GABRA2. (**h**) Quantification, showing complete rescue of the impaired gephyrin cluster distribution by GABRA2. Control x NONO RRM $^{*}P < 0.05$, Control x NONO RRM GABRA2 $^{*}P < 0.05$ using Kolmogorov-Smirnov test.

Online Methods

Patients

All human protocols were reviewed and approved by the institutional review board of the Necker Hospital and informed consent was obtained from all subjects involved in this study.

Case MCCID1 was the second child of healthy, nonconsanguineous parents. Family history is unremarkable. He was born in the 41st week of gestation, after a normal pregnancy and delivery and an Apgar score of 10/10. Parameters at birth were in the normal range (BW 3370g, LW 50.5 cm, HC 34 cm). Developmental milestones were delayed: he was able to walk alone at 3 years of age, and had limited speech with preserved comprehension. He developed absence seizures at the age of 5 years and continued to have seizures with increased frequency. He had strabismus and myopia. At the age of 15 years, he developed severe kyphoscoliosis. On examination at 17.5 years, his height was 1.79 m (+1SD), his weigh 50 kg (-1.5SD), and OFC 60.5 cm (+4SD). Hand and feet were narrow with long fingers and toes, overriding toes and bilateral ankylosis of the metacarpophalangeal joint of thumb. He had flat feet with dystrophic nails. He had long and expressionless face, malar hypoplasia, short palpebrale fissures, small and open mouth with drooling, high-arched-palate and enamel defect. He had slender build and distal amyotrophy. Speech was limited with simple sentences, severe elocution disability and nasal speech. Extensive metabolic screening was normal. Myotonic dystrophy and fragile X were excluded. Brain MRI demonstrated bilateral megalencephaly, a thick corpus callosum, enlarged white matter, septum pellucidum cyst, and a small cerebellum. High resolution cytogenetic studies (array CGH) identified a de novo 15q13.3 deletion.
Case MCCID2, a male, is the first child of healthy, non consanguineous parents with no medical family history of note. He has 3 healthy younger sisters (Figure 1A). Because hydramnios and short long bones were noted in the 2nd trimester of pregnancy, amniocentesis was performed and karyotyping showed normal chromosomes, 46,XY. He was born at 37.6 WG with low birth parameters (BW: 2540 g, BL: 46 cm, OFC: 35.5 cm) and an Apgar score of 10/10. He presented poor sucking, gastrointestinal reflux, stridor, cryptorchidism and hypotonia from birth. He

developed convergent strabismus within the first year of age. Motor skills have been delayed with head control achieved at 10 months and walking unaided at 3 years of age. At that time language was limited to a few single words. He was slender built and macrocephalic with weight and height on -2 SD and head circumference on +2 SD. His thorax was long and narrow and he developed kyphoscoliosis and pes planus. He was awkward and slow with weak patella reflexes. He suffered from drooling, persistent deglutition difficulties and severe elocution disability with nasal speech. He could not blow or smack. He had multiple dental caries due to mouth breathing. Chronic otitis media resulted in conductive hearing loss of 40 to 60 dB and has been treated with grommets. Hands and feet were narrow with overriding toes and ankylosis of the metacarpophalangeal joint of both thumbs. Although macrocephalic, his forehead was relatively short and narrow with low frontal and temporal hairline. The face was elongated with upslanting palpebral features, a convergent squint, a thin and high nasal root with deviated nasal septum and large tip with short columella, severe malar hypoplasia, a small open mouth with narrow and high palate, narrow dental arcades and crowding of teeth. Ears were normally placed and folded with hypoplastic ear lobes. He made constant progress, was toilet trained at about 7 years, speaks in sentences and is able to write his name and read simple words. He has a shy, gentle and cheerful behaviour. When last seen at 15 years of age, puberty was delayed and orthopaedic surgery of the kyphoscoliosis was planed.

Brain MRI performed at 18 months and 8 years showed a thick corpus callosum, asymmetric trigone and lateral ventricles and a Chiari malformation type I (Figure 1B). EEG showed no gross anomaly. Extensive metabolic screening was normal. Skeletal X-rays showed no malformation of the vertebrae. CytoChip^{TM} (BlueGnome, Cambridge) array-CGH did not detect any copy number variant.

Whole-exome sequencing

Agilent SureSelect librairies were prepared from 3 µg of genomic DNA sheared with a Covaris S2 Ultrasonicator as recommended by the manufacturer. Exome capture was performed with the 50 Mb SureSelect Human All Exon kit (Agilent technologies) using a multiplex approach with molecular barcodes for traceable ID of samples. Sequencing was carried with the SOLiD5500 (Life Technologies) on a pool of

barcoded exome librairies. 75+35 paired-end reads were generated and mapped on human genome reference (NCBI build37/hg19 version) using LifeScope (Life Technologies).
Sequences produced allowed a mean sequence coverage of 42-87 reads per bp. The average coverage was 70X, with more than 75% of targeted bases covered 15X. Sequence reads were aligned to the human reference genome sequence (assembly GRCh37) using Mapreads. SNPs/indels were called using Genome analysis toolkit and Picard tools. Poorly mapped (less than 3X cover) and low-quality reads (less than 20 quality score) were removed. An in-house software (PolyWeb) was used to annotate and filter the variants.

Mice

Generation of *Nono*^{gt} mice was described previously (*29*). Mice have been backcrossed greater than 12 generations to C57/Bl6J. All experiments were performed by comparing adult wild type and mutant littermates (2-3 months old). Animal housing and experimental procedures are in agreement with veterinary law of the canton of Zurich.

CT and MR Scanning and analysis

The skulls of 20 mice per genotype were scanned with in vivo 3D micro computed tomography (Quantum Fx, Perkin Elmer, Waltham MA). All mice were sacrificed prior to scanning and placed in the micro CT in ventral recumbency with the head centered to the field of view. Scans were taken with an isotropic voxel resolution of 59 µm. The protocol used 90 kV and 100 µA with 50 msec per projection resulting in a total scan time of 3 minutes for 360°. 3D surface reconstructions of all skulls were created using the Quantum Fx viewer and assessed/scored for signs of deformation and morphological anormalies by two independent investigators. Analysis of skull parameters was done as described in (*30*). Micro MR images were acquired as described in (*31*) via high-resolution MRI of mouse brain at 9.4T using a cryogenic quadrature transceiver coil. (Inplane image resolution 60x60mm2).

Mouse Behavioral Experiments

STATISTICAL MODELS: Data were analyzed using mixed ANOVA models with genotype (KO, WT) as between-subject factor. Within-subject factors were added as needed to explore the dependence of genotype effects on place, time, or stimulus. Significant interactions and, where necessary, significant main effects were further explored by Tukey-Kramer post-hoc tests or by splitting the ANOVA model, as appropriate. One-sample t-tests were used for follow-up comparisons against chance levels. Variables known to produce strongly skewed distributions and/or frequent outliers were subjected to a log transformation before ANOVA analysis (as indicated, e.g. latency measures). The significance threshold was set at 0.05. The false discovery rate (FDR) control procedure of Hochberg was applied to groups of conceptually related variables within single tests to correct significance thresholds for multiple comparisons.

Prepulse Inhibition: The session consists of a series of six 40-ms startling pulses of different intensities varying between 100 and 120 dB in order to get an average magnitude of the initial animal's startle response. The animal is then subjected to a succession of 6 discrete trials. Each trial includes a short period of background white noise (control no- stimulus condition), followed by 20-ms pre-pulses (4, 8, 12, 16, and 20 decibels above the background white noise) and 40-ms startling pulses (100 to 120 dB) presented either separately or in combination (pre-pulse + pulse, with a delay of 100 ms between the two stimuli). The session is completed with additional six 40-ms startling pulses and background noise. The time interval between two stimulus presentations can vary between 10 and 20 seconds.

Elevated plus maze: The apparatus is a crossbar-shape maze, comprising two symmetrically arranged open arms equipped with 3-mm ledges and two closed arms equipped with 20-cm walls. The intersection of the 4 arms forms a small central zone (5 cm x 5 cm). The maze is elevated 38 cm from the ground. The whole apparatus is made of semi-transparent Plexiglas. The mouse is put on the central platform, the head facing a closed arm. The session lasts 5 min, starting once it enters the four paws in to one arm, whichever close or open. The behavioral parameters are recorded on-line.

Open-field Test: The large open-field arena is circular with a diameter of 150 cm, a white plastic floor, and 35 cm high sidewalls made of white polypropylene. Illumination is by indirect diffuse room light (4 40W bulbs, 12 lux). Each subject is released near the wall and observed for 10 min. The same procedure is repeated the following day, resulting in a total observation time of 20 min. Movements are tracked using Noldus EthoVision. The number of deposited fecal boli is recorded after each session.

Light-Dark box: A 20x30 cm lit chamber with transparent Perspex walls (20 cm high) and open top is connected to a 20x15x20 cm polyvinyl-chloride box. The box is dark (ca. 10 lux) and completely enclosed, except for the 7.5x7.5 cm opening connecting it to the lit chamber. The lit chamber is under direct room light (ca. 450 lux). Each subject is released in the middle of the lit compartment and observed for 5 min. Movements are tracked using Noldus EthoVision. Rearings and grooming are recorded using the keyboard event-recorder provided by the video-tracking system.

Morris Water Maze: This test was conducted as described previously (*32*), in ca. 12-lux light in a 150cm-diameter water pool. Six trials are conducted per day, each separated by 30-60min and lasting 2min, either learning (15x15cm platform 0.5cm above the water surface), or testing (platform 0.5cm below water surface). Three days of acquisition and two days of reversal training are conducted. Movements are tracked using Noldus Ethovision. Mouse performance was evaluated using Gallagher's measure of proximity (the average distance away from the goal during the test) and Whishaw's error (% path outside a 18cm wide straight corridor connecting release point and goal) (*33, 34*).

Expression analyses

Total cultured human and mouse skin fibroblast RNAs were isolated using the RNeasy Mini Kit (Qiagen). RNA quality was assessed using RNA Nano LabChips and the 2100 Bioanalyzer (Agilent Technologies) and RNA concentration was measured by spectrophotometry (Nanodrop, Thermo Scientific). Briefly, 100 ng of total RNA was reverse transcribed, and second strand DNA was produced and

amplified by *in vitro* transcription in the presence of biotinylated ribonucleotides using the IVT Express kit (Affymetrix). Microarray experiments were performed for 2 controls and 2 patients in duplicate on the Affymetrix Human PrimeView Arrays (a genome wide array with 49293 probe sets), hybridized with fragmented amplified RNA as recommended by the manufacturer. Similarly, mouse RNAs from 2 *Nono*^{gt} and 2 WT mice were hybridized on Affymetrix GeneChip® Mouse Genome 430 2.0 Arrays (a genome wide array allowing the analysis of 39,000 transcripts). Fluorescence data were imported into two analysis softwares: Affymetrix® Expression Console™ and R Bioconductor. Gene expression levels were calculated using the RMA algorithm Expression Console and flags were computed using a custom algorithm within R [http://www.r-project.org/]. Assuming that a maximum of 80% of genes are expressed we select the 20% lowest values for each microarray to be background expression data measures. We have then computed a threshold at two standard deviations over the mean of the background. All probes which normalized intensity measures were lower than the computed threshold were flagged 0 instead of 1. The list has been created filtering probes flagged as 1 for at least half of the chips. The group comparisons were done using Student's *t* test. To estimate the false discovery rate we filtered the resulting p-values at 5% and used the Benjamini and Hochberg, Bonferroni or without correction. Cluster analysis was performed by hierarchical clustering using the Spearman correlation similarity measure and average linkage algorithm.
Meta-analysis of human and mouse samples types was performed as previously described[36].

Mouse hippocampal RNAs were extracted using a GenElute Mammalian Total RNA Miniprep Kit (Sigma, St Louis, MO, USA) according to the manufacturer's instructions. Total RNA was quantified by absorbance spectroscopy and RNA integrity and quality was assessed by 1.0% agarose gel electrophoresis. Total RNA (1 µg) was transcribed to cDNA with SuperScript II (Invitrogen, Carlsbad, CA, USA) using random hexamer primers according to the manufacturer's instructions.
For quantitative real-time PCR (qPCR), 20 ng of cDNA was used, and single transcript levels of genes were detected with the HOT FIREPol EvaGreen qPCR Mix (Solis BioDyne, Tartu, Estonia) and an AB7900 thermocycler. Primers used for detection of synaptic transcripts were as follows:

β-Actin Fwd	AGTGTGACGTTGACATCCGTA
β-Actin Rev	GCCAGAGCAGTAATCTCCTTCT
GABRA1 Fwd	GGTTGACCGTGAGAGCTGAA
GABRA1 Rev	CTACAACCACTGAACGGGCT
GABRA2 Fwd	CAGTGGCCCATAACATGACAAT
GABRA2 Rev	GGACATTCGGCTTGGACTGT
Gephyrin Fwd	GGCGACCGAGGGAATGAT
Gephyrin Rev	CCACCCAACAAAGAAGGATCTT
CamK2a Fwd	CCCCTTTCGCCTACATGTGA
CamK2a Rev	GGCTACAGTGGAGCGGCTTA

Data were analyzed using the comparative CT method (Schmittgen & Livak, 2008).

For transcriptome analysis using RNA-Seq, the quality of the isolated RNA was determined with a Qubit® (1.0) Fluorometer (Life Technologies, California, USA) and a Bioanalyzer 2100 (Agilent, Waldbronn, Germany). RNAs were then processed using The TruSeq Stranded mRNA Sample Prep Kit (Illumina, Inc, California, USA) according to the manufacturer recommendations. The TruSeq SR Cluster Kit v3-cBot-HS or TruSeq PE Cluster Kit v3-cBot-HS (Illumina, Inc, California, USA) was used for cluster generation using 8 pM of pooled normalized libraries on the cBOT. Sequencing was performed on a Illumina HiSeq 2000 system using the TruSeq SBS Kit v3-HS (Illumina, Inc, California, USA) with paired end 2 X100 reads or single end 1X100 reads.

RNA-seq reads were quality-checked with fastqc which computes various quality metrics for the raw reads. Reads were aligned to the genome and transcriptome with tophat v 1.3.3. Before mapping the low quality ends of the reads were clipped (3 bases from the read start and 10 bases from the read end). Tophat was run with default options. The fragment length parameter was set to 100 bases with a standard deviation of 100 bases. Based on these alignments the distribution of the reads across genomic features was assessed.Isoform expression was quantified with the

RSEM algorithm (http://www.biomedcentral.com/1471-2105/12/323) with the option for estimation of the read start position distribution turned on.

Meta-analysis of human and mouse samples types was performed as previously described (*35*).

Cell culture and transfection

Human primary fibroblasts were cultured at 37°C under 5% CO2 in RPMI® + glutamax or OPTI-MEM® + glutamax supplemented with 10% of fetal bovine serum (FBS) and 5% of penicillin/streptomycin (complete medium) (Life Technologies).

Mouse primary hippocampal neuron cultures were prepared as described previously (*36*). Hippocampal cultures were transfected with 0.5 µg of either eGFP–gephyrin or the specific myc–NONO construct according to the protocol described previously (*36*). Cells were transfected after 8 DIV and processed for immunofluorescence 7 days later (referred to as 8+7 DIV). In co-transfection experiments the total DNA concentration was maintained at 1.5 µg.

Plasmids used for transfection

The eGFP–gephyrin P1 variant has been described previously (*37*). Overexpression of myc-NONO and myc-NONO RRM, were conducted using the plasmids described in (*38*). GABRA2 was created amplifying rat cDNA by primers containing HindIII and XhoI sites and subsequent cloning into the pCR3.1 vector.

Western blot

Human primary fibroblasts protein extracts were prepared on ice in lysis buffer (50 mM Tris pH 8, 170 mM NaCl, 0.5% NP-40 X-100, 50 mM NaF, and Complete EDTA-free protease inhibitor 11697498001, Roche Applied Science). The Bradford protein assay was used to determine the concentration of each sample (B6916-500 Sigma). 20-30µg of protein extracts were separated by 4-20% SDS-PAGE (SDS-PAGE Mini-PROTEAN® TGX Stain Free™ #4568093 Biorad). Stain Free gels were exposed to

UV light for 2'30" prior to transfer to 0.2 µm nitrocellulose membranes (Trans-Blot Turbo Transfer Pack #1704158 Biorad). UV-induced fluorescence corresponding to total proteins were first visualized with ChemiDoc MP imaging system, then blocked with 5% nonfat dried milk powder (Invitrogen) diluted in PBS-T (1XPBS with 0.2% Tween-20) for 1-2H and incubated overnight at 4°C in 2% milk in PBS-T with the primary antibodies: NONO, SFPQ, PSPC1, and β-actin used as a control for protein loading. Membranes were then incubated with horseradish peroxidase–conjugated secondary antibodies. Proteins were visualized using ECL-Plus (GE Healthcare). Various exposure times were performed for either autoradiography films and AGFA development (Curix 60 n°1829) or Chemidoc system (Biorad). Raw signal intensities were first obtained for target proteins as well as total proteins profile, with the same sample as reference, using volume tools in the ImageLab software (Biorad). Background signal was deducted from each value. Final quantification data were given as a ratio of target signal to total signal.
Mouse brain lysate and sample preparation were performed as described[40]. Each lane was loaded with 50 µg protein and after blotting, the nitrocellulose membrane was directly blocked for 30 min with 1% solution of Western Blocking Reagent (Roche Applied Science, Indianapolis, US).

Antibodies

The following antibodies were used: Human Antibodies: mouse anti-β-actin (AM4302, 1:20,000; Ambion), rabbit anti-NONO (LS-C31127, 1:2,000; LSBio Cliniscience), rabbit anti-SFPQ (A301-320A, Bethyl), mouse anti-PSPC1 (sc-374181, 1:1,000; Santa Cruz), Mouse anti-gephyrin antibody (mAb7a, 1:3000; or 3B11, 1:10000; Synaptic Systems, Gottingen, Germany), rabbit anti-vGAT antibody (1:3000, Synaptic Systems, Gottingen, Germany), guinea pig anti-GABAAR α2 subunit antibody[41], mouse anti-Myc (1:10000, Roche), rabbit anti-NONO (1:500, (*40*)), rabbit anti-PSPC1 (1:500, (*40*)). rabbit anti-SFPQ (1:500, (*40*)), NeuN (MAB377, Milipore), GFAP (Z0334, DAKO and MAB360, Millipore), PSD-95 (MA1-045, Affinity Bioreagents), β-actin (MAB1501, Millipore). Secondary antibodies were Donkey anti-rabbit IgG-HRP antibody (1:20,000; sc-2313, Santa Cruz) or donkey anti-mouse IgG-HRP antibody (1:20,000; sc-2314, Santa Cruz).

Immunocytochemistry and Imaging on human skin fibroblasts

Cells were harvested and seeded one day prior to immunocytochemistry experiment with equal cell density for each well. 24H later, cells were rinsed twice in PBS and fixed in IC fixation buffer (FB001 Invitrogen) for 10 minutes at room temperature. Cells were then permeabilized with 0.5% Triton X-100 for 10 minutes at room temperature. After 3 PBS washes, blocking was done with 5% BSA diluted in 0.1% Triton-PBS for 30 minutes at room temperature. Hybridization was performed with the first antibodies used in Western blotting experiments in a moist chamber overnight at 4°C. After 3 x 10 minutes 0.1% Triton-PBS washes, the following detections were carried out with secondary antibodies Alexa488 anti-rabbit IgG (1:400, A-11034, Life Technologies) and Alexa594 anti-mouse IgG (1:400, A-11005, Life Technologies) for 1H at room temperature in a dark and moist chamber. After 3 x 10 minutes 0.1% Triton-PBS washes and a final PBS wash, slides were mounted with ProLong (P36935, Invitrogen). Images were taken with a Zeiss LSM700 microscope fitted with a Plan-Apochromat 40x/1.3 Oil DIC M27 objectif and the Zen 2009 software. Images montage was done using ImageJ.

Immunocytochemistry and immunohistochemistry on mouse samples

Immunocytochemistry was performed as described previously (*41*). In short, cells were rinsed in PBS and fixed for 10 minutes in 4% paraformaldehyde at room temperature. Cells were permeabilized with 0.01% Triton X-100 and detection of intracellular proteins were achieved by incubation for 60 minutes at room temperature with primary antibodies diluted in PBS containing 10% normal serum, followed by incubation with secondary antibodies coupled to Cy3 or Cy5 (1:500, Jackson ImmunoResearch) for 30 minutes at room temperature. Finally, coverslips were mounted with fluorescent mounting medium (Dako Cytomation, Carpinteria, CA). The GABAARα2 subunit antibody was incubated in living cultures for 90 minutes in culture medium (*42*).

Staining and immunhistochemical analysis of synaptic components was performed as previously described (*43*). Briefly, mice were anesthetized with pentobarbital and perfused intracardially with ice-cold, oxygenated ACSF. The brain was extracted and cut in blocks containing the regions of interest for analysis (e.g. hippocampal

formation). The Tissue was plunged into ice-cold, freshly prepared fixative (4% PFA in PBS) and postfixed for 90 min, rinsed with phosphate-buffered saline (PBS), cryoprotected overnight in 30% sucrose in PBS and frozen with powdered dry ice and stored at –80 °C.

Sections were cut from frozen blocks with a sliding microtome at a thickness of 40 µm and were collected free-floating in PBS. They were incubated under continuous agitation in primary solution (Tris buffer (pH 7.4) containing 0.2 Triton X-100, 2% normal serum and the primary antibodies) for 15–48 h at 4 °C, washed in Tris buffer and incubated for 30–60 min at room temperature in secondary antibodies coupled to a fluorochrome.

Immunofluorescence images were captured by laser scanning confocal microscopy, using a 20x, 40x or 64x lens respectively (NA 1.4, 1024 x 1024 pixels, Zeiss LSM 710). Final illustrations were prepared from the maximal intensity projection of stacks of images spaced at 0.5 µm. Signals were quantified, using a custom macro created with the ImageJ software. Images were back- ground-subtracted and filtered with a Gaussian filter, but no change in brightness and contrast was applied.

High-resolution *in-situ* hybridization

Dissociated hippocampal neurons were prepared and maintained as previously described (*41*). *In situ* hybridization was performed using the QuantiGene (QG) ViewRNA kit from Panomics as previously described with the following modifications. Cells (DIV 14) were incubated for 2 min at room temperature in PBS and fixed for 15 min using 4% formaldehyde solution (in PBS pH 7.4). After fixation, cells were permeabilized using a detergent solution (Panomics) for 5 min. Cells were washed three times with PBS followed it with in situ hybridization using GABRA2 and pan collybistin (*Arhgef9*) probes designed by Panomics, following the manufacturer's instructions. Briefly, probes were diluted 1:100 in hybridization buffer supplied by Panomics, incubated at 40°C (3hr), washed, hybridized with preamplification oligonucleotides (1:100) at 40°C (40 min), washed, hybridized with amplification oligos (1:100) at 40°C (40 min), washed, and finally hybridized with the label oligos (1:100) at 40° C (40 min). Cover-slips were dried at RT in vertical position. Coverslips were mounted with Dako-DAPI fluorescent mounting Medium (Dako S3023) and left to polymerize overnight at 4°C.

Synaptosome preparation

Synaptosomes have been prepared as described in (*44*). In brief, mouse brains were homogenized in 5 ml homogenization buffer (0.32 M sucrose, 1 mM EDTA pH 7.4, 1 mM dithiothreitol, phenylmethanesulfonyl fluoride solution (Sigma, 93482-50ML-F), complete mini-protease inhibitor (Roche Diagnostics) for 10 sec using a polytron. The homogenate was centrifuged at 1,000g for 10 min at 4 °C yielding the nuclear fraction (Nuc) and the supernatant (Sup). The supernatant was centrifuged at 31,000g for 5 min at 4°C using a discontinuous Percoll gradient. The layer between 3% and 10% of Percoll were collected, washed in 30 ml of homogenization buffer and further centrifuged at 22,000 × g for 15 min at 4°CT. The pellet was resuspended in in EBC buffer (50 mM Tris-HCl pH 8.0, 120 mM NaCl and 0.5% NP-40) containing complete mini-protease inhibitor (Roche Diagnostics) and phosphatase inhibitor cocktail 1 and 2 (Sigma–Aldrich)) for Western blot analysis or lysis buffer for RNA extraction (GenElute Mammalian Total RNA Miniprep Kit, Sigma).

Circadian analysis of patient fibroblasts.

Analysis of circadian clock function in dermal fibroblasts from patients and controls was performed exactly as described in (*45*). In brief, dermal fibroblasts were infected with the *pBluFpuro* lentivirus, containing a circadian reporter consisting of the human *Bmal1* promoter driving expression of luciferase. After selection, identical plates of cells were grown, and their circadian clocks were synchronized with the hormone dexamethasone. Subsequently, bioluminescence in each plate of cells was monitored by real-time bioluminescence for five days in a custom-constructed luminometer. Data were detrended by subtraction of a 24-hour running average, and period length and amplitude were calculated using the Lumicycle Analysis software package (Actimetrics).

References

29. E. Kowalska *et al.*, Distinct roles of DBHS family members in the circadian transcriptional feedback loop. *Molecular and cellular biology* **32**, 4585 (Nov, 2012).

30. B. Yang *et al.*, Sh3pxd2b mice are a model for craniofacial dysmorphology and otitis media. *PloS one* **6**, e22622 (2011).
31. C. Baltes, N. Radzwill, S. Bosshard, D. Marek, M. Rudin, Micro MRI of the mouse brain using a novel 400 MHz cryogenic quadrature RF probe. *NMR in biomedicine* **22**, 834 (Oct, 2009).
32. M. H. Mohajeri *et al.*, Intact spatial memory in mice with seizure-induced partial loss of hippocampal pyramidal neurons. *Neurobiology of disease* **12**, 174 (Apr, 2003).
33. M. Gallagher, R. Burwell, M. Burchinal, Severity of spatial learning impairment in aging: development of a learning index for performance in the Morris water maze. *Behavioral neuroscience* **107**, 618 (Aug, 1993).
34. I. Q. Whishaw, Cholinergic receptor blockade in the rat impairs locale but not taxon strategies for place navigation in a swimming pool. *Behavioral neuroscience* **99**, 979 (Oct, 1985).
35. J. Cros *et al.*, Human CD14dim monocytes patrol and sense nucleic acids and viruses via TLR7 and TLR8 receptors. *Immunity* **33**, 375 (Sep 24, 2010).
36. T. Buerli *et al.*, Efficient transfection of DNA or shRNA vectors into neurons using magnetofection. *Nature protocols* **2**, 3090 (2007).
37. B. Lardi-Studler *et al.*, Vertebrate-specific sequences in the gephyrin E-domain regulate cytosolic aggregation and postsynaptic clustering. *Journal of cell science* **120**, 1371 (Apr 15, 2007).
38. S. Kuwahara *et al.*, PSPC1, NONO, and SFPQ are expressed in mouse Sertoli cells and may function as coregulators of androgen receptor-mediated transcription. *Biology of reproduction* **75**, 352 (Sep, 2006).
39. J. M. Fritschy, H. Mohler, GABAA-receptor heterogeneity in the adult rat brain: differential regional and cellular distribution of seven major subunits. *The Journal of comparative neurology* **359**, 154 (Aug 14, 1995).
40. S. A. Brown *et al.*, PERIOD1-associated proteins modulate the negative limb of the mammalian circadian oscillator. *Science* **308**, 693 (Apr 29, 2005).
41. S. K. Tyagarajan *et al.*, Regulation of GABAergic synapse formation and plasticity by GSK3beta-dependent phosphorylation of gephyrin. *Proceedings of the National Academy of Sciences of the United States of America* **108**, 379 (Jan 4, 2011).

42. I. Brunig, A. Suter, I. Knuesel, B. Luscher, J. M. Fritschy, GABAergic terminals are required for postsynaptic clustering of dystrophin but not of GABA(A) receptors and gephyrin. *The Journal of neuroscience : the official journal of the Society for Neuroscience* **22**, 4805 (Jun 15, 2002).
43. T. Notter, P. Panzanelli, S. Pfister, D. Mircsof, J. M. Fritschy, A protocol for concurrent high-quality immunohistochemical and biochemical analyses in adult mouse central nervous system. *The European journal of neuroscience* **39**, 165 (Jan, 2014).
44. P. R. Dunkley, P. E. Jarvie, P. J. Robinson, A rapid Percoll gradient procedure for preparation of synaptosomes. *Nature protocols* **3**, 1718 (2008).
45. S. A. Brown *et al.*, Molecular insights into human daily behavior. *Proceedings of the National Academy of Sciences of the United States of America* **105**, 1602 (Feb 5, 2008).

SUPPLEMENTARY INFORMATION

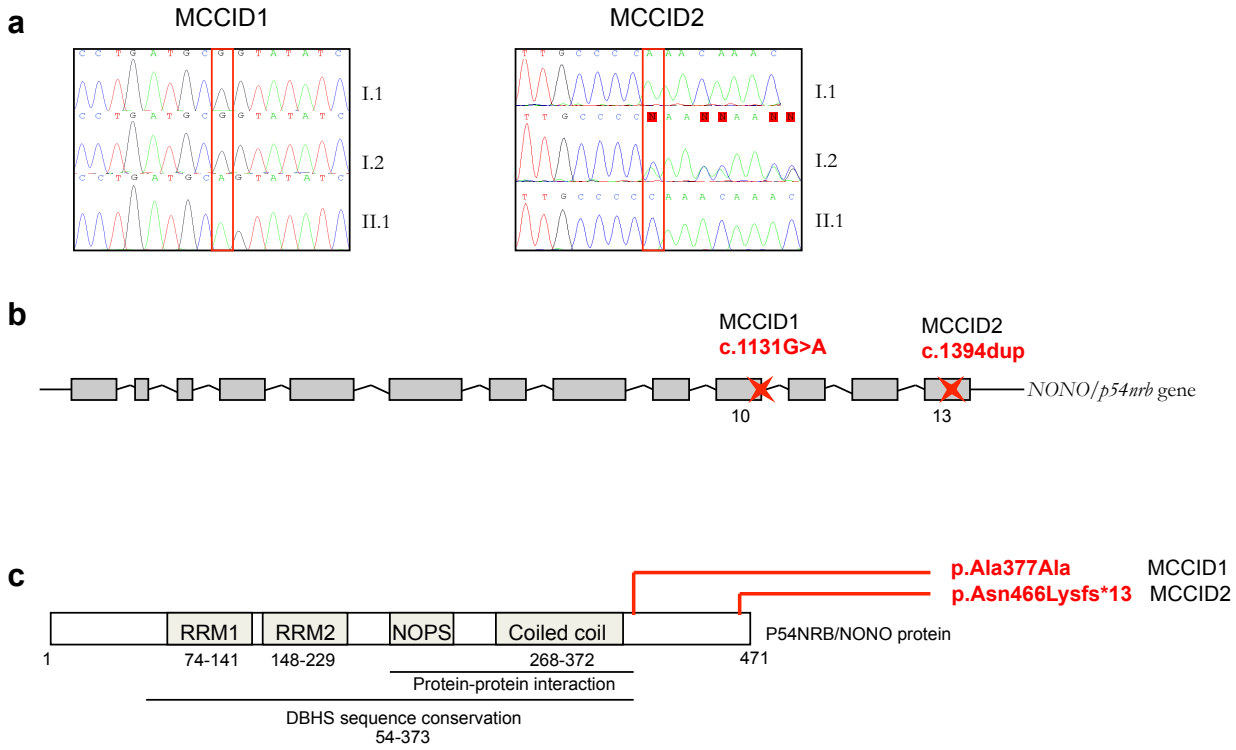

Supplementary Figure 1. Molecular analyses of patients MCCID1 and MCCID2. (**a**) Sanger sequencing chromatograms showing the NONO mutations in the probands and their parents. (**b**) Schematic representation of the NONO transcript showing exon structure. (**c**) Schematic overview of the NONO protein showing the different functional domains.

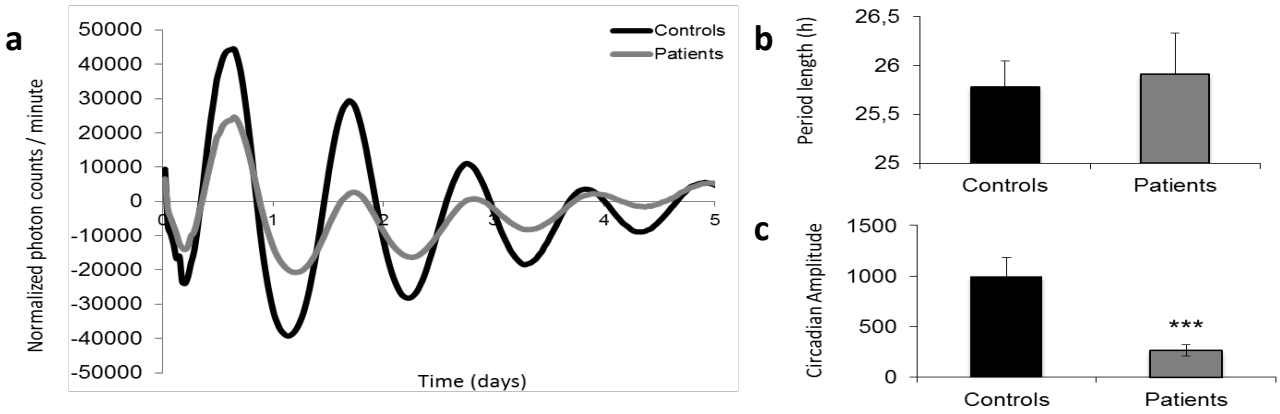

Supplementary Figure 2. Reduced circadian amplitude in patient fibroblasts. (**a**) Graph of average circadian oscillations of bioluminescence from *Bmal1-luciferase* reporter-infected fibroblasts from patients (grey) or siblings (black). Y-axis, background-subtracted bioluminescence in photons per minute; X-axis, time in days. Depicted curve is the average of three independent experiments in technical quadruplicate. (**b**) Circadian period measured in cells from controls (black bars) and patients (open bars). (**c**) Circadian amplitude measured in the same cells (arbitrary units). Student t-test, $p<0.001$. Values for both panels are the average of three independent experiments with fibroblasts from both patients and their siblings in technical quadruplicate.

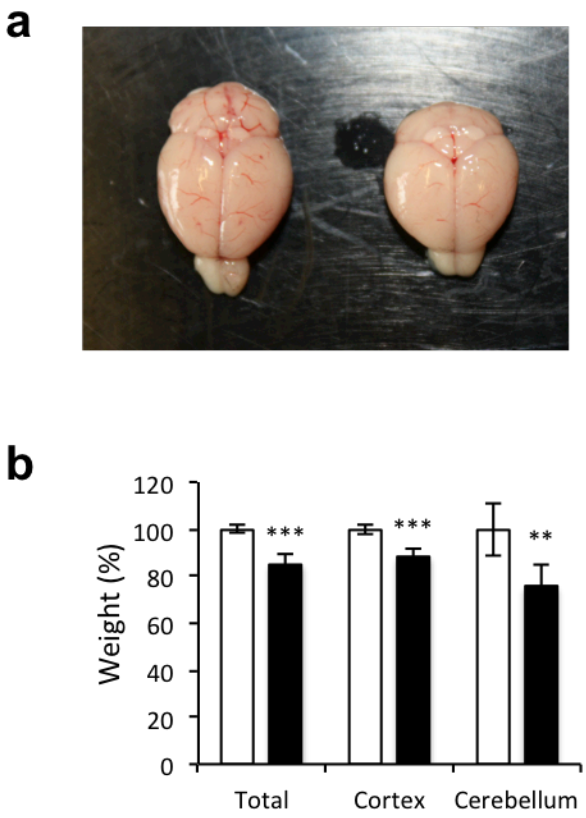

Supplementary Figure 3. Brain morphology in *Nono*^{gt} mice. (**a**) Photograph of representative brains from WT (left) and *Nono*^{gt} (right) mice. (**b**) Quantification of weight of whole brain, cortex, and cerebellum. N=5-9 mice per genotype. Student t-test. White bars, WT. Black bars, *Nono*^{gt}. In this and subsequent figures, *** p<0.001, ** p<0.01, * p<0.05. Quantification of all brain parameters from different morphological tests is shown in detail in Supplementary Table 4.

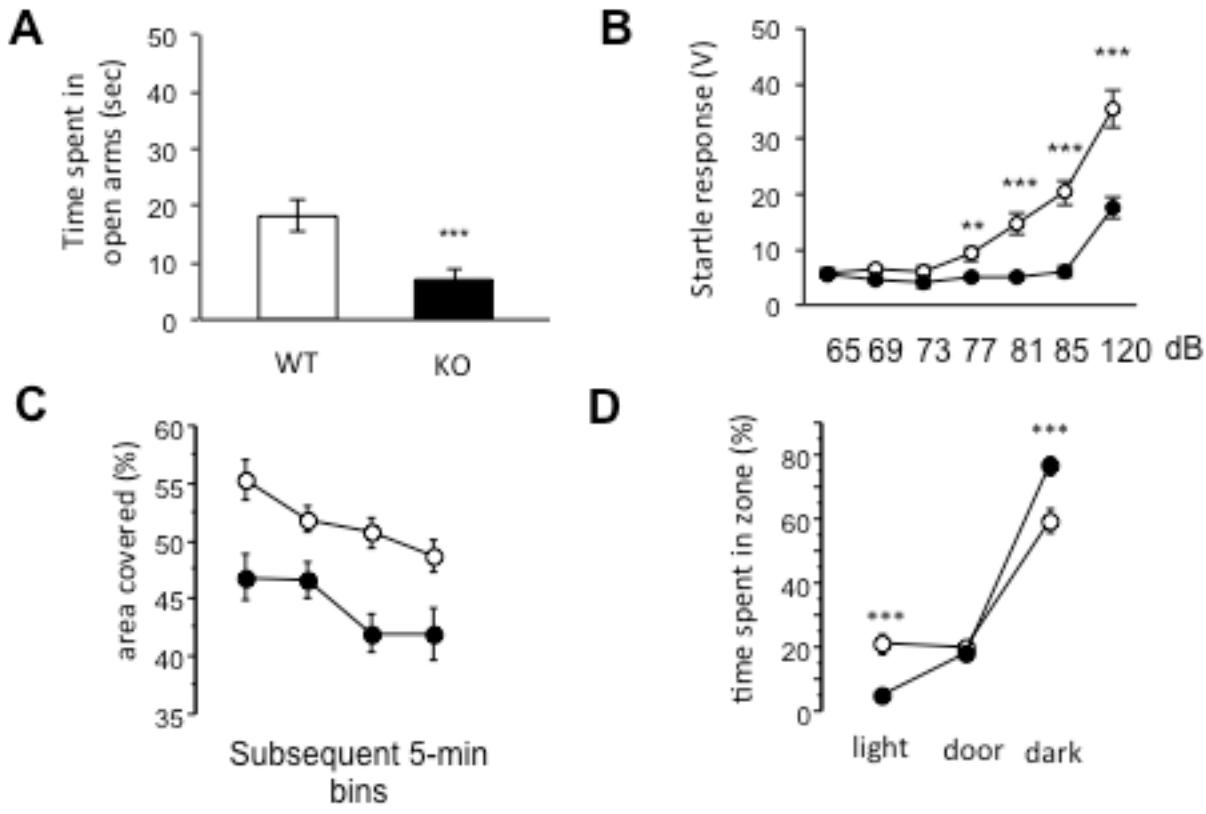

Supplementary Figure 4. Anxiety-related phenotypes in *Nono*^{gt} mice. (**a**) Percentage of time spent in open arms of elevated plus-maze. N=13-14 mice per genotype. Student t-test, p<0.001 (**b**) Post-conditioning startle response in prepulse inhibition test. Y-axis, whole-body startle response in volts; X-axis, stimulus in decibels. N=13-14 mice per genotype. Student t-test, p<0.01 or 0.001 as indicated. (**c**) Open-field exploration. Y-axis, percentage of area surface tiles visited. X-axis, subsequent 5-minute intervals after commencement of test. N=18 mice per genotype, repeated ANOVA, gene p<.0002, time p<.0001, time x gene n.s. (**d**) Light-dark transition test. Y-axis, percentage of time spent in zones indicated on X-axis. N=18 mice per genotype, repeated ANOVA, gene p<.0001, zone p<.0001, zone x gene p<0.0001. In all panels, *Nono*^{gt} mice are represented by black bars/circles, compared to WT littermates (open).

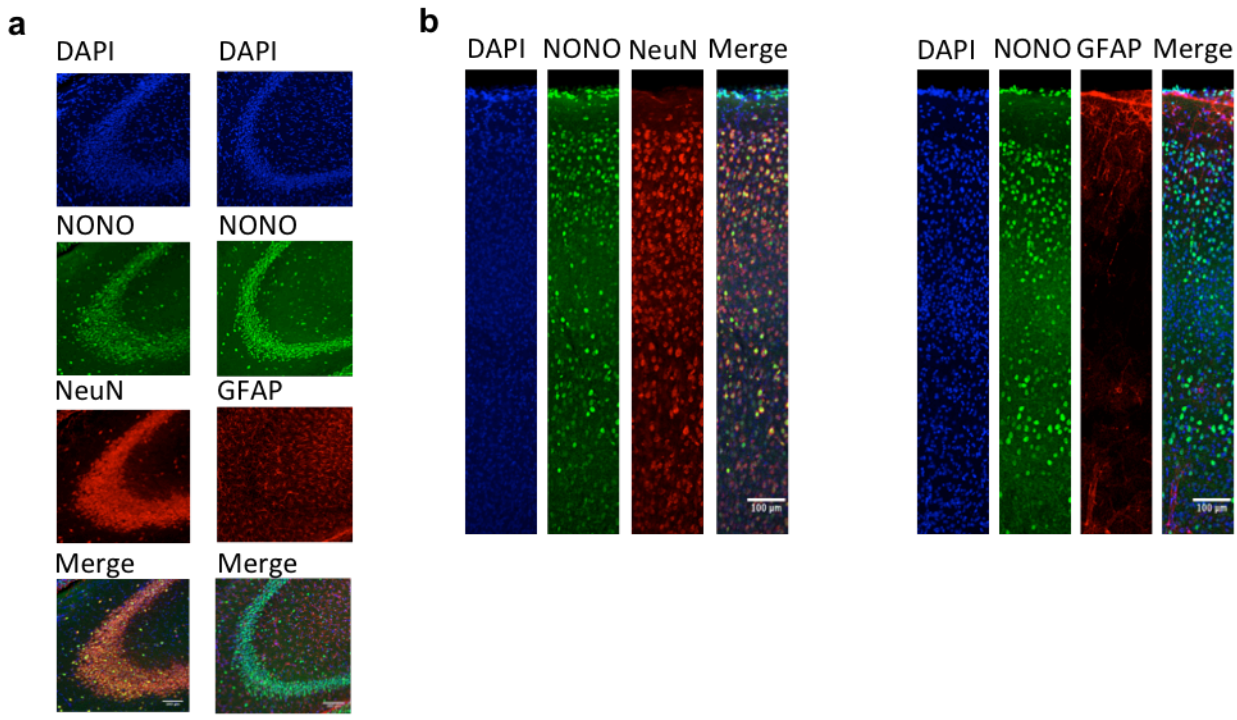

Supplementary Figure 5. Cell type and layer-specific localization of NONO in mouse brain. (**a**) Staining of hippocampal cell nuclei by DAPI (blue), anti-NONO (green), and neuron-specific anti-NeuN or astrocyte-specific anti-GFAP (red, left or right column respectively). (**b**) Identical staining of cortex.

a

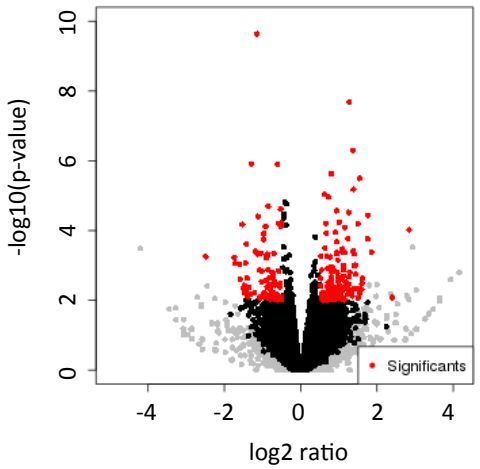

b

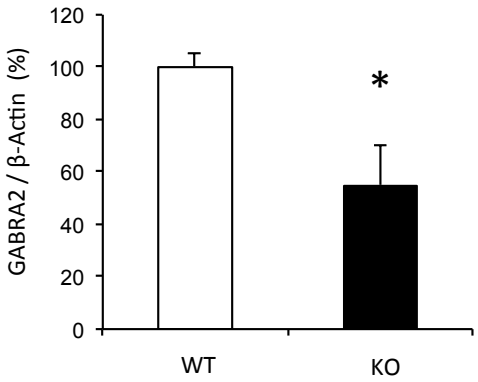

c

Identifier	Description	log2 Ratio	pValue	fdr
Nono	non-POU-domain-containing, octamer binding protein [Source:MGI Symbol;Acc:MGI:1855692]	-9.238	0	0
2900052N01Rik		-0.6108	2.99E-09	2.26E-05
Upp2	uridine phosphorylase 2 [Source:MGI Symbol;Acc:MGI:1923904]	-1.281	7.45E-09	3.75E-05
Bmper	BMP-binding endothelial regulator [Source:MGI Symbol;Acc:MGI:1920480]	0.667	3.19E-07	0.001204
Gm14420	predicted gene 14420 [Source:MGI Symbol;Acc:MGI:3652255]	-0.4389	5.07E-07	0.001532
Gpc5	glypican 5 [Source:MGI Symbol;Acc:MGI:1194894]	-0.4365	7.32E-07	0.001842
S100b	S100 protein, beta polypeptide, neural [Source:MGI Symbol;Acc:MGI:98217]	-0.4118	1.24E-06	0.002607
Gm14436		-0.5737	1.41E-06	0.002607
Gm20605	predicted gene 20605 [Source:MGI Symbol;Acc:MGI:5306917]	-0.5245	1.55E-06	0.002607
Pcdhga2		-0.8458	1.98E-06	0.002991
Fam70b		1.166	4.80E-06	0.00658
Pspc1	paraspeckle protein 1 [Source:MGI Symbol;Acc:MGI:1913895]	0.3825	5.29E-06	0.006655
Ndrg2	N-myc downstream regulated gene 2 [Source:MGI Symbol;Acc:MGI:1352498]	-0.3416	6.94E-06	0.008061
Gm14295	predicted gene 14295 [Source:MGI Symbol;Acc:MGI:3709624]	-0.5034	8.28E-06	0.008928
Sfpq	splicing factor proline/glutamine rich [Source:MGI Symbol;Acc:MGI:1918764]	0.3559	1.34E-05	0.01349
Cst3	cystatin C [Source:MGI Symbol;Acc:MGI:102519]	-0.3788	1.90E-05	0.017
Tnfrsf25	tumor necrosis factor receptor superfamily, member 25 [Source:MGI Symbol;Acc:MGI:1934667]	-0.7091	1.91E-05	0.017
Cnga4	cyclic nucleotide gated channel alpha 4 [Source:MGI Symbol;Acc:MGI:2664099]	-1.523	2.06E-05	0.01723
Rbm14	RNA binding motif protein 14 [Source:MGI Symbol;Acc:MGI:1929092]	0.3552	3.22E-05	0.02561
Gabra2	gamma-aminobutyric acid (GABA) A receptor, subunit alpha 2 [Source:MGI Symbol;Acc:MGI:95614]	-0.3623	3.47E-05	0.02622
Magt1	magnesium transporter 1 [Source:MGI Symbol;Acc:MGI:1914325]	0.4012	3.99E-05	0.02865

Supplementary Figure 6. Widespread dysregulation of transcription in *Nono*^{gt} mice hippocampi. (**a**) Volcano plot of deregulated genes. Red dots, p<0.01 and log2>0.5. (**b**) Reduced GABRA2 protein levels in hippocampi of *Nono*^{gt} mice. White bars, WT. Black bars, *Nono*^{gt}. Student t-test, N=4. (**c**) List of most severely deregulated transcripts, showing upregulation of sister DBHS family members *Sfpq* and *Pspc1*. The full dataset is available as GEO Accession number XXX.

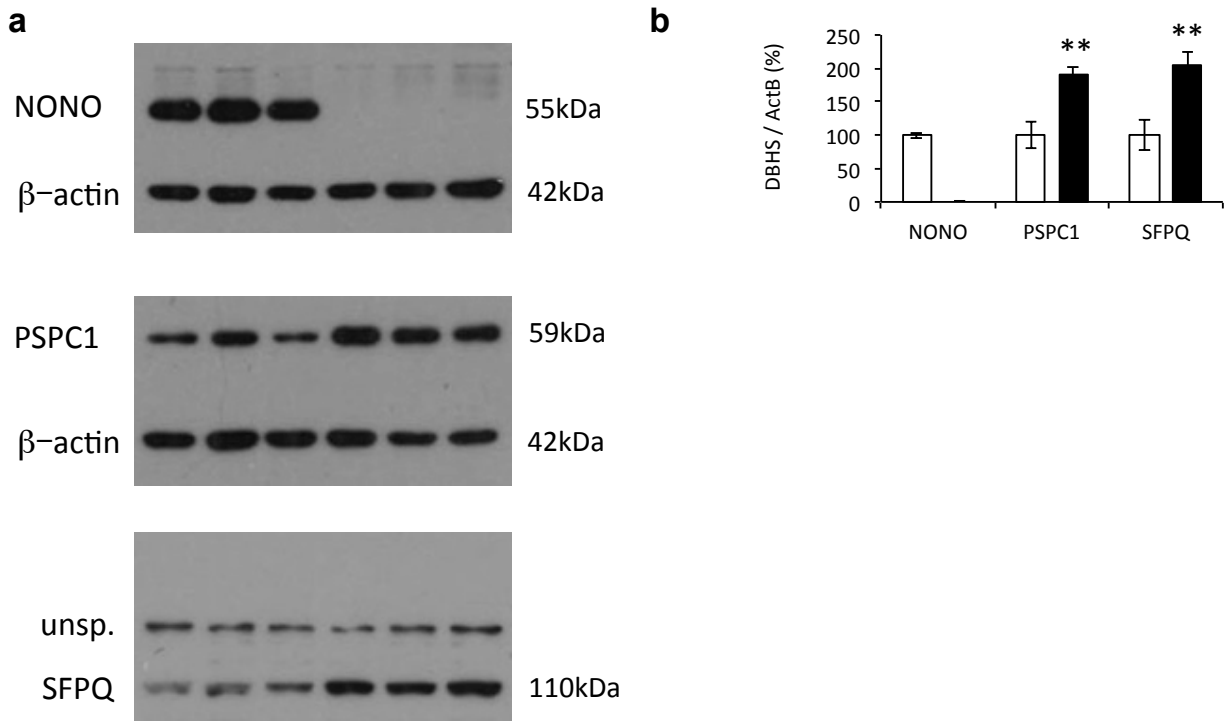

Supplementary Figure 7. Overexpression of PSPC1 and SFPQ protein in in *Nono*^{gt} mice hippocampi. (**a**) Western blots of hippocampal protein extracts from widtype and *Nono*^{gt} mice hippocampi, probed with anti-NONO, anti-PSPC1, anti-SFPQ, and anti-β-actin. N=3 mice per genotype. (**b**) Quantification of (A). White bars, WT. Black bars, *Nono*^{gt}. Student t-test, $p<0.01$.

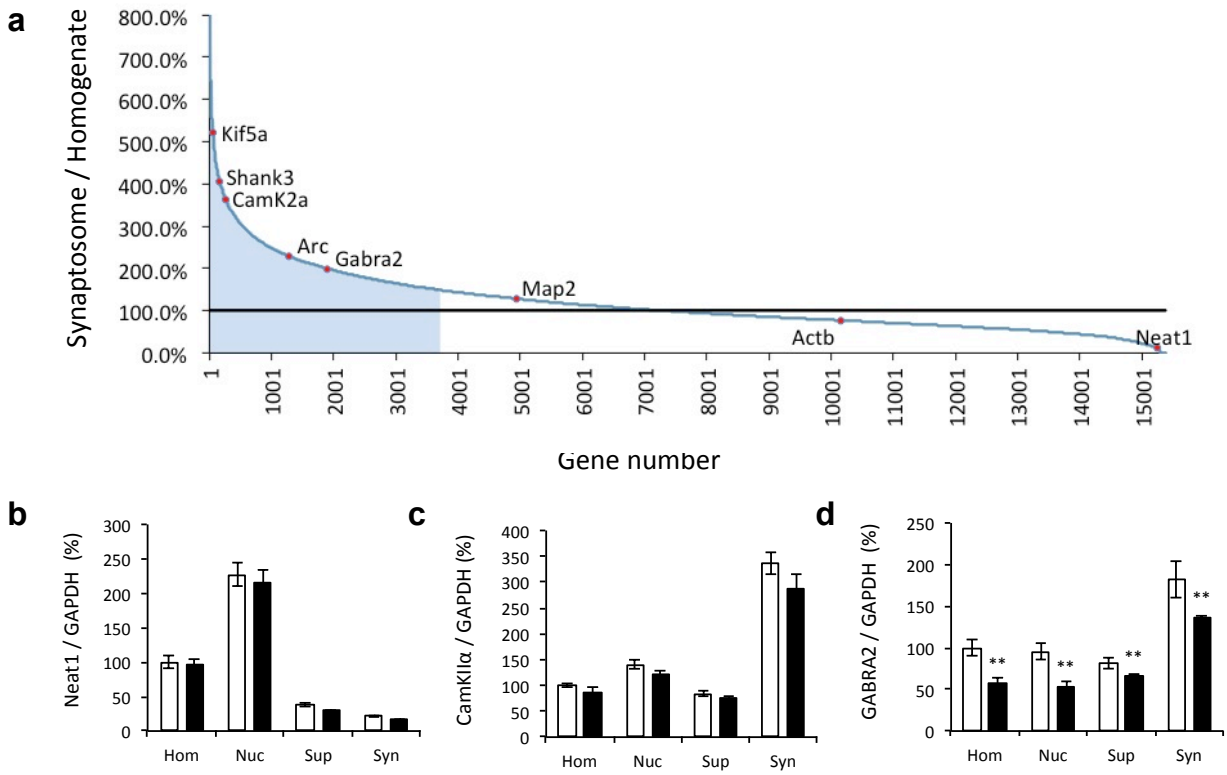

Supplementary Figure 8. Transcript abundance in different neuronal compartments in *Nono*^{gt} mice. (**a**) Profile of the mouse forebrain synaptic transcriptome. Y-axis, ratio of transcript reads from synaptome RNA sequencing compared to total. Selected transcripts previously characterized to be transported to synapses (*Kif5a, Shank3, CamK2A, Arc, Gabra2*), present throughout the cell (*Map2, Actb*), or retained in the nucleus (*Neat1*) are indicated to demonstrate the quality of synaptosomal transcript enrichment. Blue shading, transcripts more than 1.5x enriched. (**b**) Quantification of *Neat1* compared to *Gapdh* in whole-cell homogenate, purified nuclei, supernatant, or gradient-purified synaptosomes from WT (white bars) or *Nono*^{gt} mice (solid bars). (**c**) Quantification of *CamkII* compared to *Gapdh.* (**d**) Quantification of *Gabra2* compared to *Gapdh.*

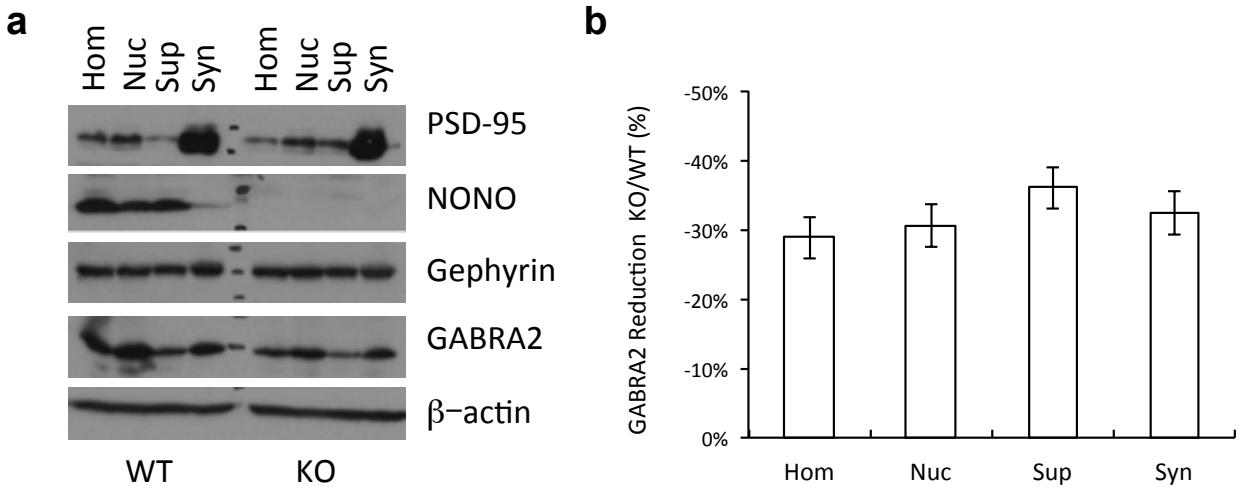

Supplementary Figure 9. Reduction of synaptic GABRA2 in *Nono*^{gt} mice. (**a**) Western blot showing fractionation of mouse forebrain into different neuronal compartments by density gradient centrifugation. Immunohistochemistry using antibodies against NONO, gephyrin, and GABA is pictured. As a control, β-actin and dendrite-enriched PSD-95 are also shown. (**b**) Quantification of the reduction in GABRA2 levels in each compartment.

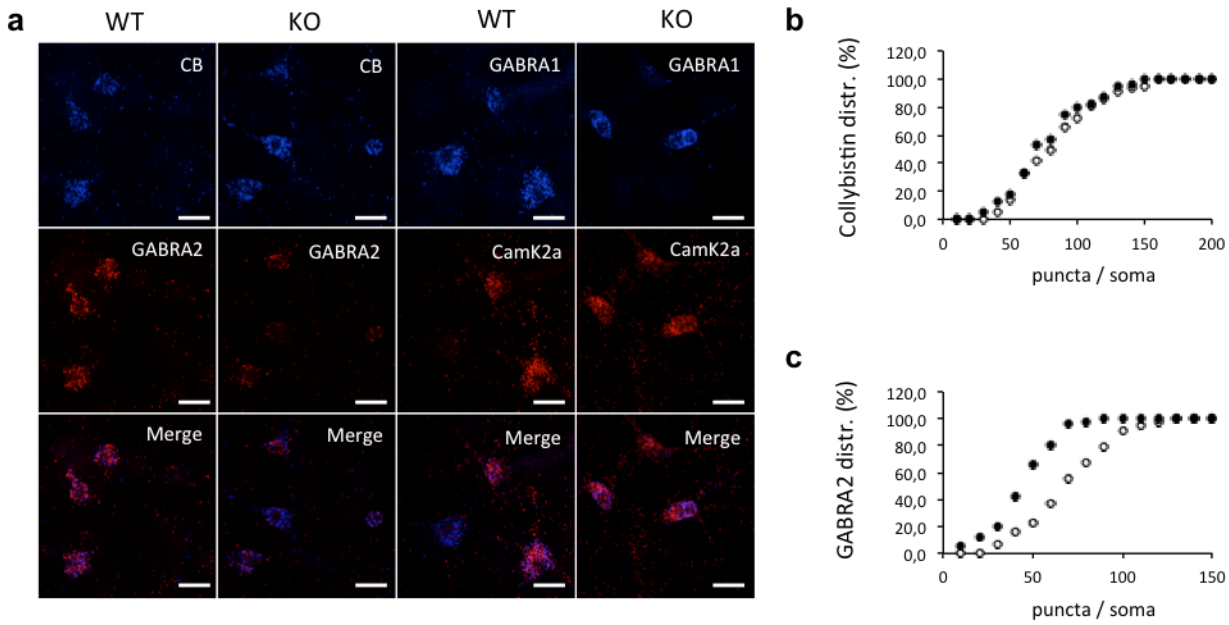

Supplementary Figure 10. Specific reduction of *Gabra2* transcript levels in cultured *Nono*^{gt} neurons. (**a**) Single-transcript-resolution RNA *in-situ* hybridization to detect abundance of *collybistin* (CB, blue), *Gabra1* (blue), *Gabra2* (red), and *CamKII* (red) in WT or *Nono*^{gt} neurons. Two transcripts were tested in different colors in a single plate of cells, and depicted in a single column. (**b**) Quantification of *collybistin* transcript distribution in puncta number per cell for 44-56 cells from 2 experiments. (**C**) Similar quantification of *Gabra2*. Solid circles, *Nono*^{gt} neurons; open circles, WT.

Supplementary Table 1: Clinical characteristics of patients with *NONO* mutations

	MCCID1	***MCCID2***
Antenatal findings	-	hydramnios
Term born	41 WG	WG
Birth parameters (BW, BL and OFC in grammes and cm)	3370 g, 50.5 cm, 34 cm	2540 g, 46 cm, 35.5 cm
Neonatal history	-	poor sucking, GR, hypotonia
Motor skills	walked at 3 y	walked at 3 y
Language	short sentences	short sentences
Nasal speach	++	++
Elocution disability	+ (severe)	+ (severe)
Drooling	+	+
ID	+	+
Epilepsy	+ (5 years)	-
Ophthalmologic findings	convergent strabismus, myopia	convergent strabismus
Behaviour	shy, gentle and cheerful	shy, gentle and cheerful
Sleep disorder	-	-
Age at examination	17 y	15 y
Growth parameters (W, H and OFS in SD)	-1.5SD, + 1SD, +4SD)	-2 SD, -2 SD, +2SD
Puberty	-	delayed
Slender built	+	+
Scoliosis	+	+++
Arachnodactyly	+	-
MCP joint ankylosis of P1	+ (bilateral)	+ (bilateral)
Pes planus	++	++
Facial features		
Long face	+	+
Palpebral fissures	up slanting	up slanting
Malar hypoplasia	++	++
Nose	Thin and high nasal root, deviated nasal septum	Thin and high nasal root, deviated nasal septum
Mouth	open	small and open
Palate	narrow and high arched	narrow and high arched
Teeth	crowding	crowding and dental caries
EEG	Abnormal	No gross anomaly
Brain MRI		
Corpus callosum	Thick (+ cyst of the septum pellucidum)	Thick
ventricles	nl	asymmetric lateral ventricles
Cerebellum	hypoplastic	Chiari malformation type I

Abbreviations are as follows:
WG : weeks of gestation; BW : birth weight; BL : birth length, OFC : occipitofrontal circumference, W : weight, H, heigth, y : year, SD : standard deviation; ID : intellectual deficiency, nl : normal, GR : gastro-oesophageal reflux, -: absent, +: present

Supplementary Table 2 : Number of variants identified by whole-exome sequencing

Patients	*MCCID1*	*MCCID2*
Total variants	64010	71478
Novel or rare variants (dbSNP130/1000GP/EVS/in-house database)	1022	1030
Coding Non-synonymous/indel/consensus SS variants	255	248
exclusively novel variants	88	87
Shared gene whose mutations co-segregate in the families	1	1

Supplementary Table 3: Differentially regulated transcripts in patients and *Nono*-deficient mice. The full dataset is available from ArrayExpress (accession E-MTAB-2894 and E-MTAB-2895),

			MCCID1			*NONO*gt mice			MCCID2		
DE Genes	Profils (MCCID1, *NONO*gt mice, MCCID2)	Full name	p-value	Fold	Delta	p-value	Fold	Delta	p-value	Fold	Delta
ACTA2	UUU	Actin, alpha 2, smooth muscle, aorta	0,00	2,93	28,06	0,00	34,96	220,94	0,02	2,34	40,08
BHLHE40	UUU	basic helix-loop-helix family, member e40	0,01	1,81	116,37	0,03	4,28	1309,55	0,01	1,63	90,20
CNN1	UUU	calponin 1, basic, smooth muscle	0,01	1,62	113,90	0,01	106,91	545,44	0,00	1,53	319,56
COL11A1	UUU	collagen, type XI, alpha 1	0,00	13,89	5906,34	0,00	697,63	4069,19	0,00	9,92	4084,12
COL12A1	UUU	collagen, type XII, alpha 1	0,00	2,06	44,11	0,01	460,70	6067,24	0,00	1,59	24,50
DKK3	UUU	dickkopf 3 homolog (Xenopus laevis)	0,01	1,52	28,35	0,03	3,36	3000,41	0,01	1,67	235,72
DLG1	UUU	discs, large homolog 1 (Drosophila)	0,00	1,75	31,84	0,01	1,58	660,25	0,00	1,82	35,24
FST	UUU	follistatin	0,01	1,61	266,91	0,05	10,45	63,58	0,01	1,60	261,20
GPC4	UUU	glypican 4	0,00	4,85	818,41	0,03	3,68	2496,10	0,00	2,07	226,85
LMCD1	UUU	LIM and cysteine-rich domains 1	0,01	1,62	73,52	0,00	83,09	479,42	0,03	2,41	828,09
MEX3B	UUU	mex-3 homolog B (C, elegans)	0,01	2,84	171,59	0,02	2,18	322,22	0,04	1,56	51,83
NCAM1	UUU	neural cell adhesion molecule 1	0,00	4,20	204,70	0,02	6,66	3332,05	0,02	1,69	43,95
PSPC1	UUU	paraspeckle component 1	0,01	2,22	494,70	0,03	2,57	615,45	0,01	2,78	721,39
RHOJ	UUU	ras homolog family member J	0,00	3,91	108,47	0,05	2,76	631,44	0,00	2,28	47,76
RNF128	UUU	ring finger protein 128, E3 ubiquitin protein ligase	0,01	2,01	33,71	0,01	11,57	102,80	0,01	3,24	74,43
SALL1	UUU	sal-like 1 (Drosophila)	0,02	2,81	139,02	0,00	57,88	280,83	0,04	2,46	71,50
SORBS2	UUU	sorbin and SH3 domain containing 2	0,00	1,79	9,28	0,03	6,09	23,75	0,01	2,19	33,14
SOX11	UUU	SRY (sex determining region Y)-box 11	0,00	1,74	8,54	0,01	30,78	155,19	0,00	4,28	37,92
TSHZ2	UUU	teashirt zinc finger homeobox 2	0,01	2,47	89,36	0,02	2,80	10,19	0,04	1,80	48,72
TWIST2	UUU	twist homolog 2 (Drosophila)	0,00	2,14	300,21	0,00	4,50	1279,81	0,00	1,98	259,25
WISP1	UUU	WNT1 inducible signaling pathway protein 1	0,00	2,40	74,30	0,01	2,21	3716,63	0,01	3,38	125,83
ABCA5	DDD	ATP-binding cassette, sub-family A (ABC1), member 5	0,00	0,41	32,25	0,04	0,25	256,57	0,00	0,59	22,15
AHR	DDD	aryl hydrocarbon receptor	0,01	0,40	579,72	0,01	0,57	31,72	0,03	0,56	429,28
ALCAM	DDD	activated leukocyte cell adhesion molecule	0,01	0,41	97,88	0,01	0,25	486,49	0,02	0,39	101,38
ARHGAP 18	DDD	Rho GTPase activating protein 18	0,00	0,47	796,59	0,00	0,21	1146,53	0,00	0,43	859,15
CCBE1	DDD	collagen and calcium binding EGF domains 1	0,00	0,25	625,52	0,02	0,18	1406,97	0,00	0,49	420,06
EBF3	DDD	early B-cell factor 3	0,00	0,28	89,36	0,02	0,24	133,74	0,04	0,37	77,64
GJC1	DDD	gap junction protein, gamma 1, 45kDa	0,03	0,58	510,20	0,02	0,38	853,36	0,05	0,60	138,37
GLCCI1	DDD	glucocorticoid induced transcript 1	0,03	0,50	85,92	0,01	0,32	177,94	0,02	0,37	107,83
GLRX	DDD	glutaredoxin (thioltransferase)	0,00	0,60	299,02	0,04	0,33	293,86	0,00	0,48	390,86

HAS2	DDD	hyaluronan synthase 2	0,02	0,62	281,41	0,01	0,32	223,83	0,00	0,44	412,14
IGF2BP3	DDD	insulin-like growth factor 2 mRNA binding protein 3	0,00	0,29	304,67	0,05	0,42	362,53	0,00	0,20	344,29
MECOM	DDD	MDS1 and EVI1 complex locus	0,00	0,55	11,32	0,03	0,49	710,76	0,00	0,63	9,14
NAV2	DDD	neuron navigator 2	0,00	0,58	262,16	0,00	0,20	155,82	0,01	0,56	277,64
NEGR1	DDD	neuronal growth regulator 1	0,01	0,56	231,28	0,01	0,04	105,79	0,03	0,58	219,71
PTER	DDD	phosphotriesterase related	0,00	0,44	157,03	0,00	0,62	262,85	0,01	0,34	42,49
RDH10	DDD	retinol dehydrogenase 10 (all-trans)	0,04	0,59	258,51	0,02	0,45	273,84	0,02	0,39	380,29
RGS20	DDD	regulator of G-protein signaling 20	0,00	0,43	65,24	0,03	0,11	325,08	0,00	0,64	40,72
RICTOR	DDD	RPTOR independent companion of MTOR, complex 2	0,00	0,45	41,60	0,01	0,55	452,22	0,01	0,54	34,98
TLE1	DDD	transducin-like enhancer of split 1 (E(sp1) homolog, Drosophila)	0,00	0,42	66,91	0,02	0,50	265,44	0,01	0,52	56,10
TRIOBP	DDD	TRIO and F-actin binding protein	0,01	0,52	69,16	0,04	0,29	1158,17	0,00	0,46	77,63
WDR20	DDD	WD repeat domain 20	0,00	0,46	99,70	0,02	0,66	60,93	0,00	0,45	102,71

D downregulated; U: upregulated

Supplementary Table 4. Quantification of brain morphology in *Nono*^{gt} mice.

	WT (%)	Stdev	NONO KO	Stdev	p Value
Brain weight	100.00	1.88	85.06	4.87	p < 0.0001
Cortex	100.00	2.13	88.25	3.69	p < 0.0001
Cerebellum	100.00	11.27	75.73	8.91	p = 0.0004
Skull lenght	100.00	1.77	91.56	4.62	p = 2.49E-7
Skull widht	100.00	2.61	96.85	6.00	p = 3.45E-6
Nose lenght	100.00	3.69	84.97	9.06	p = 6.55E-7
Relative nose length	32.47	0.90	29.86	2.67	p = 0.00019
Skull Width/Length	45.74	1.06	48.10	2.46	p = 0.00032

Supplementary Table 5. Gene ontology localization of proteins identified as dysregulated in *Nono*^{gt} mice.

#	Localizations	p-value	FDR
1	extracellular space	2.809E-13	1.103E-10
2	extracellular region part	3.250E-13	1.103E-10
3	extracellular matrix	2.233E-11	5.053E-09
4	extracellular region	7.617E-11	1.293E-08
5	plasma membrane	6.585E-10	8.943E-08
6	cell periphery	3.689E-09	4.174E-07
7	cell surface	7.807E-09	7.573E-07
8	cytoplasmic part	2.082E-08	1.767E-06
9	proteinaceous extracellular matrix	4.814E-08	3.632E-06
10	organelle	9.166E-07	6.224E-05
11	extracellular matrix part	1.813E-06	1.119E-04
12	vesicle	3.265E-06	1.848E-04
13	neuron part	4.957E-06	2.589E-04
14	plasma membrane part	6.855E-06	2.981E-04
15	neuronal cell body	7.218E-06	2.981E-04
16	external side of plasma membrane	7.241E-06	2.981E-04
17	basement membrane	7.464E-06	2.981E-04
18	neuron projection	8.693E-06	3.279E-04
19	membrane	1.022E-05	3.653E-04
20	membrane-bounded vesicle	1.111E-05	3.771E-04
21	cell body	1.958E-05	6.330E-04
22	cell projection	2.556E-05	7.890E-04
23	intracellular organelle	2.726E-05	8.047E-04
24	extracellular vesicular exosome	3.309E-05	9.362E-04
25	extracellular membrane-bounded organelle	3.969E-05	1.036E-03
26	extracellular organelle	3.969E-05	1.036E-03
27	membrane-enclosed lumen	5.667E-05	1.425E-03
28	cell projection part	7.825E-05	1.898E-03
29	integral component of plasma membrane	8.650E-05	2.025E-03
30	intrinsic component of plasma membrane	1.612E-04	3.648E-03
31	organelle lumen	1.755E-04	3.844E-03
32	dendrite	2.060E-04	4.372E-03

33	pericentriolar material	2.329E-04	4.792E-03
34	basal lamina	3.408E-04	6.807E-03
35	side of membrane	4.723E-04	9.115E-03
36	protein complex	4.833E-04	9.115E-03
37	haptoglobin-hemoglobin complex	5.051E-04	9.270E-03
38	intracellular organelle part	5.319E-04	9.505E-03
39	membrane raft	5.680E-04	9.730E-03
40	perinuclear region of cytoplasm	5.802E-04	9.730E-03
41	membrane-bounded organelle	5.875E-04	9.730E-03
42	lysosomal lumen	6.163E-04	9.964E-03
43	anchoring junction	6.784E-04	1.037E-02
44	histone acetyltransferase complex	6.835E-04	1.037E-02
45	macromolecular complex	6.872E-04	1.037E-02
46	nucleoplasm part	7.722E-04	1.119E-02
47	organelle part	7.744E-04	1.119E-02
48	vacuolar lumen	9.221E-04	1.304E-02
49	intracellular organelle lumen	9.534E-04	1.321E-02
50	lysosome	9.928E-04	1.322E-02
51	lytic vacuole	9.928E-04	1.322E-02
52	cytosol	1.061E-03	1.385E-02
53	MHC class II protein complex	1.163E-03	1.490E-02
54	perikaryon	1.266E-03	1.591E-02
55	collagen type I trimer	1.421E-03	1.750E-02
56	protein acetyltransferase complex	1.469E-03	1.750E-02
57	acetyltransferase complex	1.469E-03	1.750E-02
58	dendritic spine	1.582E-03	1.852E-02
59	paraspeckles	1.670E-03	1.916E-02
60	neuron spine	1.693E-03	1.916E-02

Supplementary Table 6. Quantification of synaptic transcripts in *Nono*^{gt} mice.

Synaptically enriched genes	3668
Total expressed genes	15393
	23.83%
NONO regulated genes	886
NONO regulated genes with synaptic localization	270
	30.47%

Chi^2 = 11.109, with 1 degree of freedom.
P = 0.0009, 2-tailed

4. General Discussion

The biological basis of learning and memory is mainly regulated by synaptic plasticity through molecular mechanisms known as Long Term Potentiation (LTP) and Long Term Depression (LTD) and it has been shown that these forms of synaptic modifications require *de-novo* protein synthesis (*164*). Over the last decades studies have demonstrated that the underlying protein translation in dendrites takes place in a small and localized fashion just next to the remodeling synapses by utilizing synaptic mRNA. Several techniques such as synaptosmal preparations and microdissections combined with high-resolution *in-situ* hybridization have greatly helped to better understand the precise local tanscriptome at the synaptic periphery. Changes of mRNA localization in the cell are the cause for regulating cell polarity and play a crucial role during development (*165*). While these mRNA dynamics at the synapse have been studied during development over long time periods (*166, 167*) or very short periods during synapse activation (*168*), determination of temporal dynamics of synaptic mRNAs over a period of 24h has not been investigated so far especially given the fact that learning and memory consolidation have been show to be regulated in a circadian fashion (*40-42*).

The fist part of the thesis focused on the identification of circadian synaptic transcpritps in the mosue brain. Transciptomic analysis identified 180 circadian genes from which only 15.5% showed rhythmicity in total brain extracts indicating a mechanism, which mainly is driven independently by the circadian transcription of transcripts in the nucleus.

One potential mechanism by which mRNA is regulated at the synapse would be the regulation of transcript stability. In mammals, mRNA localization and stability is highly regulated by its 3' untranslated region (UTR), especially by shortening of the poly(A) tail. For instance, polyadenylate-binding proteins (PABP) associate with the 3' end of mRNA to regulate polyadenylation and preventing the transcript from being degraded and therefore any factors that affect the rate of deadenylation will alter the half-life of the mRNA. One

recently identified circadian deadenylase and potential target is Nocturnin (*149*). While the role of Nocturnin (Noc) has been extensively studied in peripheral processes such as lipid metabolism, adipogenesis, glucose homeostasis, inflammation and osteogenesis, however it's localization and role in the brain remains largely unknown.

A possible link between circadian rhythms and spine formation has been recently established by the work of Passafaro and coworkers (*169*). Oligophrenin-1 is a synaptic RhoGTPase-activating protein and it has been shown to regulate dendritic spine morpholgoy in the brain (*170*). Studies of patients with X-linked intellectual disability (XLID) have revealed mutations in the gene OPHN1 gene, which codes for oligophrenin-1 (*171-176*). Interestingly, it has been found, that oligophrenin-1 and REV-ERBα, a clock genes playing a role in stabilizing the circadian rhythm by forming additional interlocked feedback loops, interact with each other at the synapse in the hippocampus. Overexpression of oligophrenin-1 in primary hippocampal neurons lead to the translocation of REV-ERBα to the synapse, while REV-ERBα localization appeared mainly nuclear upon oligophrenin-1 silencing. Furthermore, the author demonstrated, that REV-ERBα translocation is highly activity dependent. Pharmacological silencing neuronal transmission by tetrodotoxin (TTX) reduced synaptic REV-ERBα levels and blocking GABA receptors by the antagonist bicuculline showed a reciprocal effect. The synaptic localization of REV-ERBα in bicuculline treated neurons was abolished by addition of the AMPA receptor antagonist, suggesting that AMPA mediated activation induces REV-ERBα translocation to the synapse through oligophrenin-1 (*169*). By the rhythmicity of REV-ERBα in the hippocampus, a circadian synaptic translocation and modulation of the synaptic transcriptome might be a potential mechanism, by which the core clock regulates synaptic plasticity.

In previous studies, synaptic activity has been shown to initiate the active transport of mRNAs from the soma into dendrites by the association of RNA binding proteins (RBP) (*177-179*). Therefore, circadian transport of mRNA along the microtubule might be a possible mechanism in generating circadian

rhythmicity at the synapse. Given the fact, that the identified transcripts show different circadian phase, probably different RNA transport granules might be involved at different circadian time points.

An thorough analysis of Kinesin5 (Kif5) associated RNA transport granules by gel electrophoresis and subsequent proteome analysis has revealed a total of 42 proteins (134). The identified transcripts in our study show different circadian phase and therefore probably different RNA transport granules might be involved at different circadian time points. However, the precise composition of individual RNA binding granules has not been well understood and it is very likely that specific RNA binding proteins assemble differently at certain time points to transport individual mRNA transcripts.

Two of the identified proteins associated with Kif5 RNA transport granules were NONO and PSPC1. While the role of NONO and other DBHS proteins in transcription and circadian clock regulation is known, its function in synapse morphology and function is up to now unclear. In this thesis, we have shown that both NONO and PSPC1 modulate inhibitory post-synaptic structures of gephyrin and GABAA receptor α2 both *in-vitro* as well *in-vivo* using a mouse model deficient of the corresponding protein. Interestingly, NONO and PSPC1 knockout mice exhibit opposite gephyrin and $GABA_A$ receptor α2 morphology as well GABRA2 mRNA levels. This observation could be explained by two models which have been previously described in the literature for the DBHS proteins: In the first case, both NONO and PSCP1 compete as negative transcription factors with different repressive potentials for GABRA2 repression, in which NONO would be a weaker repressor compared to PSPC1 (*113, 118, 158*). In a second model, NONO would act as a positive transcription factor, while PSPC1 inhibits the transcription of GABRA2 (*92, 115, 120, 159*).

In addition, we have shown, that disrupting paraspeckles by depletion of the long-noncoding nuclear RNA Neat1 dramatically increases gephyrin and $GABA_A$ receptor α2 clustering in the mouse hippocampus. Interestingly, it has

been recently demonstrated, that nuclear speckles built along the long-nuclear RNA Malat1 (metastasis associated lung adenocarcinoma transcript 1) exhibit modulate synapse formation *in-vitro* (*180*). DNA microarray studies of Malat1 depleted neuroblastoma cells showed, that Malat1 not only regulates not only nuclear genes, but particularly genes involved in synaptogenesis such as neuroligin 1 (NLGN1) and synaptic cell adhesion molecule 1 (SynCAM1). Ultimately, depletion of Malat1 by gene silencing or overexpression in primary hippocampal neurons significantly reduced or increased synapse density (*180*). While these findings indicate a novel role for long-noncoding RNA's including Neat1 in synaptogenesis and development, the underlying mechanism still remains elusive.

Given the morphological changes in NONO deficient mice in the second part of the thesis, we aimed to look in more detail to functional consequences upon NONO depletion. We have demonstrated that NONO deficient mice exhibit behavioral and craniofacial anomalies as well as global transcriptional dysregulation in fibroblasts and hippocampal tissue. This results are strongly supported by the finding that null mutations in the NONO gene in humans are a novel cause of X-linked syndromic intellectual disability characterized by facial features as well as shy, gentle and cheerful behavior (see Study III and (*181, 182*). These findings link NONO to intellectual disability and highlight the key role of DBHS proteins in functional organization of GABAergic synapses.

Some of the most pronounced phenotypes in these patients are intellectual. A portion of these deficits might arise from effects on neural cell proliferation and differentiation, which would be consistent with the transcriptional effects that we observe upon genes related to cell growth and proliferation. Interestingly, however, in mice proliferative defects arising from NONO deficiency are closely linked to circadian clock dysfunction (*139*), and an increasing number of studies have demonstrated that alteration in the circadian system affect learning and memory. Therefore, it is possible that these symptoms are also linked to the role of DBHS proteins in the circadian transcriptional feedback loop. In Drosophila, the circadian clock controls daily changes in neuronal and synaptic structure (*145-148*). In zebrafish, induction

and/or formation of long-term memory is modulated by a circadian clock and both learning and memory formation occur better during the day than during the night (*43*). In mice, circadian fluctuations are important for learning and memory by promoting learning-associated spine formation and elimination (*66*).

In humans, several observations link cognitive disorders to circadian rhythm anomalies. Transcriptomic analyses suggest that dysregulation of circadian rhythms may be associated to bipolar disorder (*183*). Low melatonin levels have been reported in autism spectrum disorders (*54, 55, 142, 143*). Haploinsufficiency of RAI1 results in the Smith-Magenis syndrome, a disease characterized by intellectual disability, multiple congenital anomalies, obesity, neurobehavioral abnormalities and a disrupted circadian sleep-wake pattern (*184*). Moreover, RAI1 was recently shown to be a direct regulator of CLOCK, a central component of the circadian pacemaker (*185*). Finally, OPHN1, a gene responsible for X-linked ID, is required for normal circadian clock in hippocampus (*169*). Based on these observations we speculate that the impaired cognitive development observed in NONO deficient patients might be linked to aberrant circadian control of learning-dependent synaptic formation and maintenance. Further studies using more relevant cellular and animal models will be necessary to elucidate the precise mechanism underlying impaired cognitive performance in patients and potentially guide treatments.

In conclusion, our data identify NONO as a new neurodevelopmental disease gene and further support to the role of DBHS proteins in brain development and function. They suggest the existence of a clinically recognizable NONO-deficiency syndrome characterized by the association of a slender-built macrocephaly, thick corpus callosum, severe cognitive impairment and malar hypoplasia. Finally, they further argue that altered circadian rhythm may contribute to the pathogenesis of intellectual disability.

Deciphering the role of DBHS and paraspeckles in learning and memory will provide new insights into the new and unexpected role of this fascinating

regulation of RNA biology.

5. Acknowledgements

First I want to express my gratitude to my supervisor Prof. Dr. Steven A. Brown providing me the great opportunity to perform my PhD thesis in his laboratory and on this exciting field of neurobiological research. Especially I am thankful for allowing me to grow as a research scientist, for supervising this project and for the inspiring discussions. I highly esteem his scientific visions and knowledge and his motivation. I greatly enjoyed working in such a multidisciplinary field and truly appreciate his open mindedness and creativity.

Secondly, I sincerely thank my supervisor Dr. Shiva Tyagarajan, for his excellent supervision and introducing me in the complex field of inhibitory biology. I enjoyed the constructive discussions and appreciate his patient way to explain me laboratory techniques. For his encouragement and motivation I am very grateful.

I specially want to thank my committee member and partially supervisor Prof. Dr. Jean-Marc Fritschy for his help and guidance over the last years. Although he is often occupied and very busy, I was really impressed by the fact that he always took time for me when I needed his help or opinion.

Special thanks goes to my committee member Prof. Dr. Michael Kiebler for the scientific discussions and insights from a different point of view.

I want to thank my friends and labmates Christine Muheim, Ludmila Gaspar, Halim Azzi, Ermanno Moriggi, Robert Dallmann and Andreas Spinnler for they great support, motivation and scientific as well non-scientific discussions. Additionally, my thanks go to Claire de Groot and Francince Deprez for introducing me to the lab and their great support. Furthermore I want to thank Matej Žnidarič who supported me in my project and Koen Seignette for constantly challenging my view on paraspeckles.

Especially I want to thank all my collaborators, namely Prof. Laurance Colleaux, Prof. David Wolfer, Prof. Markus Rudin and Petra Seebeck, without whom this project would never have been successful as it is.

Futhermore I want to thank Giovanna Bosshard for her amazing dedication to cell culture as well bringing inspiration into my life.

Last but not least, I want to thank all my friends who have supported me during this journey.

6. List of Abbreviations

aCSF	Artificial cerebrospinal fluid
Bmal1	Brain and muscle aryl hydrocarbon receptor nuclear translocator (ARNT)-Like
CaMK	Calmodulin-dependent protein kinase
CB	Collybistin
CK1	Casein kinase 1
Clock	Circadian locomotor output cycles kaput
CNS	Central nervous system
Cry	Cryptochrome
CT	Circadian time
DBHS	Drosophila Behavior, Human Splicing protein family
DD	Constant dark
DG	Dentate Gyrus
DIV	Days in vitro
DNA	Deoxyribonucleic acid
DTT	Dithiothreitol
eGFP	Enhanced Green fluorescent protein
eIPSC	evoked inhibitory postsynaptic current
FBS	Fetal bovine serum
GABA	γ-aminobutyric acid
$GABA_AR$	$GABA_A$ Receptor
GHT	Geniculohypothalamic tract
GSK3β	Glycogen synthase kinase 3β
h	hours
KO	Knockout
lncRNA	long Non-coding RNA
LTD	Long-term potentiation
LTP	Long-trm depression
miRNA	micro RNA
MoCo	Molybdenum cofactor

mRNA	Messenger RNA
ncRNA	Non-coding RNA
NEAT1	Nuclear enriched abundant transcript 1
NMDA	N-methyl-D-aspartic acid
NONO	Non-A POU octamer binding
p54/nrb	54 kDa nuclear RNA- and DNA-binding protein
PBS	Phosphate buffer saline solution
PCR	Polymerase chain reaction
Per1	Period 1
Per2	Period 2
Poly(A)	Polyadenylation
PSD	Postsynaptic density
PSPC1	paraspeckle component 1
qPCR	Quantitative PCR
RHT	Retino hypothalamic tract
RNA	Ribonucleic acid
RRM	RNA recognition motif
SCN	Suprachiasmatic nucleus
SFPQ	splicing factor proline/glutamine-rich
vGAT	vesicular GABA transporter

7. References

1. Bell-Pedersen, D. *et al.* Circadian rhythms from multiple oscillators: lessons from diverse organisms. *Nat Rev Genet* **6**, 544-56 (2005).
2. Brown, S.A., Zumbrunn, G., Fleury-Olela, F., Preitner, N. & Schibler, U. Rhythms of mammalian body temperature can sustain peripheral circadian clocks. *Curr Biol* **12**, 1574-83 (2002).
3. Golombek, D.A. & Rosenstein, R.E. Physiology of circadian entrainment. *Physiol Rev* **90**, 1063-102 (2010).
4. Schibler, U., Ripperger, J. & Brown, S.A. Peripheral circadian oscillators in mammals: time and food. *J Biol Rhythms* **18**, 250-60 (2003).
5. Konopka, R.J. & Benzer, S. Clock mutants of Drosophila melanogaster. *Proc Natl Acad Sci U S A* **68**, 2112-6 (1971).
6. Hardin, P.E., Hall, J.C. & Rosbash, M. Feedback of the Drosophila period gene product on circadian cycling of its messenger RNA levels. *Nature* **343**, 536-40 (1990).
7. Shearman, L.P. *et al.* Interacting molecular loops in the mammalian circadian clock. *Science* **288**, 1013-9 (2000).
8. Sato, T.K. *et al.* Feedback repression is required for mammalian circadian clock function. *Nat Genet* **38**, 312-9 (2006).
9. Sangoram, A.M. *et al.* Mammalian circadian autoregulatory loop: a timeless ortholog and mPer1 interact and negatively regulate CLOCK-BMAL1-induced transcription. *Neuron* **21**, 1101-13 (1998).
10. Preitner, N. *et al.* The orphan nuclear receptor REV-ERBalpha controls circadian transcription within the positive limb of the mammalian circadian oscillator. *Cell* **110**, 251-60 (2002).
11. Guillaumond, F., Dardente, H., Giguere, V. & Cermakian, N. Differential control of Bmal1 circadian transcription by REV-ERB and ROR nuclear receptors. *J Biol Rhythms* **20**, 391-403 (2005).
12. Gallego, M. & Virshup, D.M. Post-translational modifications regulate the ticking of the circadian clock. *Nat Rev Mol Cell Biol* **8**, 139-48 (2007).

13. Dibner, C., Schibler, U. & Albrecht, U. The mammalian circadian timing system: organization and coordination of central and peripheral clocks. *Annu Rev Physiol* **72**, 517-49 (2010).
14. Morin, L.P. Neuroanatomy of the extended circadian rhythm system. *Exp Neurol* **243**, 4-20 (2013).
15. Watts, A.G., Swanson, L.W. & Sanchez-Watts, G. Efferent projections of the suprachiasmatic nucleus: I. Studies using anterograde transport of Phaseolus vulgaris leucoagglutinin in the rat. *J Comp Neurol* **258**, 204-29 (1987).
16. Watts, A.G. & Swanson, L.W. Efferent projections of the suprachiasmatic nucleus: II. Studies using retrograde transport of fluorescent dyes and simultaneous peptide immunohistochemistry in the rat. *J Comp Neurol* **258**, 230-52 (1987).
17. Abe, M. *et al.* Circadian rhythms in isolated brain regions. *J Neurosci* **22**, 350-6 (2002).
18. Granados-Fuentes, D., Tseng, A. & Herzog, E.D. A circadian clock in the olfactory bulb controls olfactory responsivity. *J Neurosci* **26**, 12219-25 (2006).
19. Jilg, A. *et al.* Temporal dynamics of mouse hippocampal clock gene expression support memory processing. *Hippocampus* **20**, 377-88 (2010).
20. Lamont, E.W., Robinson, B., Stewart, J. & Amir, S. The central and basolateral nuclei of the amygdala exhibit opposite diurnal rhythms of expression of the clock protein Period2. *Proc Natl Acad Sci U S A* **102**, 4180-4 (2005).
21. Wang, L.M. *et al.* Expression of the circadian clock gene Period2 in the hippocampus: possible implications for synaptic plasticity and learned behaviour. *ASN Neuro* **1**(2009).
22. de Jeu, M., Hermes, M. & Pennartz, C. Circadian modulation of membrane properties in slices of rat suprachiasmatic nucleus. *Neuroreport* **9**, 3725-9 (1998).
23. Green, D.J. & Gillette, R. Circadian rhythm of firing rate recorded from single cells in the rat suprachiasmatic brain slice. *Brain Res* **245**, 198-200 (1982).

24. Groos, G. & Hendriks, J. Circadian rhythms in electrical discharge of rat suprachiasmatic neurones recorded in vitro. *Neurosci Lett* **34**, 283-8 (1982).
25. Kononenko, N.I., Kuehl-Kovarik, M.C., Partin, K.M. & Dudek, F.E. Circadian difference in firing rate of isolated rat suprachiasmatic nucleus neurons. *Neurosci Lett* **436**, 314-6 (2008).
26. Kuhlman, S.J. & McMahon, D.G. Rhythmic regulation of membrane potential and potassium current persists in SCN neurons in the absence of environmental input. *Eur J Neurosci* **20**, 1113-7 (2004).
27. Pennartz, C.M., de Jeu, M.T., Bos, N.P., Schaap, J. & Geurtsen, A.M. Diurnal modulation of pacemaker potentials and calcium current in the mammalian circadian clock. *Nature* **416**, 286-90 (2002).
28. Martin, S.J., Grimwood, P.D. & Morris, R.G. Synaptic plasticity and memory: an evaluation of the hypothesis. *Annu Rev Neurosci* **23**, 649-711 (2000).
29. Barnes, C.A., McNaughton, B.L., Goddard, G.V., Douglas, R.M. & Adamec, R. Circadian rhythm of synaptic excitability in rat and monkey central nervous system. *Science* **197**, 91-2 (1977).
30. West, M.O. & Deadwyler, S.A. Circadian modulation of granule cell response to perforant path synaptic input in the rat. *Neuroscience* **5**, 1597-602 (1980).
31. Dana, R.C. & Martinez, J.L., Jr. Effect of adrenalectomy on the circadian rhythm of LTP. *Brain Res* **308**, 392-5 (1984).
32. Nishikawa, Y., Shibata, S. & Watanabe, S. Circadian changes in long-term potentiation of rat suprachiasmatic field potentials elicited by optic nerve stimulation in vitro. *Brain Res* **695**, 158-62 (1995).
33. Chaudhury, D., Wang, L.M. & Colwell, C.S. Circadian regulation of hippocampal long-term potentiation. *J Biol Rhythms* **20**, 225-36 (2005).
34. Raghavan, A.V., Horowitz, J.M. & Fuller, C.A. Diurnal modulation of long-term potentiation in the hamster hippocampal slice. *Brain Res* **833**, 311-4 (1999).
35. Nakatsuka, H. & Natsume, K. Circadian rhythm modulates long-term potentiation induced at CA1 in rat hippocampal slices. *Neurosci Res* **80**, 1-9 (2014).

36. Van der Zee, E.A. *et al.* Circadian time-place learning in mice depends on Cry genes. *Curr Biol* **18**, 844-8 (2008).
37. Mulder, C., Van Der Zee, E.A., Hut, R.A. & Gerkema, M.P. Time-place learning and memory persist in mice lacking functional Per1 and Per2 clock genes. *J Biol Rhythms* **28**, 367-79 (2013).
38. Zueger, M. *et al.* mPer1 and mPer2 mutant mice show regular spatial and contextual learning in standardized tests for hippocampus-dependent learning. *J Neural Transm* **113**, 347-56 (2006).
39. Rawashdeh, O. *et al.* PERIOD1 coordinates hippocampal rhythms and memory processing with daytime. *Hippocampus* **24**, 712-23 (2014).
40. Valentinuzzi, V.S. & Ferrari, E.A. Habituation to sound during morning and night sessions in pigeons (Columba livia). *Physiol Behav* **62**, 1203-9 (1997).
41. Valentinuzzi, V.S., Menna-Barreto, L. & Xavier, G.F. Effect of circadian phase on performance of rats in the Morris water maze task. *J Biol Rhythms* **19**, 312-24 (2004).
42. Valentinuzzi, V.S. *et al.* Memory for time of training modulates performance on a place conditioning task in marmosets. *Neurobiol Learn Mem* **89**, 604-7 (2008).
43. Rawashdeh, O., de Borsetti, N.H., Roman, G. & Cahill, G.M. Melatonin suppresses nighttime memory formation in zebrafish. *Science* **318**, 1144-6 (2007).
44. Fernandez, R.I., Lyons, L.C., Levenson, J., Khabour, O. & Eskin, A. Circadian modulation of long-term sensitization in Aplysia. *Proc Natl Acad Sci U S A* **100**, 14415-20 (2003).
45. Lyons, L.C., Green, C.L. & Eskin, A. Intermediate-term memory is modulated by the circadian clock. *J Biol Rhythms* **23**, 538-42 (2008).
46. Chaudhury, D. & Colwell, C.S. Circadian modulation of learning and memory in fear-conditioned mice. *Behav Brain Res* **133**, 95-108 (2002).
47. Pevet, P. & Challet, E. Melatonin: both master clock output and internal time-giver in the circadian clocks network. *J Physiol Paris* **105**, 170-82 (2011).

48. Benloucif, S. *et al.* Stability of melatonin and temperature as circadian phase markers and their relation to sleep times in humans. *J Biol Rhythms* **20**, 178-88 (2005).
49. Cahill, G.M. Circadian regulation of melatonin production in cultured zebrafish pineal and retina. *Brain Res* **708**, 177-81 (1996).
50. Abran, D., Anctil, M. & Ali, M.A. Melatonin activity rhythms in eyes and cerebral ganglia of Aplysia californica. *Gen Comp Endocrinol* **96**, 215-22 (1994).
51. Goto, M., Oshima, I., Tomita, T. & Ebihara, S. Melatonin content of the pineal gland in different mouse strains. *J Pineal Res* **7**, 195-204 (1989).
52. Hintermann, E., Grieder, N.C., Amherd, R., Brodbeck, D. & Meyer, U.A. Cloning of an arylalkylamine N-acetyltransferase (aaNAT1) from Drosophila melanogaster expressed in the nervous system and the gut. *Proc Natl Acad Sci U S A* **93**, 12315-20 (1996).
53. Kulman, L. While diet docs debate fats and carbs, weight loss still comes down to calories. *US News World Rep* **128**, 56 (2000).
54. Melke, J. *et al.* Abnormal melatonin synthesis in autism spectrum disorders. *Mol Psychiatry* **13**, 90-8 (2008).
55. Nir, I. *et al.* Brief report: circadian melatonin, thyroid-stimulating hormone, prolactin, and cortisol levels in serum of young adults with autism. *J Autism Dev Disord* **25**, 641-54 (1995).
56. Chung, S., Son, G.H. & Kim, K. Circadian rhythm of adrenal glucocorticoid: its regulation and clinical implications. *Biochim Biophys Acta* **1812**, 581-91 (2011).
57. Rosenfeld, P., van Eekelen, J.A., Levine, S. & de Kloet, E.R. Ontogeny of corticosteroid receptors in the brain. *Cell Mol Neurobiol* **13**, 295-319 (1993).
58. Lightman, S.L. *et al.* The significance of glucocorticoid pulsatility. *Eur J Pharmacol* **583**, 255-62 (2008).
59. Moore, R.Y. & Eichler, V.B. Loss of a circadian adrenal corticosterone rhythm following suprachiasmatic lesions in the rat. *Brain Res* **42**, 201-6 (1972).

60. Abe, K., Kroning, J., Greer, M.A. & Critchlow, V. Effects of destruction of the suprachiasmatic nuclei on the circadian rhythms in plasma corticosterone, body temperature, feeding and plasma thyrotropin. *Neuroendocrinology* **29**, 119-31 (1979).
61. Szafarczyk, A., Ixart, G., Malaval, F., Nouguier-Soule, J. & Assenmacher, I. Effects of lesions of the suprachiasmatic nuclei and of p-chlorophenylalanine on the circadian rhythms of adrenocorticotrophic hormone and corticosterone in the plasma, and on locomotor activity of rats. *J Endocrinol* **83**, 1-16 (1979).
62. Bangasser, D.A. & Shors, T.J. The hippocampus is necessary for enhancements and impairments of learning following stress. *Nat Neurosci* **10**, 1401-3 (2007).
63. de Quervain, D.J., Roozendaal, B. & McGaugh, J.L. Stress and glucocorticoids impair retrieval of long-term spatial memory. *Nature* **394**, 787-90 (1998).
64. Lupien, S.J. *et al.* Cortisol levels during human aging predict hippocampal atrophy and memory deficits. *Nat Neurosci* **1**, 69-73 (1998).
65. Liston, C. & Gan, W.B. Glucocorticoids are critical regulators of dendritic spine development and plasticity in vivo. *Proc Natl Acad Sci U S A* **108**, 16074-9 (2011).
66. Liston, C. *et al.* Circadian glucocorticoid oscillations promote learning-dependent synapse formation and maintenance. *Nat Neurosci* **16**, 698-705 (2013).
67. Ruby, N.F. *et al.* Hippocampal-dependent learning requires a functional circadian system. *Proc Natl Acad Sci U S A* **105**, 15593-8 (2008).
68. McIntire, S.L., Reimer, R.J., Schuske, K., Edwards, R.H. & Jorgensen, E.M. Identification and characterization of the vesicular GABA transporter. *Nature* **389**, 870-6 (1997).
69. Aguilar-Roblero, R. *et al.* Circadian rhythmicity in the GABAergic system in the suprachiasmatic nuclei of the rat. *Neurosci Lett* **157**, 199-202 (1993).
70. Saxena, N.C. & Macdonald, R.L. Properties of putative cerebellar gamma-aminobutyric acid A receptor isoforms. *Mol Pharmacol* **49**, 567-79 (1996).

71. Perrais, D. & Ropert, N. Effect of zolpidem on miniature IPSCs and occupancy of postsynaptic GABAA receptors in central synapses. *J Neurosci* **19**, 578-88 (1999).
72. Brickley, S.G. & Mody, I. Extrasynaptic GABA(A) receptors: their function in the CNS and implications for disease. *Neuron* **73**, 23-34 (2012).
73. Fritschy, J.M. & Mohler, H. GABAA-receptor heterogeneity in the adult rat brain: differential regional and cellular distribution of seven major subunits. *J Comp Neurol* **359**, 154-94 (1995).
74. Tyagarajan, S.K. & Fritschy, J.M. Gephyrin: a master regulator of neuronal function? *Nat Rev Neurosci* **15**, 141-56 (2014).
75. Jacob, T.C., Moss, S.J. & Jurd, R. GABA(A) receptor trafficking and its role in the dynamic modulation of neuronal inhibition. *Nat Rev Neurosci* **9**, 331-43 (2008).
76. Kralic, J.E. *et al.* Compensatory alteration of inhibitory synaptic circuits in cerebellum and thalamus of gamma-aminobutyric acid type A receptor alpha1 subunit knockout mice. *J Comp Neurol* **495**, 408-21 (2006).
77. Panzanelli, P. *et al.* Distinct mechanisms regulate GABAA receptor and gephyrin clustering at perisomatic and axo-axonic synapses on CA1 pyramidal cells. *J Physiol* **589**, 4959-80 (2011).
78. Essrich, C., Lorez, M., Benson, J.A., Fritschy, J.M. & Luscher, B. Postsynaptic clustering of major GABAA receptor subtypes requires the gamma 2 subunit and gephyrin. *Nat Neurosci* **1**, 563-71 (1998).
79. Megias, M., Emri, Z., Freund, T.F. & Gulyas, A.I. Total number and distribution of inhibitory and excitatory synapses on hippocampal CA1 pyramidal cells. *Neuroscience* **102**, 527-40 (2001).
80. Stallmeyer, B. *et al.* The neurotransmitter receptor-anchoring protein gephyrin reconstitutes molybdenum cofactor biosynthesis in bacteria, plants, and mammalian cells. *Proc Natl Acad Sci U S A* **96**, 1333-8 (1999).
81. Tretter, V. *et al.* The clustering of GABA(A) receptor subtypes at inhibitory synapses is facilitated via the direct binding of receptor alpha 2 subunits to gephyrin. *J Neurosci* **28**, 1356-65 (2008).
82. Saiepour, L. *et al.* Complex role of collybistin and gephyrin in GABAA receptor clustering. *J Biol Chem* **285**, 29623-31 (2010).

83. Maric, H.M., Mukherjee, J., Tretter, V., Moss, S.J. & Schindelin, H. Gephyrin-mediated gamma-aminobutyric acid type A and glycine receptor clustering relies on a common binding site. *J Biol Chem* **286**, 42105-14 (2011).
84. Levi, S., Logan, S.M., Tovar, K.R. & Craig, A.M. Gephyrin is critical for glycine receptor clustering but not for the formation of functional GABAergic synapses in hippocampal neurons. *J Neurosci* **24**, 207-17 (2004).
85. Sander, B. *et al.* Structural characterization of gephyrin by AFM and SAXS reveals a mixture of compact and extended states. *Acta Crystallogr D Biol Crystallogr* **69**, 2050-60 (2013).
86. Sola, M. *et al.* Structural basis of dynamic glycine receptor clustering by gephyrin. *EMBO J* **23**, 2510-9 (2004).
87. Kneussel, M. *et al.* Gephyrin-independent clustering of postsynaptic GABA(A) receptor subtypes. *Mol Cell Neurosci* **17**, 973-82 (2001).
88. Tyagarajan, S.K. *et al.* Extracellular signal-regulated kinase and glycogen synthase kinase 3beta regulate gephyrin postsynaptic aggregation and GABAergic synaptic function in a calpain-dependent mechanism. *J Biol Chem* **288**, 9634-47 (2013).
89. Tyagarajan, S.K. *et al.* Regulation of GABAergic synapse formation and plasticity by GSK3beta-dependent phosphorylation of gephyrin. *Proc Natl Acad Sci U S A* **108**, 379-84 (2011).
90. Dejanovic, B. *et al.* Palmitoylation of gephyrin controls receptor clustering and plasticity of GABAergic synapses. *PLoS Biol* **12**, e1001908 (2014).
91. Brown, S.A. *et al.* PERIOD1-associated proteins modulate the negative limb of the mammalian circadian oscillator. *Science* **308**, 693-6 (2005).
92. Kowalska, E. *et al.* Distinct roles of DBHS family members in the circadian transcriptional feedback loop. *Mol Cell Biol* **32**, 4585-94 (2012).
93. Li, S. *et al.* Double-strand break repair deficiency in NONO knockout murine embryonic fibroblasts and compensation by spontaneous upregulation of the PSPC1 paralog. *Nucleic Acids Res* **42**, 9771-80 (2014).

94. Yang, Y.S. *et al.* NonO, a non-POU-domain-containing, octamer-binding protein, is the mammalian homolog of Drosophila nonAdiss. *Mol Cell Biol* **13**, 5593-603 (1993).
95. Dong, B., Horowitz, D.S., Kobayashi, R. & Krainer, A.R. Purification and cDNA cloning of HeLa cell p54nrb, a nuclear protein with two RNA recognition motifs and extensive homology to human splicing factor PSF and Drosophila NONA/BJ6. *Nucleic Acids Res* **21**, 4085-92 (1993).
96. Myojin, R. *et al.* Expression and functional significance of mouse paraspeckle protein 1 on spermatogenesis. *Biol Reprod* **71**, 926-32 (2004).
97. Fox, A.H., Bond, C.S. & Lamond, A.I. P54nrb forms a heterodimer with PSP1 that localizes to paraspeckles in an RNA-dependent manner. *Mol Biol Cell* **16**, 5304-15 (2005).
98. Passon, D.M., Lee, M., Fox, A.H. & Bond, C.S. Crystallization of a paraspeckle protein PSPC1-NONO heterodimer. *Acta Crystallogr Sect F Struct Biol Cryst Commun* **67**, 1231-4 (2011).
99. Passon, D.M. *et al.* Structure of the heterodimer of human NONO and paraspeckle protein component 1 and analysis of its role in subnuclear body formation. *Proc Natl Acad Sci U S A* **109**, 4846-50 (2012).
100. Fox, A.H. *et al.* Paraspeckles: a novel nuclear domain. *Curr Biol* **12**, 13-25 (2002).
101. Prasanth, K.V. *et al.* Regulating gene expression through RNA nuclear retention. *Cell* **123**, 249-63 (2005).
102. Clemson, C.M. *et al.* An architectural role for a nuclear noncoding RNA: NEAT1 RNA is essential for the structure of paraspeckles. *Mol Cell* **33**, 717-26 (2009).
103. Sunwoo, H. *et al.* MEN epsilon/beta nuclear-retained non-coding RNAs are up-regulated upon muscle differentiation and are essential components of paraspeckles. *Genome Res* **19**, 347-59 (2009).
104. Sasaki, Y.T., Ideue, T., Sano, M., Mituyama, T. & Hirose, T. MENepsilon/beta noncoding RNAs are essential for structural integrity of nuclear paraspeckles. *Proc Natl Acad Sci U S A* **106**, 2525-30 (2009).

105. Bond, C.S. & Fox, A.H. Paraspeckles: nuclear bodies built on long noncoding RNA. *J Cell Biol* **186**, 637-44 (2009).
106. Chen, L.L. & Carmichael, G.G. Altered nuclear retention of mRNAs containing inverted repeats in human embryonic stem cells: functional role of a nuclear noncoding RNA. *Mol Cell* **35**, 467-78 (2009).
107. Andersen, J.S. *et al.* Directed proteomic analysis of the human nucleolus. *Curr Biol* **12**, 1-11 (2002).
108. Fox, A.H. & Lamond, A.I. Paraspeckles. *Cold Spring Harb Perspect Biol* **2**, a000687 (2010).
109. Nakagawa, S. & Hirose, T. Paraspeckle nuclear bodies--useful uselessness? *Cell Mol Life Sci* **69**, 3027-36 (2012).
110. Zhang, Z. & Carmichael, G.G. The fate of dsRNA in the nucleus: a p54(nrb)-containing complex mediates the nuclear retention of promiscuously A-to-I edited RNAs. *Cell* **106**, 465-75 (2001).
111. Kawano, S., Miyaji, M., Ichiyasu, S., Tsutsui, K.M. & Tsutsui, K. Regulation of DNA Topoisomerase IIbeta through RNA-dependent association with heterogeneous nuclear ribonucleoprotein U (hnRNP U). *J Biol Chem* **285**, 26451-60 (2010).
112. Shav-Tal, Y. & Zipori, D. PSF and p54(nrb)/NonO--multi-functional nuclear proteins. *FEBS Lett* **531**, 109-14 (2002).
113. Amelio, A.L. *et al.* A coactivator trap identifies NONO (p54nrb) as a component of the cAMP-signaling pathway. *Proc Natl Acad Sci U S A* **104**, 20314-9 (2007).
114. Bianconcini, A. *et al.* Transcriptional activity of the murine retinol-binding protein gene is regulated by a multiprotein complex containing HMGA1, p54 nrb/NonO, protein-associated splicing factor (PSF) and steroidogenic factor 1 (SF1)/liver receptor homologue 1 (LRH-1). *Int J Biochem Cell Biol* **41**, 2189-203 (2009).
115. Dong, X., Sweet, J., Challis, J.R., Brown, T. & Lye, S.J. Transcriptional activity of androgen receptor is modulated by two RNA splicing factors, PSF and p54nrb. *Mol Cell Biol* **27**, 4863-75 (2007).

116. Dong, X. *et al.* p54nrb is a transcriptional corepressor of the progesterone receptor that modulates transcription of the labor-associated gene, connexin 43 (Gja1). *Mol Endocrinol* **23**, 1147-60 (2009).
117. Hata, K. *et al.* Paraspeckle protein p54nrb links Sox9-mediated transcription with RNA processing during chondrogenesis in mice. *J Clin Invest* **118**, 3098-108 (2008).
118. Ishitani, K. *et al.* p54nrb acts as a transcriptional coactivator for activation function 1 of the human androgen receptor. *Biochem Biophys Res Commun* **306**, 660-5 (2003).
119. Keil, J.M., Liu, X. & Antonetti, D.A. Glucocorticoid induction of occludin expression and endothelial barrier requires transcription factor p54 NONO. *Invest Ophthalmol Vis Sci* **54**, 4007-15 (2013).
120. Mathur, M., Tucker, P.W. & Samuels, H.H. PSF is a novel corepressor that mediates its effect through Sin3A and the DNA binding domain of nuclear hormone receptors. *Mol Cell Biol* **21**, 2298-311 (2001).
121. Roepcke, S. *et al.* A tandem sequence motif acts as a distance-dependent enhancer in a set of genes involved in translation by binding the proteins NonO and SFPQ. *BMC Genomics* **12**, 624 (2011).
122. Yadav, S.P. *et al.* The transcription-splicing protein NonO/p54nrb and three NonO-interacting proteins bind to distal enhancer region and augment rhodopsin expression. *Hum Mol Genet* **23**, 2132-44 (2014).
123. Buxade, M., Morrice, N., Krebs, D.L. & Proud, C.G. The PSF.p54nrb complex is a novel Mnk substrate that binds the mRNA for tumor necrosis factor alpha. *J Biol Chem* **283**, 57-65 (2008).
124. Kaneko, S., Rozenblatt-Rosen, O., Meyerson, M. & Manley, J.L. The multifunctional protein p54nrb/PSF recruits the exonuclease XRN2 to facilitate pre-mRNA 3' processing and transcription termination. *Genes Dev* **21**, 1779-89 (2007).
125. Rosonina, E. *et al.* Role for PSF in mediating transcriptional activator-dependent stimulation of pre-mRNA processing in vivo. *Mol Cell Biol* **25**, 6734-46 (2005).

126. Ito, T. *et al.* Brm transactivates the telomerase reverse transcriptase (TERT) gene and modulates the splicing patterns of its transcripts in concert with p54(nrb). *Biochem J* **411**, 201-9 (2008).
127. Kameoka, S., Duque, P. & Konarska, M.M. p54(nrb) associates with the 5' splice site within large transcription/splicing complexes. *EMBO J* **23**, 1782-91 (2004).
128. Marko, M., Leichter, M., Patrinou-Georgoula, M. & Guialis, A. hnRNP M interacts with PSF and p54(nrb) and co-localizes within defined nuclear structures. *Exp Cell Res* **316**, 390-400 (2010).
129. Bladen, C.L., Udayakumar, D., Takeda, Y. & Dynan, W.S. Identification of the polypyrimidine tract binding protein-associated splicing factor.p54(nrb) complex as a candidate DNA double-strand break rejoining factor. *J Biol Chem* **280**, 5205-10 (2005).
130. Salton, M., Lerenthal, Y., Wang, S.Y., Chen, D.J. & Shiloh, Y. Involvement of Matrin 3 and SFPQ/NONO in the DNA damage response. *Cell Cycle* **9**, 1568-76 (2010).
131. Ha, K., Takeda, Y. & Dynan, W.S. Sequences in PSF/SFPQ mediate radioresistance and recruitment of PSF/SFPQ-containing complexes to DNA damage sites in human cells. *DNA Repair (Amst)* **10**, 252-9 (2011).
132. Rajesh, C., Baker, D.K., Pierce, A.J. & Pittman, D.L. The splicing-factor related protein SFPQ/PSF interacts with RAD51D and is necessary for homology-directed repair and sister chromatid cohesion. *Nucleic Acids Res* **39**, 132-45 (2011).
133. Krietsch, J. *et al.* PARP activation regulates the RNA-binding protein NONO in the DNA damage response to DNA double-strand breaks. *Nucleic Acids Res* **40**, 10287-301 (2012).
134. Kanai, Y., Dohmae, N. & Hirokawa, N. Kinesin transports RNA: isolation and characterization of an RNA-transporting granule. *Neuron* **43**, 513-25 (2004).
135. Huang, C.J., Tang, Z., Lin, R.J. & Tucker, P.W. Phosphorylation by SR kinases regulates the binding of PTB-associated splicing factor (PSF) to the pre-mRNA polypyrimidine tract. *FEBS Lett* **581**, 223-32 (2007).

136. Proteau, A. *et al.* The multifunctional nuclear protein p54nrb is multiphosphorylated in mitosis and interacts with the mitotic regulator Pin1. *J Mol Biol* **346**, 1163-72 (2005).
137. Karhumaa, P. *et al.* Nuclear NonO/p54(nrb) protein is a nonclassical carbonic anhydrase. *J Biol Chem* **275**, 16044-9 (2000).
138. Duong, H.A., Robles, M.S., Knutti, D. & Weitz, C.J. A molecular mechanism for circadian clock negative feedback. *Science* **332**, 1436-9 (2011).
139. Kowalska, E. *et al.* NONO couples the circadian clock to the cell cycle. *Proc Natl Acad Sci U S A* **110**, 1592-9 (2013).
140. Sutton, M.A. & Schuman, E.M. Dendritic protein synthesis, synaptic plasticity, and memory. *Cell* **127**, 49-58 (2006).
141. Medioni, C., Mowry, K. & Besse, F. Principles and roles of mRNA localization in animal development. *Development* **139**, 3263-76 (2012).
142. Gumy, L.F. *et al.* Transcriptome analysis of embryonic and adult sensory axons reveals changes in mRNA repertoire localization. *RNA* **17**, 85-98 (2011).
143. Zivraj, K.H. *et al.* Subcellular profiling reveals distinct and developmentally regulated repertoire of growth cone mRNAs. *J Neurosci* **30**, 15464-78 (2010).
144. Steward, O., Wallace, C.S., Lyford, G.L. & Worley, P.F. Synaptic activation causes the mRNA for the IEG Arc to localize selectively near activated postsynaptic sites on dendrites. *Neuron* **21**, 741-51 (1998).
145. Stubblefield, J.J., Terrien, J. & Green, C.B. Nocturnin: at the crossroads of clocks and metabolism. *Trends Endocrinol Metab* **23**, 326-33 (2012).
146. Valnegri, P. *et al.* A circadian clock in hippocampus is regulated by interaction between oligophrenin-1 and Rev-erbalpha. *Nat Neurosci* **14**, 1293-301 (2011).
147. Fauchereau, F. *et al.* The RhoGAP activity of OPHN1, a new F-actin-binding protein, is negatively controlled by its amino-terminal domain. *Mol Cell Neurosci* **23**, 574-86 (2003).
148. Bergmann, C. *et al.* Oligophrenin 1 (OPHN1) gene mutation causes syndromic X-linked mental retardation with epilepsy, rostral ventricular enlargement and cerebellar hypoplasia. *Brain* **126**, 1537-44 (2003).

149. Billuart, P. *et al.* Oligophrenin 1 encodes a rho-GAP protein involved in X-linked mental retardation. *Pathol Biol (Paris)* **46**, 678 (1998).
150. Govek, E.E. *et al.* The X-linked mental retardation protein oligophrenin-1 is required for dendritic spine morphogenesis. *Nat Neurosci* **7**, 364-72 (2004).
151. Khelfaoui, M. *et al.* Loss of X-linked mental retardation gene oligophrenin1 in mice impairs spatial memory and leads to ventricular enlargement and dendritic spine immaturity. *J Neurosci* **27**, 9439-50 (2007).
152. Philip, N. *et al.* Mutations in the oligophrenin-1 gene (OPHN1) cause X linked congenital cerebellar hypoplasia. *J Med Genet* **40**, 441-6 (2003).
153. Tentler, D. *et al.* Deletion including the oligophrenin-1 gene associated with enlarged cerebral ventricles, cerebellar hypoplasia, seizures and ataxia. *Eur J Hum Genet* **7**, 541-8 (1999).
154. Holt, C.E. & Bullock, S.L. Subcellular mRNA localization in animal cells and why it matters. *Science* **326**, 1212-6 (2009).
155. Doyle, M. & Kiebler, M.A. Mechanisms of dendritic mRNA transport and its role in synaptic tagging. *EMBO J* **30**, 3540-52 (2011).
156. Zhang, G., Neubert, T.A. & Jordan, B.A. RNA binding proteins accumulate at the postsynaptic density with synaptic activity. *J Neurosci* **32**, 599-609 (2012).
157. Kuwahara, S. *et al.* PSPC1, NONO, and SFPQ are expressed in mouse Sertoli cells and may function as coregulators of androgen receptor-mediated transcription. *Biol Reprod* **75**, 352-9 (2006).
158. Song, K.S., Kim, K., Chung, K.C., Seol, J.H. & Yoon, J.H. Interaction of SOCS3 with NonO attenuates IL-1beta-dependent MUC8 gene expression. *Biochem Biophys Res Commun* **377**, 946-51 (2008).
159. Bernard, D. *et al.* A long nuclear-retained non-coding RNA regulates synaptogenesis by modulating gene expression. *EMBO J* **29**, 3082-93 (2010).
160. Hu, H. *et al.* X-exome sequencing of 405 unresolved families identifies seven novel intellectual disability genes. *Mol Psychiatry* (2015).

161. Deciphering Developmental Disorders, S. Large-scale discovery of novel genetic causes of developmental disorders. *Nature* **519**, 223-8 (2015).
162. Mehnert, K.I. *et al.* Circadian changes in Drosophila motor terminals. *Dev Neurobiol* **67**, 415-21 (2007).
163. Fernandez, M.P., Berni, J. & Ceriani, M.F. Circadian remodeling of neuronal circuits involved in rhythmic behavior. *PLoS Biol* **6**, e69 (2008).
164. Pyza, E. & Gorska-Andrzejak, J. External and internal inputs affecting plasticity of dendrites and axons of the fly's neurons. *Acta Neurobiol Exp (Wars)* **68**, 322-33 (2008).
165. Damulewicz, M. & Pyza, E. The clock input to the first optic neuropil of Drosophila melanogaster expressing neuronal circadian plasticity. *PLoS One* **6**, e21258 (2011).
166. Akula, N. *et al.* RNA-sequencing of the brain transcriptome implicates dysregulation of neuroplasticity, circadian rhythms and GTPase binding in bipolar disorder. *Mol Psychiatry* **19**, 1179-85 (2014).
167. Kulman, G. *et al.* Evidence of pineal endocrine hypofunction in autistic children. *Neuro Endocrinol Lett* **21**, 31-34 (2000).
168. Tordjman, S., Anderson, G.M., Pichard, N., Charbuy, H. & Touitou, Y. Nocturnal excretion of 6-sulphatoxymelatonin in children and adolescents with autistic disorder. *Biol Psychiatry* **57**, 134-8 (2005).
169. Elsea, S.H. & Williams, S.R. Smith-Magenis syndrome: haploinsufficiency of RAI1 results in altered gene regulation in neurological and metabolic pathways. *Expert Rev Mol Med* **13**, e14 (2011).
170. Williams, S.R., Zies, D., Mullegama, S.V., Grotewiel, M.S. & Elsea, S.H. Smith-Magenis syndrome results in disruption of CLOCK gene transcription and reveals an integral role for RAI1 in the maintenance of circadian rhythmicity. *Am J Hum Genet* **90**, 941-9 (2012).

8. Curriculum Vitae

Personal Details

Name Mircsof

First name Dennis

Birth Date 12.01.1986

Nationality Swiss

Education

PhD thesis November 2010 - present

Title: “Identification of circadian synaptic transcripts and the role of DBHS proteins in inhibitory synaptic biology” Institute of Pharmacology and Toxicology, University of Zurich, Switzerland Supervisor: Prof. Dr. Steven A. Brown and Dr. Shiva Tyagarajan; Affiliation to the PhD program in Neuroscience Neuroscience Center Zurich (ZNZ), University of Zurich and ETH Zurich, Switzerland

Master of Sciences in Pharmaceutical Science August 2009

Federal Diploma as Pharmacist Swiss Federal Institute of Technology Zurich (ETH), Switzerland Institute of Pharmaceutical Sciences

Master thesis Nov. 2007- May 2008

Titel: “Construction of a DNA-encoded chemical library: A two round 'split and pool' strategy“ Institute of Pharmaceutical Science, ETH Zurich, Switzerland Supervisor: Prof. Dr. Dario Neri

Bachelor of Sciences in Pharmaceutical Science May 2007

Swiss Federal Institute of Technology Zurich (ETH) Institute of Pharmaceutical Sciences

Conferences and Poster Presentations

2015	SSN Annual Meeting; 24/01 2015; Fribourg (Switzerland)
	Swiss RNA workshop 23/01 2015; Bern (Switzerland)
2014	EMBO: The Complex Life of mRNA; 05–8/10 2014; Heidelberg (Germany)
	ZNZ Symposium 11/09 2014; Zurich (Switzerland)
	Pharmacology & Toxicology Poster Day; 8/09/2014; Zurich (Switzerland)
	SSN Annual Meeting; 25/01 2014; Bern (Switzerland)
	Swiss RNA workshop 24/01 2014; Bern (Switzerland)

2013	Neuroscience 2013 - Society for Neuroscience (SFN); 09-13/11 2013, San Diego (United States of America)
	ISN-FENS Summer School on Local protein synthesis in axons and dendrites; 24–28/09 2013; Kolymbari (Greece)
	Gordon Research Conference on Inhibition in the CNS; 16–21/6 2013; Les Diablerets (Switzerland)
	British Neuroscience Festival; 7–10/4 2013; London (United Kingdom)
	ZNZ PhD Retreat; 25–27/4 2013; Valens (Switzerland)
	Synergia Meeting; 27/02–1/3 2013; Chexbres (Switzerland)
	Swiss RNA workshop; 25/02 2013; Bern (Switzerland)
2012	Zurich Pharmacology Poster Day 2011: 4/10 2012; Zurich (Switzerland)
	EMBO: The Complex Life of mRNA; 07–10/10 2012; Heidelberg (Germany)
	NCCR Neuro Concluding Symposium and ZNZ Annual Symposium; 14–15/06 2012; Zurich (Switzerland)
	Swiss RNA workshop 03/02 2012; Bern(Switzerland)
2011	ZNZ Symposium 16/09 2011; Zurich (Switzerland)
	12th International Course on Chronopharmacology 25/07–02/08 2011; Mannheim (Germany)
	SSN Annual Meeting; 26/03 2011; Basel (Switzerland)

Publications

Mircsof D, Langouët M, Rio M, Moutton S, Siquier-Pernet K, Bole-Feysot C, Cagnard N, Nitschke P, Gaspar L, Žnidaric M, Alibeu O, Fritz A-K, Wolfer D.P., Schröter A, Bosshard G, Rudin M, Koester C, Crestani F, Seebeck P, Boddaert N, Fritschy J-M, Munnich A, Amiel J, Brown S. A., Tyagarajan S. K., Colleaux L. ; NONO mutations are a novel cause of syndromic intellectual disability and inhibitory synaptic defects; in submission

Notter, T., Panzanelli, P., Pfister, S., **Mircsof, D**. and Fritschy, J.-M. (2013), A protocol for concurrent high-quality immunohistochemical and biochemical analyses in adult mouse central nervous system. European Journal of Neuroscience. doi: 10.1111/ejn.12447

Mircsof D. and Brown S.A. (2013) The Influence of Light, Exercise, and Behavior upon Circadian Rhythms. In: Kushida C. (ed.) The Encyclopedia of Sleep, Vol. 1, pp. 435-441. Waltham, MA: Academic Press.

Buller F, Steiner M, Frey K, **Mircsof D**, Scheuermann J, Kalisch M, Bühlmann P, Supuran CT, Neri D; Selection of Carbonic Anhydrase IX Inhibitors from One Million DNA-Encoded Compounds; ACS Chem Biol. 2011 Apr 15;6(4):336-44.